SUGILITE AND ASSOCIATED METAMORPHIC SILICATE MINERALS FROM WESSELS MINE KALAHARI MANGANESE FIELD

BY

Roger Dixon

THESIS SUBMITTED IN FULFILMENT OF THE REQUIREMENTS

FOR THE DEGREE

MAGISTER SCIENTIAE

IN THE FACULTY OF SCIENCE AT THE

UNIVERSITY OF CAPE TOWN

1988

This represents the original research of the author

except where specific acknowledgement is made.

Signed by candidate

signature removed

ABSTRACT

Sugilite, a purple mineral belonging to the milarite group, occurs in the lower manganese orebody at Wessels Mine, in the Kalahari Manganese Field. This orebody was formed in the lowermost manganiferous horizon of the Hotazel Member of the Voëlwater Jasper Formation, part of the volcanogenic sedimentary iron formation of the Griqualand West Sequence. At Wessels Mine, which is located northwest of Kuruman in the northwestern Cape Province, evidence of a widespread and pervasive hydrothermal event which took place around 1 300 Ma is found in the form of upgrading of the manganese-ore horizons and the formation of zoned silicate-mineral assemblages. The presence of unusual minerals such as glaucochroite, iron akermanite, xonotlite and hydrogarnets of various types constrains the main phase of metamorphism to between 400 and 450 °C in a low pressure, hydrous environment with $X_{CO2} \leq 0,02$. All the minerals which occur in these assemblages are described and discussed in terms of their chemistry and formation.

ACKNOWLEDGEMENTS

I would like to thank:

The Chief Director of the Geological Survey, Dr C. Frick, for the opportunity afforded to me to pursue this research and for his encouragement.

My supervisors, Prof A. M. Reid and Dr J. Moore.

SAMANCOR, and in particular Messers D. Bird, R. Arnot and C. Steenkamp, for permission to visit Wessels Mine and for guidance underground and sample collection.

This work would not have been completed without the assistance of Dr Feo Walraven (isotopic determinations), Dr G. du Plessis and Mr R. Rickards (microprobe analyses), Ms M. Schatz (SEM), Mr M. Kohler (photography), and Dr R. A. Edge and Messers J. Trojak and D. A. Burnett (chemical analyses). E. Roux and L Smit drew the illustrations

CONTENTS

ABSTRACT
ACKNOWLEDGEMENTS
CONTENTS

		PAGE
1	INTRODUCTION	1
1.1	Study aim.	1
1.2	Sample collection	2
1.3	Analytical methods.....	3
2	GEOLOGICAL SETTING	7
2.1	Stratigraphy	7
2.2	The Hotazel Member	9
2.3	Manganese ores in the Black Rock area.....	12
2.3.1	Host-rock composition.....	16
2.4	Location of sugilite and associated minerals	19
3	MINERALOGY OF THE SUGILITE ASSEMBLAGE.....	25
3.1	Milarite group	25
3.1.1	Sugilite	28
3.1.2	Mineral X	36
3.1.3	Chemistry	41
3.1.4	Formation	46
4	MINERALS ASSOCIATED WITH THE SUGILITE ASSEMBLAGE	48
4.1	Amphibole group.....	48
4.1.1	Chemistry and classification	48
4.2	Garnet	64
4.2.1	Mn^{3+} in the garnet structure	79
4.2.2	The garnet-hydrogarnet series	83
4.2.3	Compositional variation in the garnets	85
4.3	Sheet silicates	91
4.3.1	Chlorite	91
4.3.2	Phlogopite.....	91

4.4	Olivine and melilite	94
4.4.1	Glaucochroite-kirschsteinite	94
4.4.2	Akermanite	102
4.4.3	Formation of glaucochroite and akermanite	107
4.5	Wollastonite group	110
4.5.1	Pectolite-serandite.....	111
4.5.2	Wollastonite	114
4.5.3	Formation	114
4.6	Pyroxene	116
4.6.1	Acmite	116
4.6.2	Diopside	117
4.7	Vesuvianite.....	120
4.8	Quartz	125
5	**AGE OF METAMORPHISM.....**	**126**
5.1	Sampling and analysis	126
5.1.1	Sugilite Rb-Sr isotopes	127
5.1.2	Sugilite Pb isotopes	127
5.1.3	Galena Pb isotopes	127
5.1.4	Bostonite Rb-Sr isotopes	128
5.1.5	Bostonite Pb isotopes	128
5.2	Discussion	129
6	**METAMORPHIC CONDITIONS .....**	**131**
6.1	Depth and pressure of formation	132
6.2	Original composition of the rock.....	132
6.3	Sequence of metamorphic mineral formation.	133
6.4	Discussion	135
6.4.1	Stage 1	135
6.4.2	Stage 2	138
7	**CONCLUSIONS .....**	**142**
8	**REFERENCES .....**	**143**

1 INTRODUCTION

Sugilite, a member of the milarite group of minerals, is a sodium-potassium ferric-iron silicate first described by Murakami et al. (1976) in an aegirine syenite from Iwagi Islet, southwest Japan. It was described from the Wessels Manganese Mine near Kuruman, northwestern Cape Province, by Dunn et al. (1980) and subsequently from Madhya Pradesh, India (Clark et al. 1980). The mineral from Wessels Mine has a purple-violet colour and occurs interbedded with layered manganese ores, with most of the mineral occurring in the vicinity of the upper gradational contact of the lower manganese-ore layer with the overlying banded iron formation. It has been found in small quantities in several localitites in the mine and is being mined as a gemstone. Since the initial discovery at the Wessels Mine the sugilite has also been found in association with several other unusual minerals and, in places, it occurs together with a zoned sequence of minerals such as is found in infiltration metasomatic calc-alkaline skarns.

1.1 STUDY AIM

The aim of this study is to describe the sugilite and the silicate minerals associated with it which occur in the lower manganese-ore layer at Wessels Mine in the Kalahari Manganese Field, and to determine the conditions of formation of these minerals. This mineralisation appears to be linked to an

hydrothermal event which affected the northwestern portion of the Kalahari Manganese Field. The present high manganese content of the ores and the relative absence of carbonate material is in striking contrast to the low manganese and high carbonate contents of the ores in the rest of the Manganese Field. This presumed hydrothermal event appears to have resulted in the upgrading of the ore and the removal of large amounts of carbonate material. Rb-Sr and Pb isotope studies have been undertaken to determine the age of this hydrothermal event so as to find the heat source and mechanism for the event.

1.2 SAMPLE COLLECTION

The sugilite occurrences are highly localised in Wessels Mine and are usually found exposed immediately after blasting has taken place, after which the material is collected by hand and sold by the company. This makes the acquisition of material difficult, but not impossible. Underground visits were made on two occasions to collect material and obtain accurate information as to where the sugilite formed in the ore. The majority of the material used in this study, however, was obtained from mineral dealers and collectors. The sugilite originally discovered at the Mine was discarded as waste by the management and subsequently obtained by dealers as lapidary material, of which the finest quality sold for up to 1 000 US dollars per carat in polished form. As a result of this generally haphazard acquisition of material, the exact

locations of some of the samples in the Mine are indeterminate. Due to the nature of the mineralisation and its generally widespread occurrence in the mine this is not considered to be a serious drawback.

1.3 ANALYTICAL METHODS

The major analytical method employed in this study was electron microprobe analysis and two instruments were used: the Jeol JXA 50A microprobe at the Geological Survey in Pretoria and the Cameca microprobe in the Department of Geochemistry at the University of Cape Town.

Analyses were obtained using the JEOL JXA 50A electron microprobe at 15 kV and a beam current of 0,255 μA. Standards used were wollastonite for Si and Ca, corundum for Al, periclase for Mg, hematite for Fe, pyrolusite for Mn, albite for Na, orthoclase for K and celestite for Sr, using the correction procedures of Bence and Albee (1968).

On the Cameca microprobe four standard sets were used for the various mineral species: olivine, amphibole, garnet and pyroxene. In the olivine set the standards were Mg-olivine for Si, Fe and Mg, Kakanui pyrope for Al and Ca, and rhodonite for Mn. In the amphibole set Kakanui hornblende for Na, K, Si, Al, Fe, Mg and Ca, and rhodonite for Mn. In the garnet set Kakanui pyrope for Si, Al, Fe, Mg and Ca, rhodonite for Mn and Kakanui hornblende for Na. The pyroxene set used diopside for Si, Mg

and Ca, Kakanui pyrope for Al and Fe, rhodonite for Mn and Kakanui hornblende for Na and K.

All the analyses presented in Chapter 4 were determined by microprobe. Those mineral analyses with low totals are not necessarily inaccurate but may reflect the presence of water (and in the case of the sugilite, lithium) which cannot be detected by microprobe. Other elements are not suspected of causing these low summations, since bulk samples containing many of the mineral phases in question were analysed as described below and no alternative light elements were identified.

The accuracy of the microprobe is limited to 1 or 2 per cent. The outer limits are substantially greater when dealing with unusual compositions. The problem derives in part from the fact that standards were not available which closely match the unknown minerals. Because of this and because of the uncertainty in standards the errors can be correspondingly great.

Most of the minerals analysed in this study have analytical totals that do not add up to 100 per cent. This is a common phenomenon in microprobe analysis and may reflect error, due to something as simple as the quality of the sample surface, or the oxidation state of elements such as iron and manganese, which occurr in large amounts in some of the minerals.

X-ray fluorescence analysis was used for the rock-sample analyses presented in Chapter 2. Other methods used were wet chemistry determinations of FeO, atomic absorption spectroscopy for Li, F and Cl, and infrared spectroscopy for S, CO_2 and H_2O.

A Jeol JSM35 scanning electron microscope was used to help identify and locate mineral phases that were too small to observe by means of optical microscopy, and to locate phases containing elements occurring in minor amounts in the bulk samples (Figs 1 and 2).

From all the analytical techniques employed only Si, Al, Fe, Mn, Mg, Ca, Na and K were found in concentrations high enough to analyse for by microprobe, although Li, Sr and P were present in significant amounts in certain assemblages.

X-ray diffraction was used to identify nearly all of the minerals discussed in this study. The diffraction data presented were obtained using either grain mounts in a Gandolfi camera or powders in a diffraction scan (or a combination of both). CaF_2 was used as an internal standard for the powder diffraction. In all cases Cu-Kα radiation (1,5418 Å) was used. The calculated d-spacings given in the thesis were obtained by using the Appleman computer program.

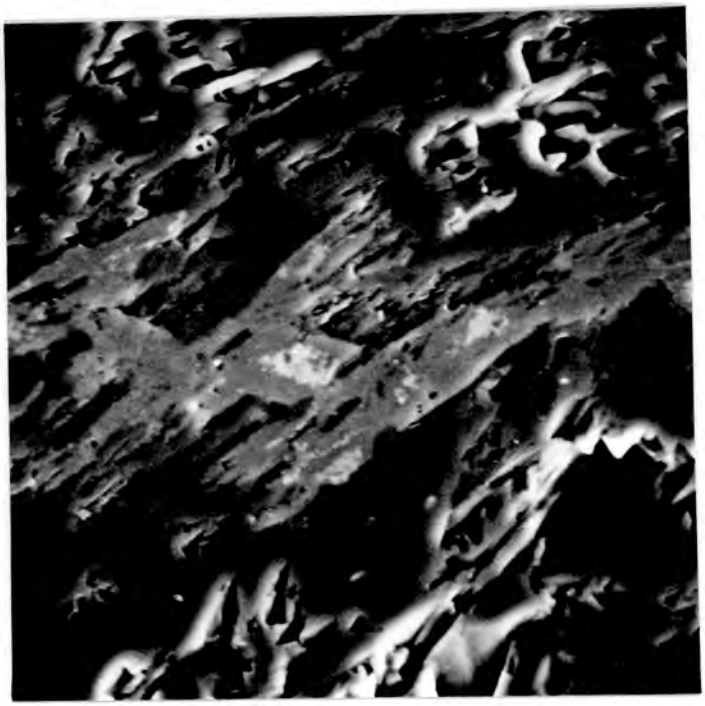

Figure 1. The light-grey laths are an unidentified CaSrP-rich mineral, and the white inclusions in them are an unidentified CaSr-rich phase. The dark-grey mineral is pectolite. Sample RDW3A, SEM, 1000X.

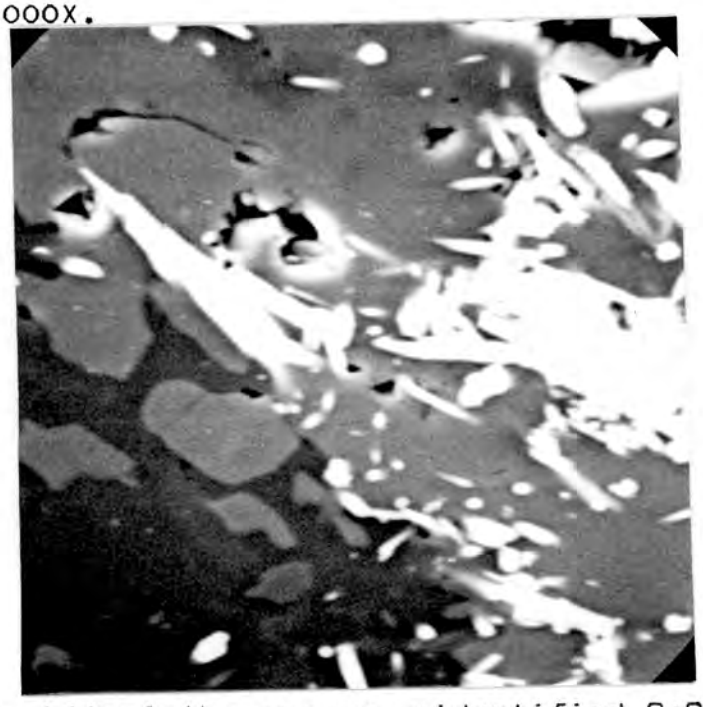

Figure 2. The white laths are an unidentified CaSr-rich phase, the medium-grey is wollastonite and the dark-grey pectolite. Sample RDW2, SEM, 1000X.

2 GEOLOGICAL SETTING

2.1 STRATIGRAPHY

The strata-bound ore deposits of the Kalahari Manganese Field in the Kuruman area, northern Cape Province, South Africa, are the largest sedimentary manganese deposits in the world. They are considered to represent a single episode of manganese deposition at or before 2 100 Ma (Söhnge 1977). According to SACS (1980) the manganese deposits of the Griqualand West Sequence lie in the Hotazel Member of the Voëlwater Jasper Formation, immediately above the Ongeluk Andesite Formation. The Voëlwater is stratigraphically succeeded by the Olifantshoek Sequence consisting mainly of the Mapedi Shale Formation, the Lucknow Quartzite Formation, the Hartley Andesite Formation and the Volop Quartzite Group, giving a total thickness of more than 4 500 m.

The Cox Group, consisting of the Ongeluk Andesite Formation and the Hotazel and Mooidraai Members of the Voëlwater Jasper Formation, represents a mixed volcanogenic-chemical sedimentary rock unit in the Griqualand West Sequence (Söhnge 1977; Beukes 1980) (Fig. 3). The Ongeluk lavas crop out extensively but the Voëlwater is largely covered by the Cretaceous to Tertiary Kalahari Group, the Karoo Sequence and the Olifantshoek Sequence.

The Hotazel Member is preserved in the form of erosional

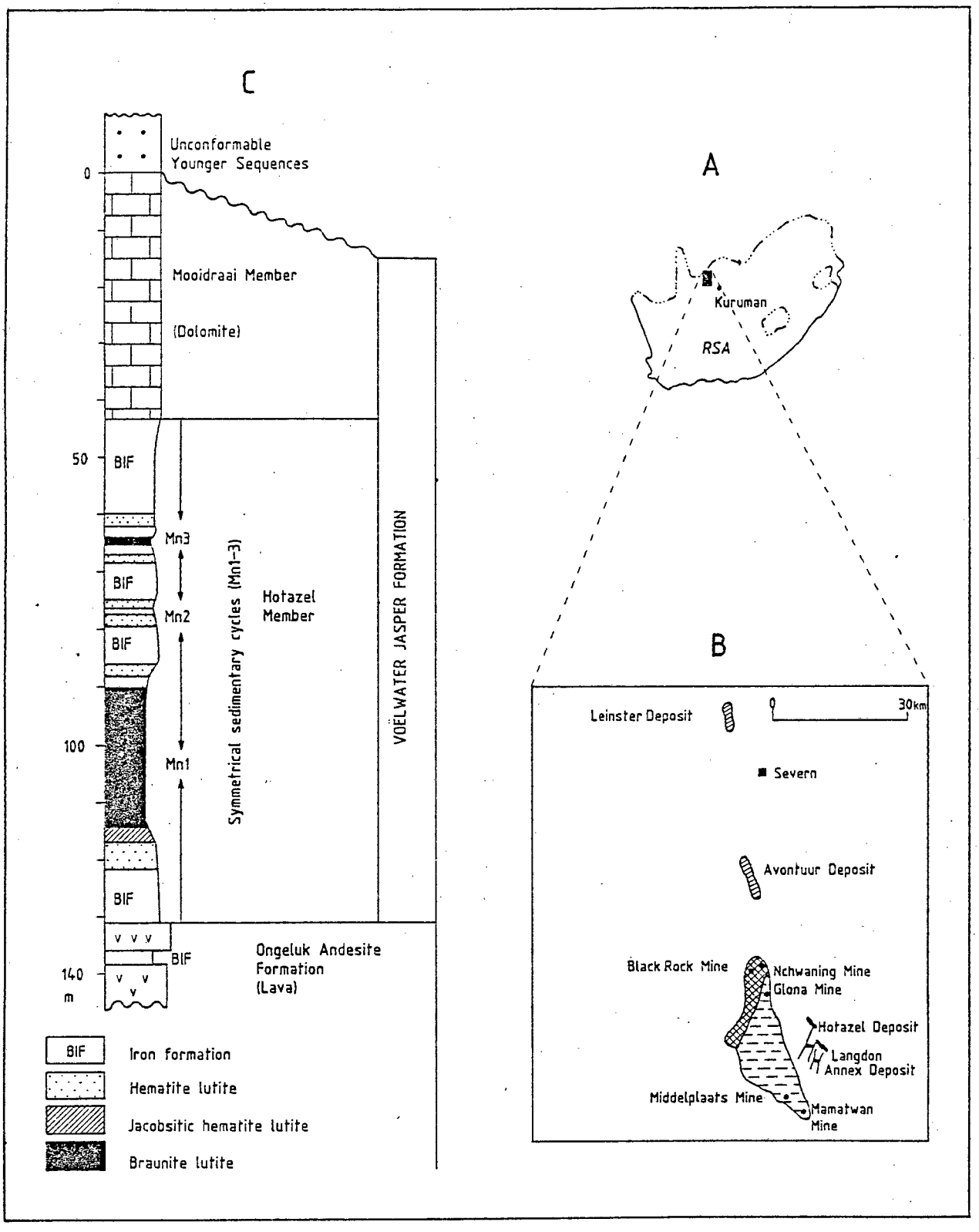

Fig. 3 - Locality map of the Kalahari Manganese Field (A) showing areal distribution of deposits and main ore types (B), and stratigraphic setting of braunite lutite beds in the Voëlwater Jasper Formation (C) (after Miyano and Beukes, 1987).

relics in a number of structural basins. The Mamatwan, Middelplaats, N'chwaning and Wessels Manganese Mines are situated in the largest known, westernmost basin. The base of the Hotazel Member in this area consists of a bright-red jasper unit, overlying hyaloclastic breccias and pillow-lava flows of the mafic Ongeluk Formation. Similar jasper beds also cap pillow-lava flows and hyaloclastite units in the upper part of the Ongeluk Formation to the south of the study area (Grobler and Botha 1976) suggesting an interfingering relationship between the lava and the Hotazel Formation* (Beukes 1980). Red hematite dust also forms part of the matrix of some of the hyaloclastic breccias.

Dykes of bostonite cut through the mine area. The main dyke is approximately 30 m wide and the only metamorphic effect visible on the manganese ore is a 10 mm-thick jacobsitic rim around the dyke (De Villiers 1983).

2.2 THE HOTAZEL MEMBER

An iron formation is defined as an iron-rich sedimentary rock consisting of chert and microcrystalline iron minerals (Beukes 1980). The chert occurs either as chert mesobands and microbands or as interstitial grains between the iron-mineral

---

* SACS 1980 HOTAZEL MEMBER

particles. The iron formations display textural and structural features resembling those of carbonate rocks.

The chert content of the basal jasper unit of the Hotazel Member decreases upwards. In the sequence the jasper unit grades into kutnahorite-bearing pisolitic hematite lutite, which in turn gradually grades into microcrystalline kutnahoritic pisolitic braunite lutite (see Fig. 3). The kutnahorite is concentrated in the pisoliths which represent partly compacted, early diagenetic concretions in hematite and braunite lutite. Although pisoliths are the most abundant spherical particles in the lutites, ovoids of less than 2 mm in diameter are also present. These fall in the oolith size range and are of a concretionary origin (Beukes 1980).

The sequence described above represents the lower section of the lowermost of three jasper–manganolutite–jasper sedimentary cycles present in the Hotazel Member. Each of the cycles consists of jasper and/or jaspilite–kutnahoritic hematite lutite–kutnahoritic braunite lutite. The braunite lutite bed of the lower cycle is between 5 m and 40 m thick. With a manganese content of between 20 and 48 wt. per cent it is the major ore unit in the Kalahari Manganese Field. At Wessels Mine it is about 5 m thick and contains up to 45 wt. per cent manganese and little carbonate.

The middle manganolutite unit (cycle 2) is approximately 2 m thick and consists essentially of a braunitic hematite lutite

which is of no economic significance. The upper manganese orebody, which was mined in earlier years, rarely exceeds 5 m in thickness. Grey-coloured hematitic and magnetitic minnesotaite ribbon- and bandlutite are present between the lower and middle manganolutite units. Thin chlorite-bearing mesobands interbedded with the iron formations may represent altered volcanic-ash bands.

The kutnahoritic hematite lutite which overlies the uppermost manganolutite unit is in turn overlain by hematite pillowlutite. This unit is increasingly sideritic and grades into laminated and cross-laminated siderite ribbonlutites and bandlutites. This siderite facies banded iron formation forms the top of the Hotazel Member and is overlain by brecciated and laminated cherty dolomite of the Mooidraai Member (Beukes 1983).

The above-mentioned association of sedimentary manganese deposits and jasper, together with the hyaloclastites and pillow lavas of the underlying Ongeluk Andesite Formation, is similar to the greenstone–jasperoid association of volcanogenic–sedimentary manganese deposits (Stanton 1972; Roy 1981). According to Beukes (1983) the cyclical jasper to manganese-oxide variations in the Voëlwater are due to transgressions and regressions relative to a volcanic source. Divalent manganese ions take longer to be oxidised than ferrous ions and are therefore deposited further away from the volcanogenic source (Bonatti et al. 1972). Frick (1986), on

the basis of geochemical evidence, states that the banded iron formations of the Voëlwater resulted from extreme chemical leaching and deposition controlled by hydrothermal activity, their deposition probably controlled by the interplay of the concentration of elements and the temperature of the water during this volcanically active period.

2.3 MANGANESE ORES IN THE BLACK ROCK AREA

The high-grade manganese ores in the northwestern portion of the Kalahari Manganese Field (Wessels, Black Rock and the N'chwaning Mines) consist of braunite II, bixbyite, hausmannite, hematite, calcite and andradite, with trace amounts of braunite. In contrast to this, the low-grade (diagenetic to very low-grade metamorphic) Mamatwan-type ores to the southeast consist mainly of braunite, hausmannite, jacobsite, hematite, kutnahorite and calcite (see Table 1). In addition the ores of the former contain such minerals as rhodonite and tephroite, with the iron formation showing development of acmite. De Villiers (1970) proposed that the Kalahari Manganese Field underwent thermal metamorphism to varying degrees some time after deposition of the Voëlwater. Kleyenstüber (1984) has shown that a thermal event was experienced with the northwestern portion of the Kalahari Manganese Field reaching temperatures of around 300 °C. De Villiers (1983), on the basis of the Fe content in bixbyite, proposed temperatures for the Black Rock and Wessels areas of 400 °C or more.

Hematite	$Fe^{3+}_2O_3$
Bixbyite	$(Mn^{3+},Fe^{3+})_2O_3$
Braunite	$Mn^{2+}(Mn^{3+},Fe^{3+})_6SiO_{12}$
Braunite II	$Ca_{0,5}(Mn^{3+},Fe^{3+})_7Si_{0,5}O_{12}$
Hausmannite	$Mn^{2+}(Mn^{3+},Fe^{3+})_2O_4$
Jacobsite	$(Mn^{2+},Fe^{2+},Mg)(Fe^{3+},Mn^{3+})_2O_4$
Kutnahorite	$CaMn(CO_3)_2$
Marokite	$CaMn^{3+}_2O_4$
Rhodochrosite	$MnCO_3$
Tephroite	Mn_2SiO_4
Pyrolusite	MnO_2

TABLE 1. Some minerals found in the manganese ores in the Wessels Mine and others nearby.

Mineralogical differences between Mamatwan-type and Wessels-type ores are reflected in the average chemical composition of the ore types. The low-grade (lower manganese content) ores contain more CaO, H_2O and CO_2, and less Fe_2O_3 and Mn_2O_3 than the high-grade ores (Table 2). The low content of CO_2, CaO and MgO in the Wessels-type ore illustrates its deficiency in carbonates relative to the carbonate-rich Mamatwan-type ore. In areas where sugilite occurs the total CO_2 content of the rocks is less than 0,5 per cent. The manganese content of the Mamatwan ores at around 38 per cent was originally considered too low-grade to mine (Nel 1984), in comparison with the higher grade ores in the Hotazel and Black Rock areas, which in some exceptional cases consist of almost pure hausmannite with a manganese content of up to 60 per cent.

A recent study by Miyano and Beukes (1987) based on the manganese-oxide assemblages of the two ore types has dealt with the mechanism of manganese enrichment from the low- to high-grade ores in a quartz-deficient hydrothermal system. The hydrothermal alteration took place in a stockwork fashion along bedding planes, joints and faults, and resulted in the formation of high-grade high-temperature Wessels-type ore from the low-grade Mamatwan-type ore at temperatures of between 300 to 400 °C. Because the CaO content of the Wessels-type ore is very low relative to Mamatwan-type ore, considerable CaO must have been leached from the system during the hydrothermal process, during which Ca^{2+} from carbonates became available

	Mamatwan-type wt. percent	Wessels-type wt. percent
SiO_2	4-6	6-9
Al_2O_3*	1,00	1,00
Fe_2O_3**	5,7-8,6	15,7-20,0
Mn_2O_3	53,2-54,6	67,5-69,0
CaO	14,00	5,00
MgO	4,00	1,00
Na_2O	0,40	0,40
K_2O	0,05	0,02
S	0,10	0,15
P	0,05	0,05
CO_2	16,00	2,00
H_2O	3,50	2,30

*
**Total Fe as Fe_2O_3
Total Mn as Mn_2O_3

TABLE 2 - Average bulk composition of low-grade Mamatwan-type and high-grade Wessels-type ore (after SAMANCOR, 1979).

for the formation of braunite II which replaced braunite. The hydrothermal solutions became enriched in silica derived from braunite to such an extent that, in the presence of sufficient Ca^{2+}, andradite and other higher temperature silicate minerals precipitated.

2.3.1 HOST-ROCK COMPOSITION

Table 3 shows the variation in composition of banded lutites just above manganese ore in a sequence progressing upwards into sugilite over a distance of 40 cm. The variation is illustrated in Figure 4. A striking feature is the distinct mineralogical, chemical and colour difference between the lower and upper portions of the section. From the manganese ore, which is black and contains a large amount of Mn and Fe, samples 1 to 6 are bright red, contain high iron and consist mainly of hematite and acmite. Samples 7 to 9 are black in colour, contain acmite with no hematite, and much less iron. The uppermost sample 10 is purple in colour, has the lowest iron content and a wide range of minerals, especially pectolite and sugilite.

The change in colour between the black acmite-rich samples and the purple sugilite-rich sample is gradational over a distance of about 20 mm, whereas the colour change between the red hematite-bearing samples and the hematite-deficient black layers above is sharply defined on a microscopic scale. This latter boundary also has a distinct chemical signature (Fig.

	1	2	3	4	5	6	7	8	9	10
SiO_2	11,85	25,99	43,82	45,32	28,99	28,15	52,27	53,73	52,40	56,04
TiO_2	0,09	0,08	0,06	0,06	0,06	0,05	0,05	0,06	0,06	0,09
Al_2O_3	0,12	0,32	0,00	0,00	0,00	0,00	0,00	0,00	0,00	1,29
Fe_2O_3	60,57	55,42	43,59	40,49	62,54	65,14	31,77	29,04	26,32	21,48
FeO	0,25	0,25	0,25	0,25	0,25	0,25	0,25	0,25	0,25	0,25
Mn_2O_3	17,30	9,12	0,86	1,45	0,86	1,25	2,24	4,67	6,60	5,65
MgO	3,12	2,60	0,79	1,34	0,66	0,77	0,77	1,24	1,26	1,18
CaO	1,26	1,20	0,53	0,79	0,45	0,41	0,57	0,64	1,14	1,58
Na_2O	0,96	3,74	8,56	8,44	4,61	3,99	10,06	9,28	9,69	8,18
K_2O	1,21	0,78	0,00	0,11	0,00	0,00	0,00	0,04	0,10	1,33
P_2O_5	0,24	0,20	0,17	0,13	0,12	0,04	0,03	0,07	0,06	0,06
H_2O	2,79	0,44	0,26	0,20	0,13	0,08	0,11	0,15	0,20	0,51
CO_2	0,11	0,12	0,10	0,09	0,07	0,06	0,09	0,08	0,15	0,15
TOTAL	99,72	100,01	98,74	98,52	98,49	99,94	97,94	98,98	98,58	97,49

Total Mn as Mn_2O_3 because the Mn^{3+} ion is present in braunite and hausmannite at the bottom of the section, and in the sugilite at the top, and analytical techniques available did not permit the determination of Mn^{2+} and Mn^{3+}.

TABLE 3. Chemical composition of lutites just above manganese ore in a sequence progressing upwards into sugilite over a distance of 40 cm.

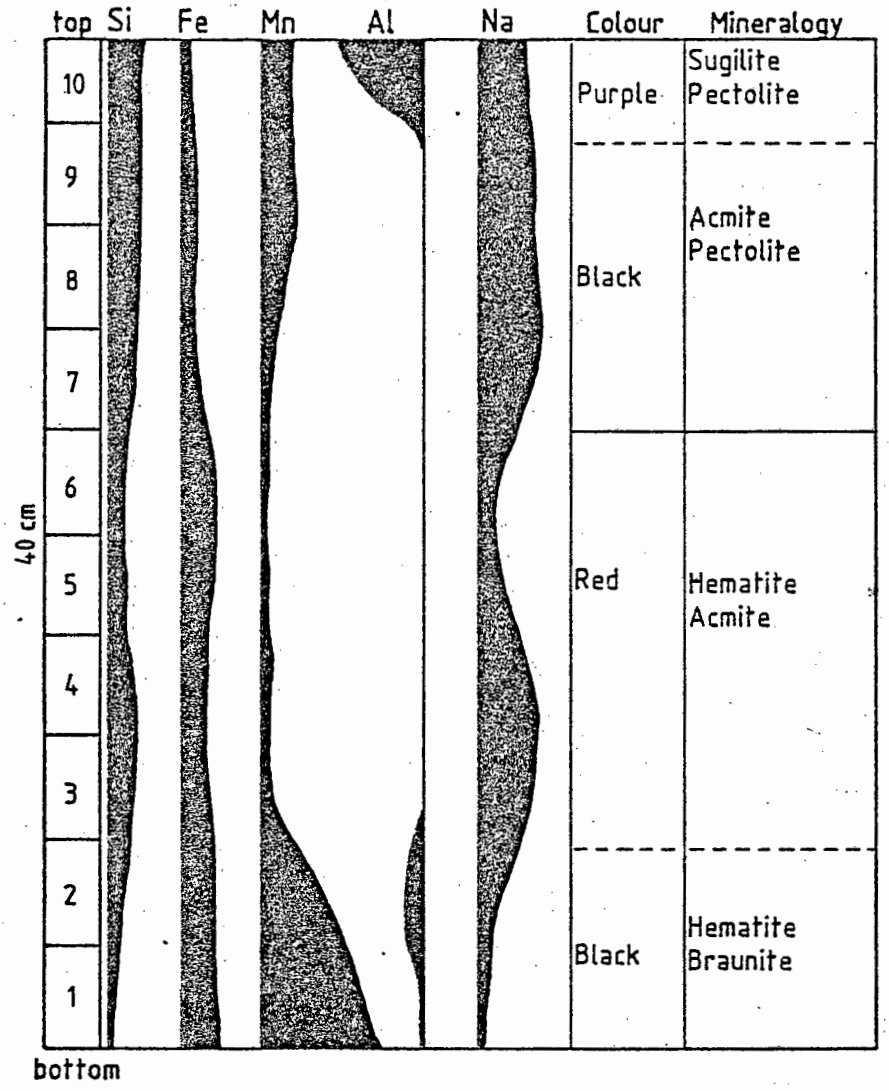

Fig. 4 - Diagram illustrating the variation in colour, chemistry and mineralogy through the section whose analyses are given in Table 3.

4) and cuts across the pre-existing undulose sedimentary banding.

The gradual or sudden increases in the amounts of Al, K, Si and Na towards the sugilite-rich sample 10, and the variation in the other elements upwards from the manganese ore appear to indicate that some process of element movement was operative at the time of sugilite formation.

2.4 LOCATION OF SUGILITE AND ASSOCIATED MINERALS

Sugilite and associated mineral assemblages are uncommon and have a patchy but widespread distribution restricted to the lower manganese-ore layer at Wessels Mine, as outlined below:

i) in the vicinity of the contact between the braunite lutite of the first sedimentary cycle and the jaspilite of the bottom of the second sedimentary cycle (the hanging wall, most common occurrence)(Fig. 5 A),

ii) in the vicinity of the contact between the hematite lutite and the braunite lutite of the first sedimentary cycle (the footwall, less common than (i))(Fig. 5 B),

iii) in small brecciated areas in the middle of the braunite lutite of the first sedimentary cycle (this is only

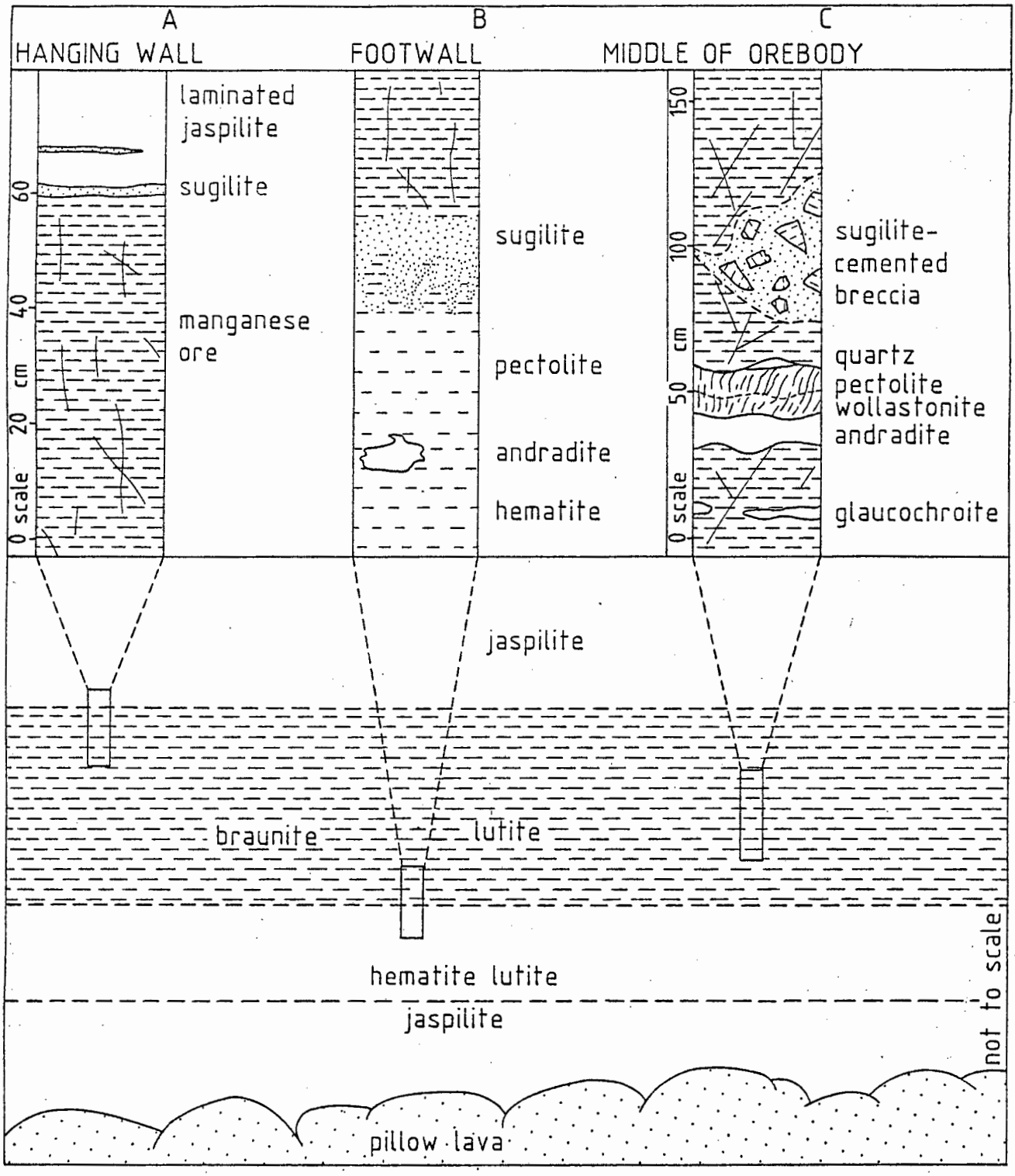

Fig. 5 - Idealised profiles of the sugilite occurrences in the lower manganese ore body of the Voëlwater Jasper Formation above the Ongeluk Andesite Formation at Wessels Mine. All contacts not indicated in bold are gradational. Cross-section not to scale (Dixon, 1985).

occasionally observed, and is more the exception than the rule) (Fig. 5 C), and

iv) in cracks and fissures cutting through the braunite lutite (occasional occurrence).

There have been a number of sugilite discoveries in the mine. The occurrences are up to 100 m apart and their relationship to each other is uncertain. Some of the occurrences, including the largest (± 10 t of sugilite removed), are related to cracks and fissures whilst the smaller occurrences, which are planar in habit and partially conformable with bedding, covering a few square metres, do not appear to be associated with major fracturing of the host rock.

The initial description of sugilite from Wessels Mine (Dunn et al. 1980) was of massive material interlayered with fine-grained acmite and manganese oxides, chiefly braunite. Sugilite also occurs as a component in an assemblage showing mineralogical zoning charcterised by sharp zone boundaries, a small number of mineral species per zone and a very distinct chemical zonation. Development of this assemblage appears to be by the preferential development of sugilite along certain bedding planes. This is then followed by a gradual transgression of the original layering resulting in the formation of the zoned assemblage which in places can approach 40 cm in thickness.

In the zoned assemblages several distinct zones have been identified each of which is between 1 mm and 10 cm thick. There is a very distinct chemical variation from zone to zone, and the number of zones in a particular assemblage appears to be proportional to the total thickness of the assemblage. The thicker assemblages occur only in a few localised areas. The zones are characterised by the sequential predominance of andradite, wollastonite, pectolite, vesuvianite, quartz and sugilite. The interrelationship of the zones is complex. The sugilite zone, which also has the highest alkali content (see Table 3, sample 10), forms the topmost layer. There is a tendency for the andradite, wollastonite, pectolite, vesuvianite and quartz zones to develop as coherent units which can be separate from the sugilite. In Figure 6 most of the zones developed can be seen.

An orange-coloured garnet and olivine bearing calc-silicate layer up to 5 cm thick occurs just below the top of the manganese ore in the lower orebody, usually below the zoned assemblage and sugilite occurrences, and persists laterally for tens of metres. This layer is far more widespread than the sugilite-bearing assemblages, but appears to have formed syngenetically with the former and will be discussed as such. This layer is fine grained and relatively homogenous in appearance. In thin section (Fig. 7) it can be seen to consist of a dark orange-brown groundmass, very fine grained, and containing abundant Fe- and Mn-silicate minerals, such as andradite. The flattened light-coloured blebs contain Ca and

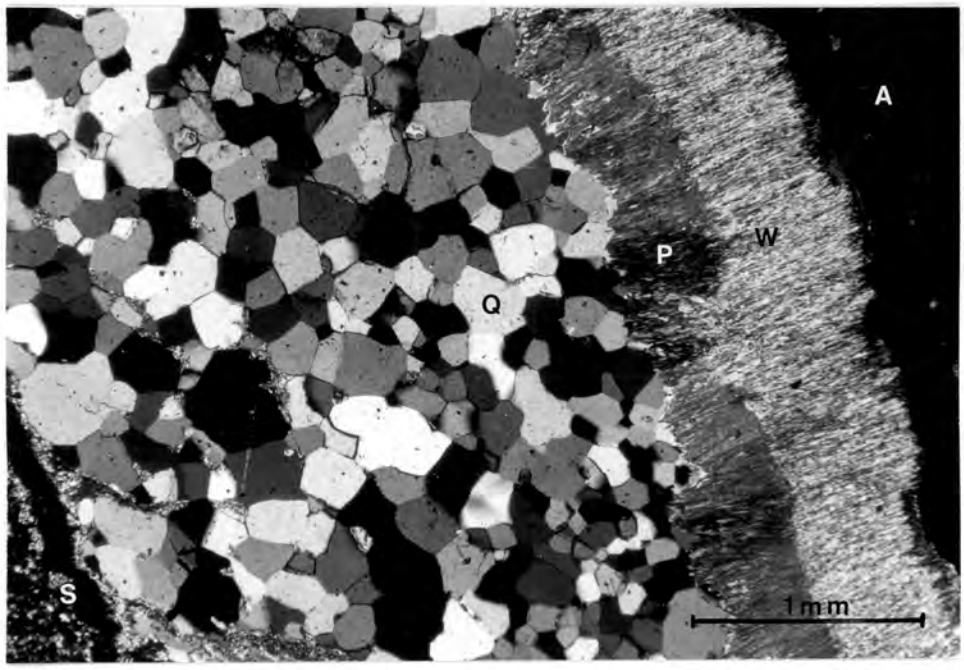

Figure 6. Photomicrograph showing the development of mineralogical layering. From bottom (right) to top (left) the sequence is: A = andradite, W = wollastonite, P = pectolite, Q = quartz and S = sugilite. Plane polarised light, field of view 4mm.

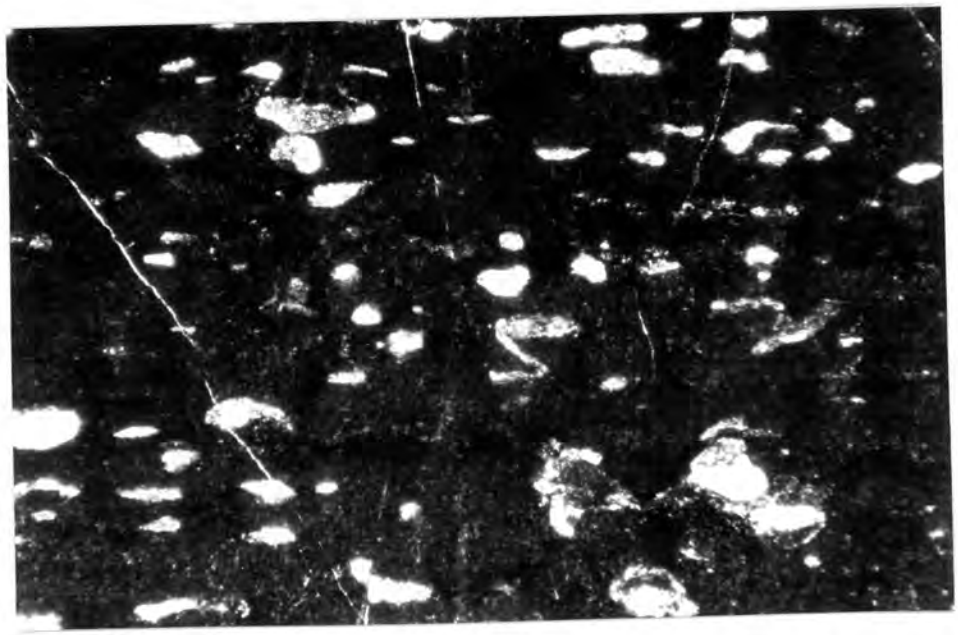

Figure 7. Photomicrograph of the orange calc-silicate layer which consists of CaMg-rich blebs in a groundmass of FeMn-rich minerals. Field of view 4mm, plane polarised light.

Mg silicates such as diopside and pectolite, and are considered to represent recrystallised carbonate pisoliths.

3. MINERALOGY OF THE SUGILITE ASSEMBLAGE

3.1 MILARITE GROUP

A violet mineral of gem quality was discovered at Wessels Mine in 1973 and identified as sogdianite (Bank et al. 1978). This identification was shown to be wrong by Dunn et al. (1980) and the mineral was in fact sugilite, a member of the milarite group, first described from Iwagi Islet, southwest Japan by Murakami et al. (1976). Sugilite has also been described from a manganese mine in Madhya Pradesh, India (Clark et al. 1980).

The milarite group comprises a series of silicate minerals characterised by the six-membered double-ring milarite-type structure (Ito et al. 1952). The structure of milarite is illustrated in Figure 8. Hexagonal $Si_{12}O_{30}$ double rings of silicate tetrahedra are linked by tetrahedrally coordinated T(2) cations and octahedrally coordinated A cations into a three-dimensional tetrahedral framework. Sandwiched between adjacent A octahedra are the B sites, each surrounded by nine oxygens; alternating along the tunnels formed by the stacking of the double hexagonal silicate rings are the C and D sites, each surrounded by twelve and eighteen oxygens, respectively (Černy et al. 1980). Forbes et al. (1972) proposed the following general formula for milarite-type minerals

$$A_2^{[6]}B_2^{[9]}C^{[12]}D^{[18]}T(2)_3^{[4]}T(1)_{12}^{[4]}O_{30}$$

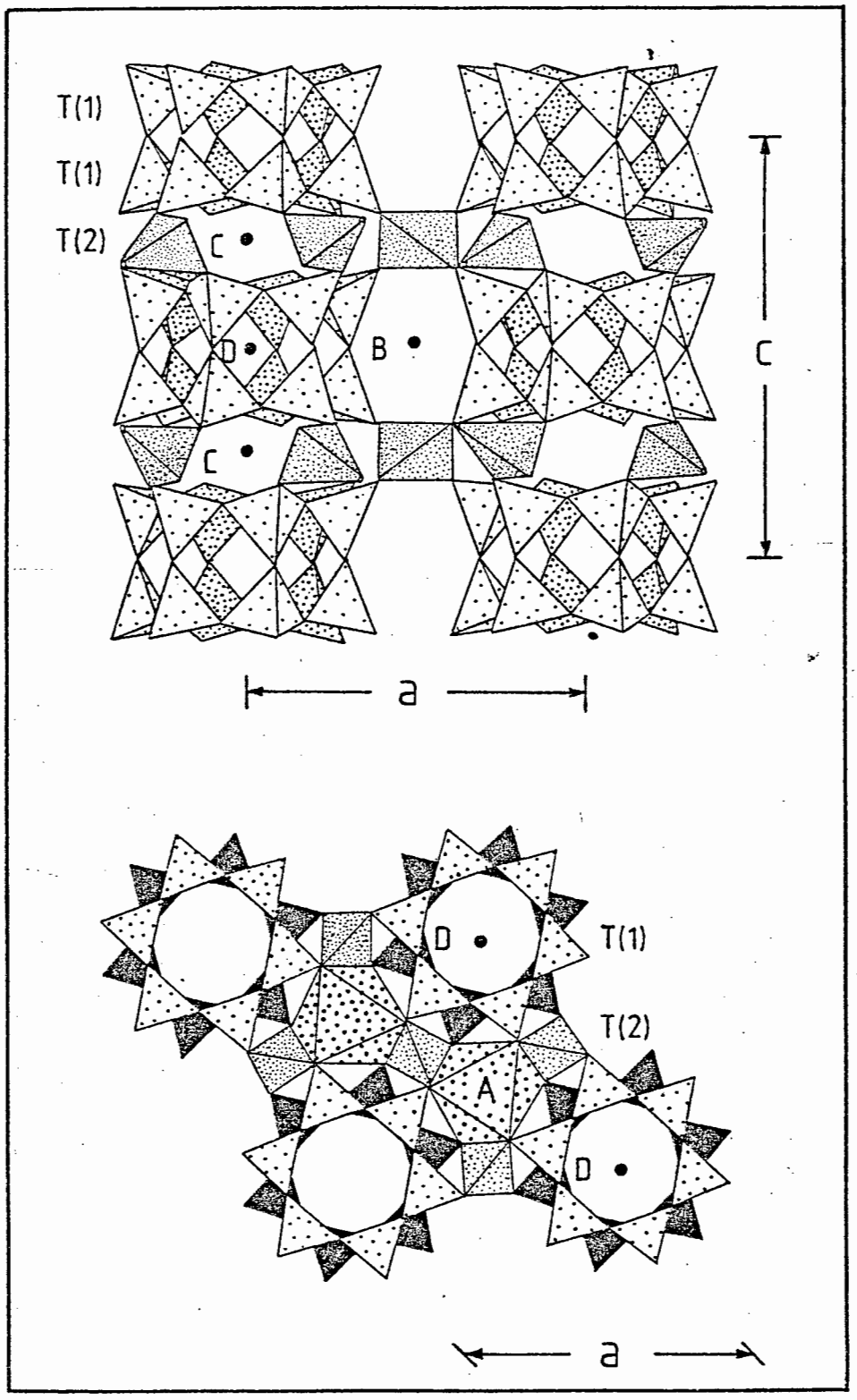

Fig. 8 - Crystal structure of milarite viewed parallel to [101] and [001]. Octahedral A sites located at the level of the T(2) octahedra are omitted in the horizontal projection for clarity (Černy et al. 1980).

where A, B, C, T(1) and T(2) are various sites in the structure, and [ ] indicates the coordination number of the specific site. Sugilite is characterised by the high content of ferric iron in 6-coordination and lithium in the 4-coordinated T(2) site. The 12-coordination site is occupied mainly by K, while the 9-coordination site is occupied by Na and vacant sites. The ideal formula for sugilite can be written as

$$(K,Na)^{12}Na^{9}_{2}(Fe^{3+},Na,Ti)^{6}_{2}(Li,Al,Fe^{3+})^{4}_{3}Si^{4}_{12}O_{30}$$

A number of minerals belong to the milarite group, a modified classification of which is proposed in Table 4. Sugilite most closely resembles sogdianite (Dusmatov et al. 1968), but differs from the latter in lacking Zr and containing a high Fe^{3+} content. Brannockite (White et al. 1973) resembles sugilite in containing Li in a tetrahedral site [T(2)], as does darapiosite (Semenov et al. 1975). These four minerals have similar cell dimensions and other physical properties.

The above four minerals differ from the osumilite subgroup of Abraham et al. (1983), which includes osumilite (Miyashiro 1956), roedderite (Fuchs et al. 1966), merrihueite (Dodd et al. 1965), yagiite (Bunch et al. 1969) and eifelite (Abraham et al. 1983). Mineral X is described later in this chapter. This group has the simplest major-element composition involving only K^{+}, Na^{+}, Mg^{2+}, Fe^{2+}, Fe^{3+} and Al^{3+}, while the remaining members of the milarite group carry essential amounts of some of the elements Li, Be, Ca, Mn, Zn, Zr, and Sn. The

general formula for the osumilite subgroup can be given as

$$W_{1-2}X_2Y_3Z_{12}O_{30}$$

where W = K,Na; X = Mg,Fe^{2+}; Y = Mg,Fe^{2+},Al,Fe^{3+}; Z = Si,Al.

A similar formula can be given for the rest of the milarite group in which the tetrahedral T(2) site is occupied mainly by Be and Al, and the octahedral site by Ca (Černy et al. 1980). In this manner it is possible to separate out three subgroups of the milarite group, the **milarite subgroup** (milarite, armenite), the **osumilite subgroup** (osumilite, roedderite, merrihueite, yagiite, eifelite) and the **sugilite subgroup** (sugilite, sogdianite, brannockite, darapiosite).

A further subgroup of the milarite group of double-chain silicates is the orthorhombic (pseudohexagonal) subgroup (Clark et al. 1980) comprising tuhualite (Hutton 1956), zektzerite (Dunn et al. 1977) and emeleusite (Upton et al. 1978).

3.1.1 SUGILITE

Sugilite has an ideal formula of

$$(K,Na)(Na)_2(Fe^{3+},Na,Ti)_2(Li,Al,Fe^{3+})_3(Si_{12}O_{30})$$

(Murakami et al. 1976). Sugilite was originally described as a light brownish-yellow mineral comprising 3-8 per cent by volume of an aegirine syenite, associated with albite, aegirine, pectolite and an unidentified Ca-K-Ti silicate.

In Table 5 the various optical and physical properties of sugilite from the three known localitites are compared. The distinct difference in colour between the type material and the two other occurrences is due to the presence of trivalent manganese. Absorption curves of sugilite obtained with a Pye-Unicam UV/VIS spectrophotometer, and compared with the absorption spectra of other manganese- and iron-bearing minerals, indicate that the purple colour can be attributed to both manganese (as Mn^{3+}) and iron (as Fe^{3+}) (Shigley et al. 1987). The strength of the spectral features increases in intensity as the colour of the sugilite darkens. An absorption spectrum of sugilite is illustrated in Figure 9. In Table 6 analyses of sugilite from the literature are presented, and in Table 7 X-ray diffraction data for sugilite from Iwagi (Murakami et al. 1976) and Wessels (this study).

In the manganese orebody at Wessels Mine sugilite is found around cracks and spreading laterally along what appear to be compositionally suitable layers. In places the whole rock has been altered, but even then the original bedding layers can be identified. The patches in the ore where the sugilite occurs are usually of a restricted lateral extent, not more than 100 m^2, and limited to a narrow band of usually not more than 1 m

Locality	Iwagi Islet	Madhya Pradesh	Wessels Mine
Habit	Small, vitreous grains.	Massive, small grains. Small prismatic crystals.	Massive, granular Crystals to 15 mm in size.
Colour	Light brownish yellow.	Deep amethystine pink.	Light to dark bluish to reddish purple.
Cleavage	0001, weak		Weak.
Colour in T/Section	Colourless	Pink to drab light brown.	Purple to yellow brown.
Hardness	6–6,5	4,5	5,5–6,5
Relative Density	2,80 calculated 2,74 measured		2,74–2,80 measured.
Optics	Uniaxial (-)	Uniaxial (-) Non-pleochroic	Uniaxial (-) Very weakly pleochroic.
w	1,610	1,595	1,610
e	1,607	1,590	1,606
Cell	Hexagonal	Hexagonal	Hexagonal
a	10,007 ± 2	10,002 ± 7	10,040 ± 5
c	14,000 ±2	13,959 ± 5	14,062 ± 3
Space Gp.	D^2_{6n}-P6/mcc		

Data from Murakami et al. (1976), Dunn et al. (1980), Clark et al. (1980), Shigley et al. (1987) and this study.

TABLE 5. Physical and optical properties of sugilite

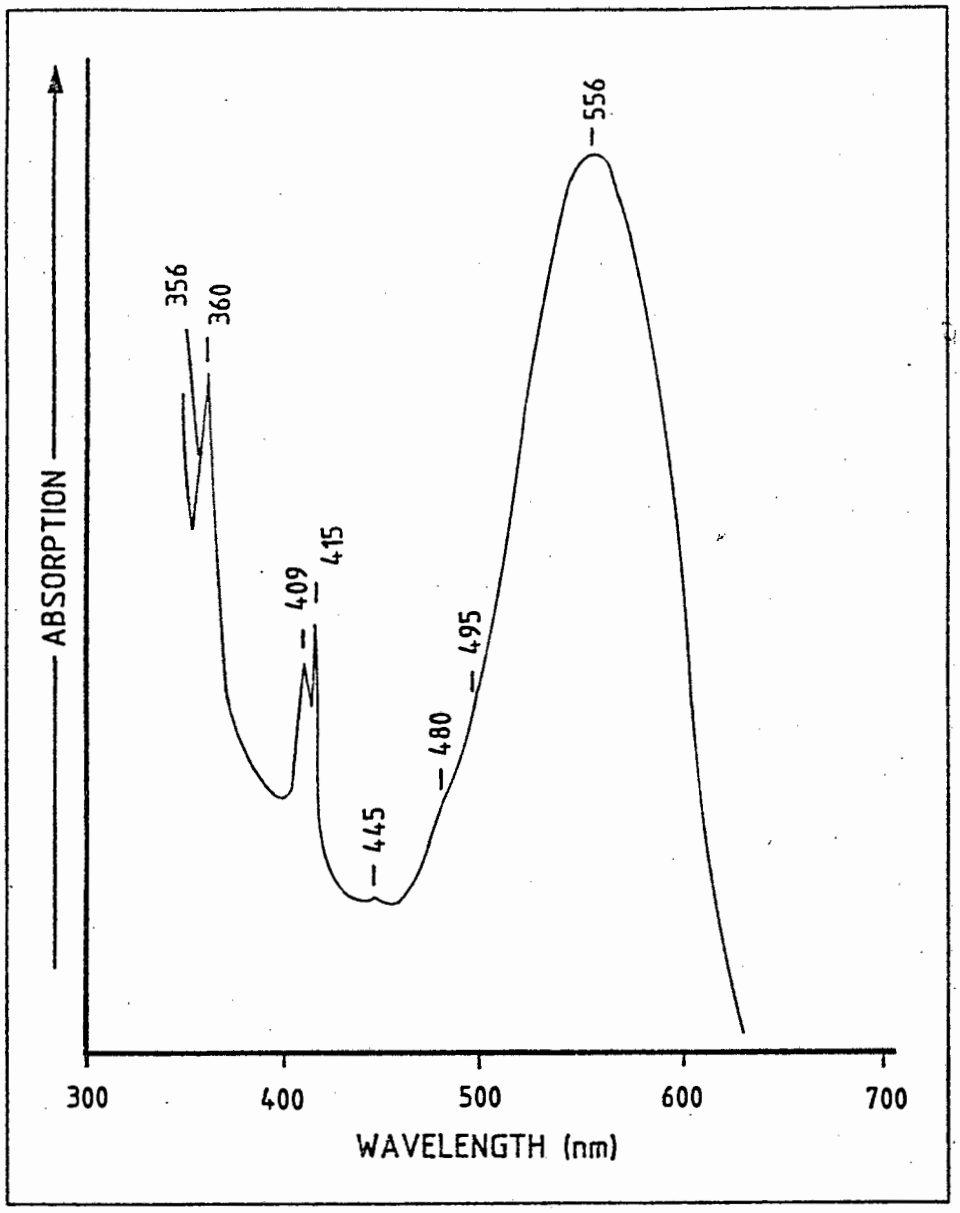

Fig. 9 - The spectrophotometer absorption curve of a polycrystalline sample of purple manganoan sugilite. The curve was obtained with a Pye-Unicam PU8800 UV/VIS spectrophotometer with a 1 nm bandwidth and a 1 nm/sec scanning speed. The path length through the sample was approximately 1,56 mm (Shigley et al. 1987).

	1	2	3	4	5
SiO_2	71,38	70,38	68,22	67,91	69,6
TiO_2	0,51	0,19	nd	0,01	nd
Al_2O_3	2,97	2,98	0,48	0,09	nd
Fe_2O_3	12,96	8,03	13,14	15,16	13,9
FeO	0,19	nd	nd	nr	nr
Mn_2O_3	nd	3,61	2,03	1,02	2,1
MgO	nd	nr	na	0,82	nd
CaO	nd	nr	na	0,25	nd
Na_2O	4,37	5,29	5,47	5,77	6,0
K_2O	3,76	4,53	4,50	3,95	4,7
Li_2O	3,14	2,54	4,10	(5,02)	(3,7)
H_2O	0,93	nr	nr	nr	nd
TOTAL	100,01	97,55	97,94	94,98	96,3
STRUCTURAL FORMULAE CALCULATED TO 30 OXYGENS					
Si	12,15	12,23	11,98	11,71	12,03
Ti^{3+}	0,06	0,03	-	-	-
Al^{2+}	0,60	0,61	0,10	0,02	-
Fe^{3+}	1,63	1,05	1,74	1,97	1,81
Fe	0,03	-	-	-	-
Mn	-	0,48	0,27	0,13	0,28
Mg	-	-	-	0,21	-
Ca	-	-	-	0,05	-
Na	1,44	1,78	1,86	1,93	2,01
K	0,82	1,00	1,01	0,87	1,04
Li	2,15	1,78	2,90	3,48	2,57
H_2O	0,92	-	-	-	-
TOTAL	19,80	18,96	19,86	20,37	19,74

nr = not reported, nd = not detected
( ) = difference to 100%

1. Iwagi Islet, Japan. Murakami et al. (1976).
2. BM 1955, 169. Madhya Pradesh, India. Clark et al. (1980).
3. BM 1979, 180. Wessels Mine. Clark et al. (1980).
4. Wessels Mine. Olivier et al. (1983).
5. NMNH 137289. Wessels Mine. Dunn et al. (1980).

TABLE 6. Sugilite analyses from the literature.

Wessels Mine			Iwagi Islet			
d(obs.)	I_o	d(calc)	d(obs.)	I_o	d(calc.)	hkil
8,647	12	8,676	8,65	7	8,67	$10\bar{1}0$
7,002	21	7,013	6,98	13	7,00	0002
5,441	7	5,454				$10\bar{1}2$
			4,78	7	4,71	$11\bar{2}1$
4,339	100	4,338	4,32	100	4,33	$20\bar{2}0$
4,078	52	4,076	4,06	57	4,07	$11\bar{2}2$
3,688	14	3,689	3,68	13	3,68	$20\bar{2}2$
3,504	30	3,507	3,50	24	3,50	0004
3,279	26	3,279	3,27	7	3,28	$21\bar{3}0$
3,251	29	3,251	3,25	8	3,25	$10\bar{1}4$
3,192	96	3,193	3,19	81	3,19	$21\bar{3}1$
2,974	11	2,971				$21\bar{3}2$
2,8740	80	2,8727	2,876b	51	2,889	$30\bar{3}0$
					2,868	$11\bar{2}4$
2,8287	12	2,8325				$30\bar{3}1$
2,7280	21	2,7271	2,725	13	2,723	$20\bar{2}1$
			2,678	11	2,681	$21\bar{3}3$
2,5155	24	2,5046	2,499	18	2,502	$22\bar{4}0$
2,4072	13	2,4064	2,401	7	2,404	$31\bar{4}0$
2,3394	13	2,3377				0006
2,2824	15	2,2761	2,273	6	2,273	$31\bar{4}2$
2,2550	10	2,2572				$10\bar{1}6$
2,2336	15	2,2311	2,231	8	2,228	$30\bar{3}4$
2,1620	14	2,1691	2,159	13	2,167	$40\bar{4}0$
2,0566	6	2,0580				$20\bar{2}6$
1,9881	17	1,9905	1,983	13	1,988	$32\bar{5}0$
1,8961	12	1,8933	1,890	8	1,891	$41\bar{4}0$
1,8786	16	1,8763	1,874	11	1,874	$41\bar{5}1$
1,8273	18	1,8279	1,827	8	1,829	$32\bar{5}3$
			1,820b	7	1,826	$41\bar{5}2$
					1,815	$30\bar{3}6$
1,7549	12	1,7549	1,757	7	1,750	0008
1,7118	13	1,7098	1,711	8	1,707	$21\bar{3}7$
1,666	13	1,6660	1,666	10	1,668	$33\bar{6}0$
			1,627	6	1,623	$20\bar{2}8$
1,5510	11	1,5488	1,551	7	1,557	$51\bar{6}0$
					1,553	$50\bar{5}4$
1,5104	15	1,5076	1,508	8	1,506	$33\bar{6}4$
1,4843	13	1,4853				$42\bar{5}4$
1,4491	9	1,4460	1,439	7	1,444	$60\bar{6}0$
1,4386	9	1,4384				$60\bar{6}1$
1,4202	7	1,4190	1,420	5	1,425	$43\bar{7}0$
			1,391	10	1,396	$43\bar{7}2$
1,3905	9	1,3893	1,385	5	1,388	$52\bar{7}0$

TABLE 7 Powder diffraction data for sugilite from Iwagi Islet, Japan (Murakami et al. 1976) and from Wessels Mine, (Cu Kα 1,5418 Å), this study.

thick. The original sedimentary bedding features are usually preserved, with sugilite developed as poikiloblastic polygonal grains up to 3 mm across and the residual Ca- and Mg-rich material forming spherical clumps (Figs 10,11). With increased development of the sugilite, small segregations or vugs containing pale-green material are found in these layers. The sugilite lining these vugs often displays euhedral crystal habit - hexagonal and platy, and up to 0,3 mm in maximum dimension. Locally reddish-purple crystals of prismatic habit up to 3 mm long are found in open vuggy sugilite and, in exceptional cases, hexagonal prisms up to 5 mm in size and light purplish pink in colour are found in small pockets associated with pectolite and quartz.

The green material mentioned above consists of hexagonal prismatic crystals, 0,1 mm by 0,01 mm, anhedral manganoan pectolite and rarely quartz. In places where this feature is more common the sedimentary layering is almost destroyed and the assemblage has a swirled and inhomogeneous appearance. The relict clots of material mentioned above are no longer evident (Fig. 12). The polygonal sugilite is Fe-rich and contrasts with that in the most inhomogeneous areas where dark yellowish brown (high Fe, low Mn) and pale-purple (high Mn, high Al) sugilite coexist.

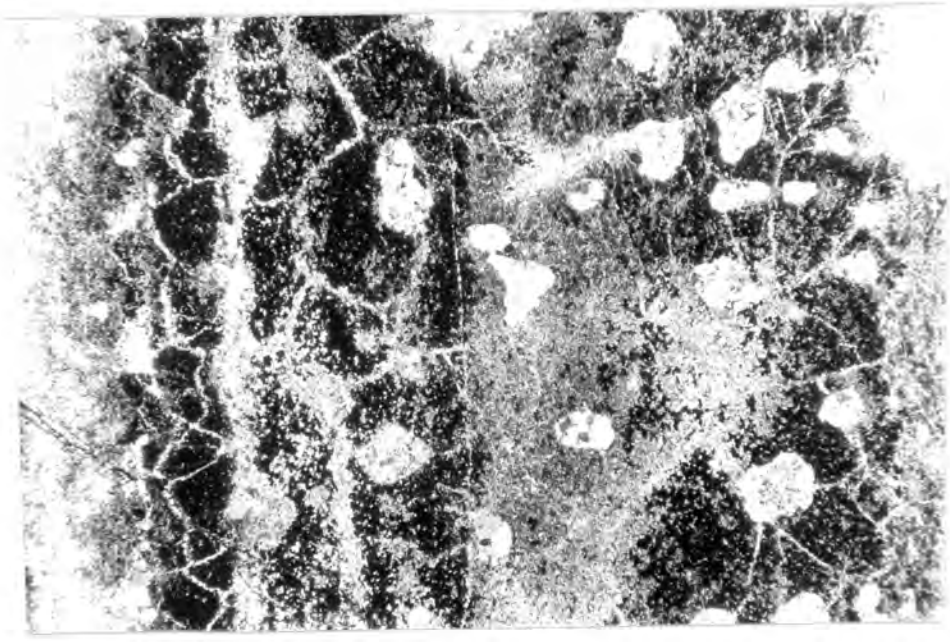

Fig. 10 - Photomicrograph showing the replacement of the original rock by sugilite. Note the polygonal texture of the sugilite and the relict (dark) ooid material. Original bedding is preserved. Width of sample 14 mm. Plane polarised light.

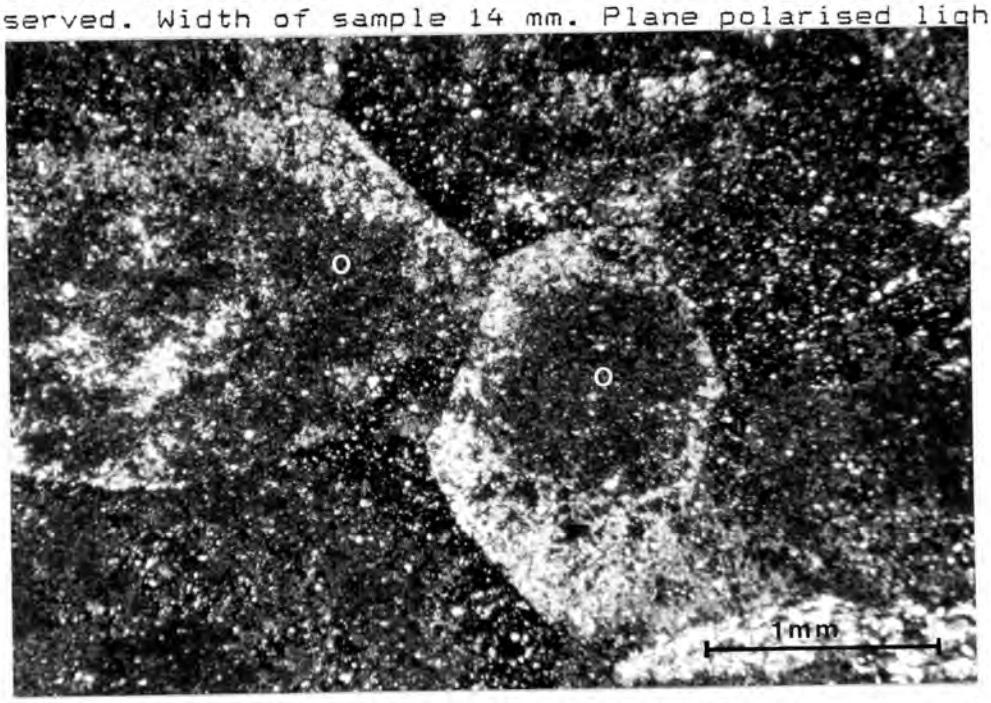

Fig. 11 - Photomicrograph of polygonal sugilite grains showing triple junctions. The sugilite does not take Ca and Mg into its structure and this fine-grained material (O) often shows the original shapes of the ooids in which it was first concentrated. Crossed nicols. Field of view 4 mm.

3.1.2 MINERAL X

In the more inhomogeneous areas of the assemblage other minerals in addition to sugilite are found. These include serandite, a Sr-bearing phosphate, manganoan magnesio--arfvedsonite. Another presumed milarite group mineral, mineral X, occurs as hexagonal euhedral crystals (Fig. 12) up to 0,05 mm long lining sugilite-rich areas which are up to 1 mm across. Crystals are rectangular in outline, with a maximum size of 0,05 mm long by 0,01 mm wide, intimately intergrown with sugilite (Fig. 13). In some places the crystals are matted together and this forms areas that are almost monominerallic, yielding consistent microprobe analyses. These crystals are pale green in colour. The interference colours are first-order yellow and white, with an anomalous blue colour in places. The mineral is uniaxial (-). It is not pleochroic. Due to the very small size, and the fact that it has proved impossible to obtain a pure separate, an accurate RD was not obtained. Similarly, the refractive indices were difficult to establish, and a value of 1,63 $\pm$ 2 was arrived at by comparing the mineral with the sugilite and pectolite, whose indices bracket those of the former. X-ray diffraction by means of a Gandolfi camera and powder diffractometry gives a hexagonal cell with dimensions of a = 10,312 $\pm$ 7 Å and c = 14,383 $\pm$ 22 Å (see Table 8).

Compositionally, microprobe analyses (Table 9) give a calculated formula of:

TABLE 4 THE MINERALS OF THE MILARITE GROUP

		a	b	c	sign	D	colour
MILARITE SUBGROUP							
Milarite	$(K, Na)_2\ (Na, K, H_2O)_2\ Ca_4\ (Be, Al)_6\ Si_{24}\ O_{60}$	hex 10,40		13,80	-	2,57	pale green to colourless
Armenite	$Ba\ Ca_2\ Al_3\ (Si, Al)_{12}\ O_{30} \cdot 2H_2O$	hex 10,69		13,90		2,76	colourless or green
OSUMILITE SUBGROUP							
Osumilite	$(K, Na)\ (Fe^{2+}, Mg)_2\ (Al, Fe^{3+})_3\ (Si, Al)_{12}\ O_{30} \cdot H_2O$	hex 10,17		14,34	+	2,64	light blue to colourless
Osumilite-(Mg)	$(K, Na)\ (Mg, Fe^{2+})_2\ (Al, Fe^{3+})_3\ (Si, Al)_{12}\ O_{30} \cdot H_2O$	hex 10,08		14,35	+		light blue to colourless
Roedderite	$(K, Na)\ Na\ (Mg, Fe^{2+})_2\ Mg_3\ Si_{12}\ O_{30}$	hex 10,14		14,28	+	2,63	colourless
Eifelite	$K\ Na_2\ (Na, Mg)_2\ Mg_3\ Si_{12}\ O_{30}$	hex 10,14		14,22	+	2,67	colourless to very light yellow or green.
Merrihueite	$K\ Na\ Fe_2\ (Mg, Fe)_3\ Si_{12}\ O_{30}$	hex 10,16		14,32		2,87	greenish blue
Yagiite	$(K, Na)\ Na_2\ Mg_4\ (Mg, Al)_6\ Si_{24}\ O_{60}$	hex 10,09		14,29	+	2,70	colourless
Mineral X	$(K, Na)\ (Na, Ca)_2\ (Mg, Na, Mn)_2\ (Mg, Fe, Al)_3\ (Si, Al)_{12}\ O_{30}$	hex 10,31		14,38	-		pale green
SUGILITE SUBGROUP							
Sugilite	$(K, Na)\ Na_2\ (Fe^{3}, Na, Mn^{3+})_2\ (Li, Al, Fe^{3+})_3\ Si_{12}\ O_{30}$	hex 10,007		14,000	-	2,74	yellow brown to purple
Sugilite-(Al)	$K\ Na_2\ (Al, Mn^{3+})_2\ (Li, Al, Fe^{3+})_3\ Si_{12}\ O_{30}$	hex -		-	-		purple
Sogdianite	$K\ (Na, K)\ (Zr, Fe^{3+}, Ti, Fe^{2+})_2\ (Li, Al, Fe^{3+})_3\ Si_{12}\ O_{30}$	hex 10,09		13,98	-	2,90	violet
Brannockite	$(K, Na)\ Sn_2\ Li_3\ Si_{12}\ O_{30}$	hex 10,017		14,245	-	2,98	colourless
Darapiosite	$K\ (Na, K)_2\ Mn\ Zn\ Li\ Zr\ Si_{12}\ O_{30}$	hex 10,32		14,39	-	2,92	colourless to white
ZEKTZERITE SUBGROUP							
Zektzerite	$Na\ Zr\ Li\ Si_6\ O_{15}$	orth 14,306	17,330	10,140	-	2,79	colourless to pink
Tuhualite	$K\ Na\ Fe_2\ Fe_2\ Si_{12}\ O_{30}$	orth 14,31	17,28	10,11	+	2,89	blue
Emeleusite	$Na\ Na_2\ (Na, Fe^{3+})_2\ (Li_2\ Fe^{3+})_3\ Si_{12}\ O_{30}$	orth 10,037	17,550	14,010	-	2,76	colourless

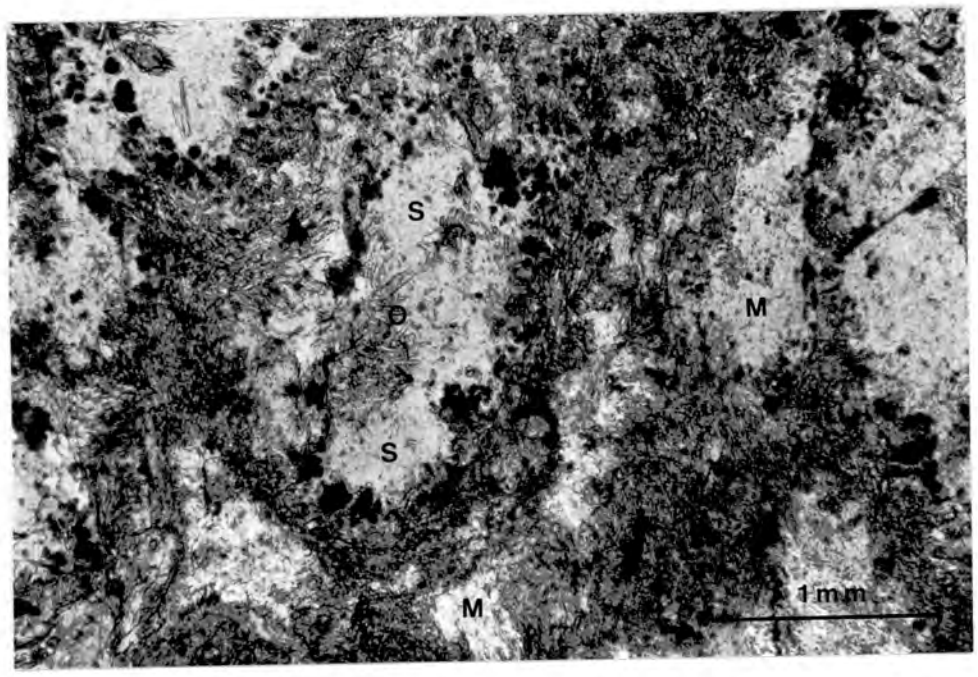

Fig. 12 - Photomicrograph showing the development of the inhomogeneous sugilite assemblage. Light areas consist predominantly of AlMn-rich sugilite and are rimmed with dark grains of Fe-rich sugilite. Amphiboles are also present. S = sugilite, O = mineral X and M = manganoan pectolite. Crossed nicols. Field of view 4 mm.

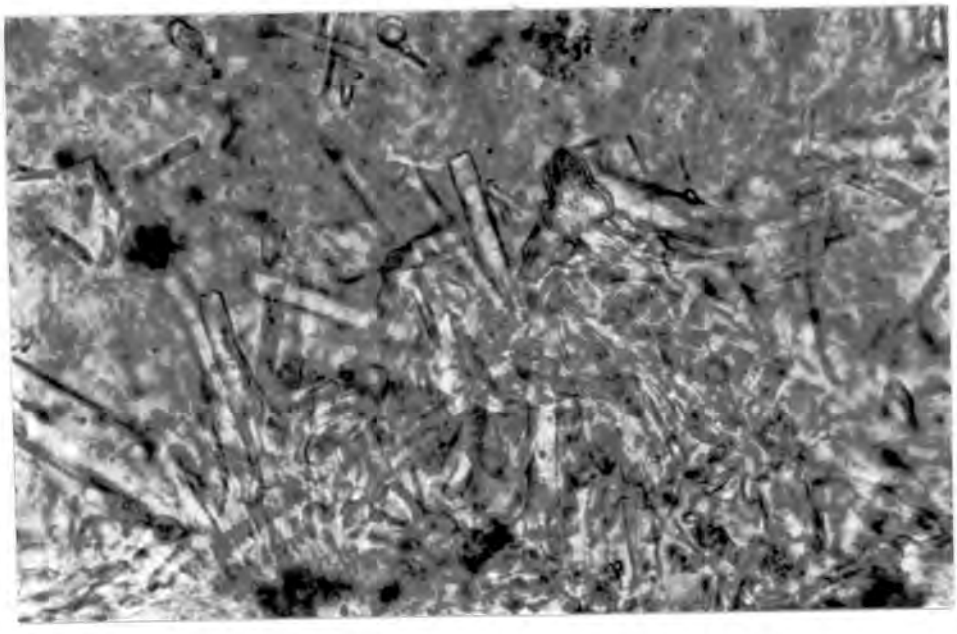

Fig. 13 - Photomicrograph of mineral-X crystals in sugilite. Field of view 0,5 mm. Plane polarised light.

Mineral X			Roedderite			
d(obs.)	Io	d(calc.)	d(obs.)	Io	d(calc.)	hkil
7,225	75	7,192	7,15	64	7,14	0002
5,556	25	5,601	5,540	36	5,538	$10\bar{1}2$
			5,084	22	5,069	$11\bar{2}0$
4,451	17	4,465	4,391	32	4,390	$20\bar{2}0$
4,191	42	4,190				$11\bar{2}2$
			3,747	66	3,740	$20\bar{2}2$
3,613	50	3,596	3,570	100	3,569	0004
3,500	100	3,511				$11\bar{2}3$
3,378	83	3,375				$21\bar{3}0$
			3,35b	13	3,319	$12\bar{3}0$
			3,309	26	3,306	$10\bar{1}4$
3,284	50	3,286				$21\bar{3}1$
			3,239	77	3,233	$12\bar{3}1$
3,058	58	3,055				$21\bar{3}2$
			2,922	67	2,927	$30\bar{3}0$
2,958	100	2,949			2,920	$11\bar{2}4$
			2,772	44	2,769	$20\bar{2}4$
			2,720	14	2,722	$12\bar{3}3$
			2,435	12	2,433	$12\bar{3}4$
2,397	25	2,397	2,375	9	2,379	0006
2,341	83	2,342				$31\bar{3}2$
2,284	50	2,293				$30\bar{3}4$
2,231	42	2,233				$40\bar{4}0$
			2,171	9	2,168	$13\bar{4}3$
2,137	33	2,132	2,094	11	2,098	$40\bar{4}2$
					2,092	$02\bar{2}6$
2,048	50	2,049				$32\bar{5}0$
			1,936	5	1,934	$12\bar{3}6$
1,929	33	1,931				$41\bar{5}1$
			1,902	5	1,899	$14\bar{5}1$
1,893	17	1,897				$40\bar{4}4$
1,875	25	1,877				$31\bar{4}5$
			1,853	8	1,855	$14\bar{5}2$
			1,784	13	1,784	0008
1,753	42	1,755	1,737	10	1,737	$21\bar{3}7$
1,645	25	1,643	1,621	5	1,616	$42\bar{6}2$
			1,570	5	1,567	$24\bar{6}3$
			1,335	5	1,333	$16\bar{7}1$
					1,335	$23\bar{5}8$
1,311	25	1,310				$61\bar{7}3$

The roedderite has a = 10,139±0,01 and c = 14,275±0,01 Å.
Roedderite data from Fuchs et al. (1966).
Mineral-X data, this study, obtained using Cu Kα radiation.

TABLE 8. Powder diffraction data for mineral X and roedderite

	RDW44	RDW41	SMLSUG5	SMLSUG7
SiO_2	66,41	67,75	69,85	65,03
Al_2O_3	1,03	0,23	1,75	0,70
FeO	9,86	7,56	6,45	10,41
MnO	1,39	2,41	5,61	4,11
MgO	8,54	6,71	5,86	8,54
CaO	1,02	1,66	nd	0,55
Na_2O	7,37	7,34	5,35	6,20
K_2O	4,17	3,92	4,75	4,51
TOTAL	99,79	97,58	99,62	100,05
STRUCTURAL FORMULAE ON THE BASIS OF 30 OXYGENS				
Si	11,881	12,269	12,334	11,774
Al^{3+}	0,217	0,049	0,364	0,149
Fe^{2+}	1,475	1,145	0,953	1,576
Mn^{2+}	0,211	0,370	0,839	0,630
Mg	2,277	1,811	1,542	2,304
Ca	0,196	0,322	0,000	0,107
Na	2,557	2,577	1,832	2,177
K	0,952	0,906	1,070	1,042
TOTAL	19,765	19,449	18,934	19,759

Total Fe and Mn assumed to be divalent.

TABLE 9. Mineral X (osumilite subgroup) analyses.

$(K,Na,Sr)(Na,Ca)_{0,7-1,8}(Mg,Na,Mn)_2(Mg,Fe,Al,Ti)_3(Si,Al)_{12}O_{30}$

The analyses given in Table 9 are distinctly different from those of sugilite on the basis of MgO and CaO content, and the diffraction pattern shows quite distinctly that it is not an amphibole, but rather that it is probably a member of the milarite group, specifically the osumilite sub-group. A comparison of the diffraction patterns of roedderite and the unknown green-phase mineral X (Table 8) shows the strong resemblance in the two patterns.

3.1.3 CHEMISTRY

Sugilite has been shown to have its Fe and Mn in a trivalent state, with very little of these two elements in the divalent state (Clark et al. 1980, Shigley et al. 1987). The mineral-X analyses, on the other hand, which are rich in Mg, have Fe and Mn allocated to the divalent state on the basis of the mineral classification as a presumed member of the osumilite subgroup. The members of this subgroup are Mg rich and have most, if not all, Fe in the divalent state. The sugilite is brightly coloured while mineral X is pale green, an additional indication of the oxidation state of Fe and Mn. Other minerals occurring in the assemblages demonstrate the same dichotomous distribution of the di- and trivalent Fe and Mn, such as pectolite and diopside (green, containing Mg and Mn^{2+}) and the garnets and acmite (orange to brown, containing Fe^{3+} and Mn^{3+}).

Analyses of sugilite from Wessels mine from this study are presented in Table 10. In Figure 14 the variation between total Mn, total Fe and Mg for sugilite and mineral X is shown and the two minerals are quite distinct. Two of the analyses (at the Mn apex and with the mineral-X points) are of a purple sugilite whose predominant trivalent cation is Al, so much so that they could be considered to approach an Al end member in composition, and as such will be called sugilite-(Al), with the following ideal formula:

$$KNa_2(Al,Mn^{3+})_2(Li,Al,Fe^{3+})_3(Si_{12}O_{30})$$

It would appear as if the presence of large amounts of Mg causes the amphibole structure to form in most cases, but that when the A site in the amphibole structure is filled by K+, the double-ring structure of the milarite group appears to be stabilised, with the C(12) site being filled.

The presence of Al in sugilite, sometimes in considerable amounts, and the spread along the Fe-Al axis of the diagram in Figure 15 are in direct contrast with the pronounced Fe-Mn substitution trend observed for the amphiboles with their very low Al contents (see Chapter 4.1). This is most probably indicative of the oxidation state of the Fe and Mn in the two mineral species. Fe^{3+} will rather substitute for Al^{3+}, but when a large proportion of the cations are divalent the Fe^{2+}-Mn^{2+} substitution is preferred.

TABLE 10 MICROPROBE ANALYSES OF SUGILITE FROM WESSELS MINE

	1	2	3	4	5	6	7	8	9	10	11	12	13	14	15	16	17	18	19	20	21	22	23	24	25	26
	RDW43	RDW49	V8L10	RDW44	H1019	RDW46	RDW47	S52	H105	H107	H1018	RDW42b	H106	V8L4	RDW42	H23	RDW41	S54	H22	H89	BS4	RDW410	RDW42a	BS3	H83	H85
SiO_2	67,67	68,69	67,71	69,01	69,25	68,12	69,50	69,97	69,28	69,01	71,26	67,84	69,52	69,71	69,21	70,64	68,29	68,58	71,13	70,42	69,36	68,89	69,54	69,46	71,16	73,2
Al_2O_3	0,68	0,69	0,13	1,63	0,19	0,92	1,00	0,88	0,26	0,16	0,16	1,21	0,32	0,88	1,72	0,27	2,13	1,32	0,38	0,76	2,65	4,10	2,20	3,45	8,97	9,1
Fe_2O_3*	14,57	14,51	13,85	13,48	13,23	13,18	12,89	12,88	12,87	12,57	12,44	12,34	12,02	11,20	10,80	10,59	10,50	10,29	9,75	9,64	8,92	8,64	8,63	8,57	1,95	nd
Mn_2O_3*	1,07	0,89	2,78	0,96	2,30	1,50	0,70	2,37	2,52	2,64	2,98	1,54	2,85	3,25	2,58	4,43	2,53	3,08	4,91	4,66	2,90	1,36	3,95	2,25	0,99	1,4
MgO	nd	nd	0,89	nd	nd	0,18	0,12	nd	nd	nd	nd	0,93	nd	nd	nd	nd	nd	nd	nd	nd	0,48	nd	nd	1,27	1,69	nd
CaO	0,15	nd	nd	nd	nd	nd	nd	nd	nd	nd	nd	0,17	nd	nd	nd	nd	nd	nd	nd	nd	0,13	0,15	nd	0,50	nd	nd
SrO	na	na	na	0,74	na	na	na	na	na	na	na	na	na	na	na	na	na	na	na	na	0,88	na	0,56	na	na	na
Na_2O	5,94	5,56	6,27	5,53	5,38	5,17	5,41	6,25	6,28	6,20	3,91	5,74	6,37	5,88	5,77	5,83	5,25	5,62	5,78	6,37	5,78	5,34	5,32	6,14	6,38	6,3
K_2O	4,83	5,09	4,12	5,16	4,36	4,97	5,21	5,03	4,37	4,55	3,77	4,99	4,35	4,44	5,12	4,25	5,03	4,78	4,07	4,54	5,03	4,92	4,93	5,00	4,46	4,8
Li_2O**	5,09	4,57	4,25	3,49	5,29	5,96	5,17	2,62	4,42	4,87	5,48	5,24	4,57	4,64	4,80	4,00	6,27	6,33	3,98	3,59	3,87	6,60	4,87	3,36	4,42	5,0
TOTAL***	94,91	95,43	95,75	96,51	94,71	94,04	94,83	97,38	95,58	95,13	94,52	94,76	95,43	95,36	95,20	96,00	93,73	93,67	96,02	96,41	96,1[illegible]	93,40	95,13	96,64	95,58	94,9
STRUCTUAL FORMULAE BASED ON 30 OXYGENS																										
Si	11,705	11,855	11,821	11,945	11,869	11,685	11,897	12,114	11,932	11,883	12,046	11,672	11,947	11,937	11,857	12,098	11,641	11,700	12,139	12,092	11,908	11,605	11,878	11,868	11,736	11,9
Al^{3+}	0,139	0,140	0,027	0,333	0,038	0,186	0,202	0,180	0,053	0,032	0,032	0,245	0,065	0,178	0,347	0,054	0,428	0,265	0,076	0,154	0,536	0,814	0,443	0,694	1,740	1,7
Fe^{3+}	1,896	1,884	1,819	1,756	1,706	1,701	1,660	1,678	1,668	1,629	1,582	1,598	1,554	1,443	1,392	1,365	1,349	1,321	1,253	1,246	1,152	1,095	1,109	1,102	0,242	-
Mn^{3+}	0,141	0,117	0,369	0,126	0,306	0,195	0,091	0,312	0,330	0,346	0,383	0,202	0,373	0,424	0,336	0,577	0,328	0,400	0,638	0,609	0,379	0,174	0,514	0,293	0,124	0,1
Mg	-	-	0,232	-	-	0,046	0,031	-	-	-	-	0,239	-	-	-	-	-	-	-	-	0,123	-	-	0,323	0,416	-
Ca	0,028	-	-	-	-	-	-	-	-	-	-	0,031	-	-	-	-	-	-	-	-	0,024	0,027	-	0,092	-	-
Sr	-	-	-	0,074	-	-	-	-	-	-	-	-	-	-	-	-	-	-	-	-	0,088	-	0,055	-	-	-
Na	1,992	1,861	2,122	1,856	1,788	1,719	1,795	2,098	2,097	2,076	1,282	1,915	2,122	1,952	1,917	1,936	1,735	1,859	1,914	2,121	1,924	1,744	1,762	2.034	2,040	2,01
K	1,066	1,121	0,918	1,139	0,953	1,088	1,138	1,111	0,960	0,999	0,813	1,095	0,954	0,970	1,119	0,928	1,094	1,040	0,903	0,994	1,102	1,057	1,074	1,080	0,938	1,0
Li	3,541	3,172	2,984	2,430	3,647	4,112	3,559	1,824	3,062	3,372	3,726	3,626	3,159	3,196	3,308	2,755	4,299	4,343	2,728	2,479	2,672	4,472	3,346	2,309	2,932	3,3

nd = not detected
na = not analysed
* Fe and Mn assumed to be trivalent.
** Li_2O given as difference to 100%
*** Total does not include Li_2O

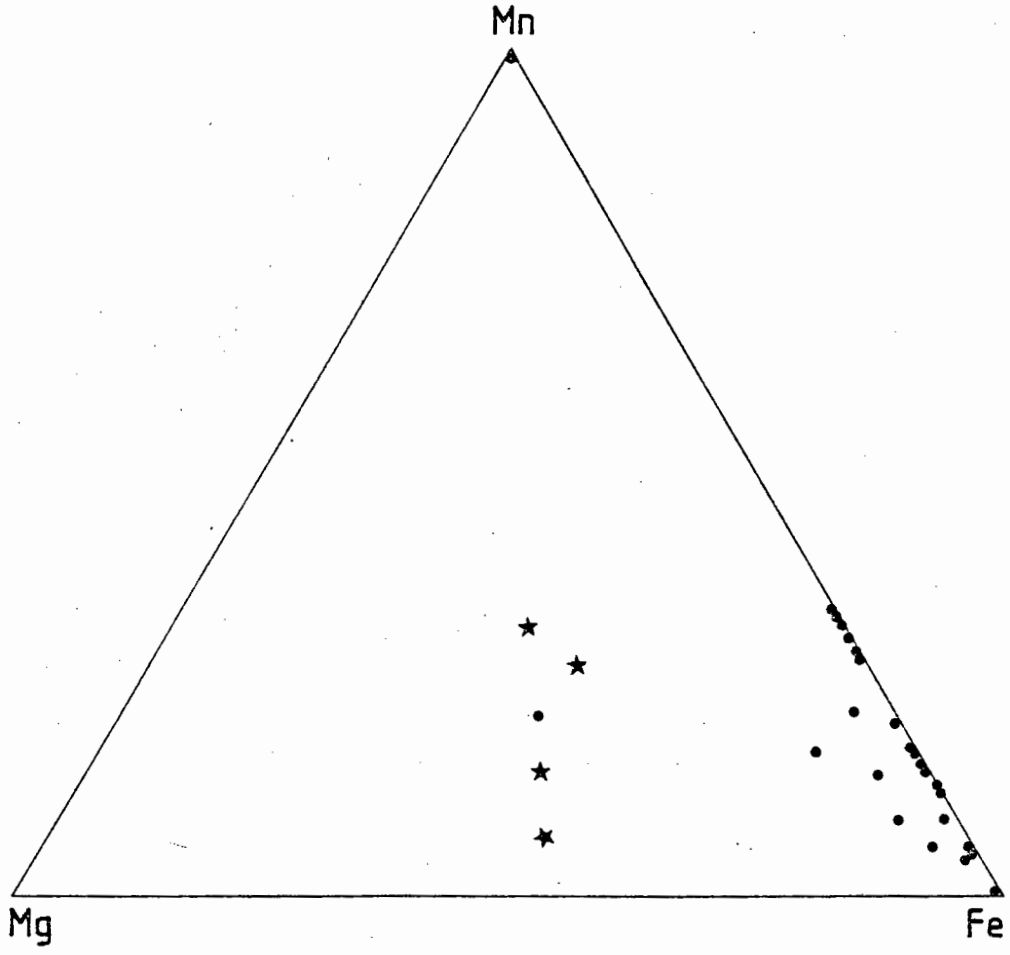

Fig. 14 - Variation between wt. per cent Mn_2O_3, Fe_2O_3 and MgO for sugilite (filled circles), and between MnO, FeO and MgO for mineral X (stars). The two sugilite points, one at the Mn apex and the other with the stars, are of sugilite-(Al).

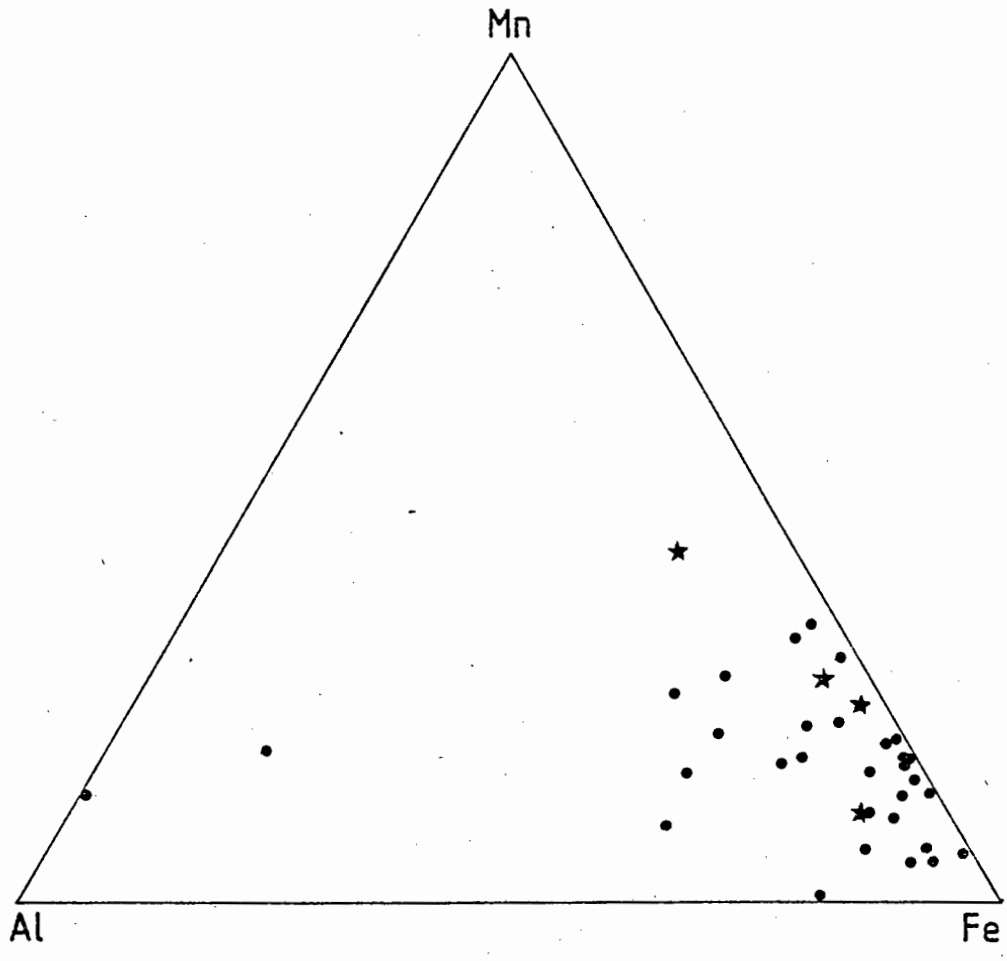

Fig. 15 - Variation between wt. per cent Al_2O_3, Mn_2O_3 and Fe_2O_3 for sugilite (filled circles) and between Al_2O_3, MnO and FeO for mineral X (stars).

3.1.4 FORMATION

Schreyer and Seifert (1967) used a composition similar to that of the sugilite zone, but simplified to the system K_2O-4MgO-$5Al_2O_3$-$20SiO_2$, to hydrothermally synthesise a phase within the osumilite group. The best results were obtained at between 0,5 and 1 kbar pH_2O and at temperatures of 550 to 700 °C. This osumilite phase formed as minute rods, commonly in spherulitic intergrowths typical of devitrification products. This texture is comparable with the textures in the sugilite zone (Figs. 12,13), which contains the other osumilite group phases. The presence of Li, Mn, Na, Ca and Fe may have a stabilising effect on the formation of osumilite-group phases at lower temperatures than the above experimental results.

Abraham et al. (1983) described the minerals eifelite and roedderite from the Bellerberg volcano in the Eifel, West Germany. These are members of the osumilite subgroup but are enriched in sodium and magnesium and deficient in aluminium, and bear a strong compositional and structural resemblance to the green osumilite-type mineral-X phase mentioned above. The roedderite is considered to be a precipitate from highly alkaline, Mg,Si-rich but Al-deficient gases percolating through contact-metamorphosed basement.

Natural occurrences of the sugilite-type minerals are limited to a few localities, but in general all have common features.

The sugilite from the Iwagi Islet syenite was formed as a product of metasomatic alteration of a biotite granite (Murakami et al. 1976). Sogdianite occurs together with darapiosite in pegmatitic veins roughly equivalent to alkalic granite in composition. This highly alkaline environment, similar to that in which hypothermal quartz veins are formed, explains why the minerals are extremely silica rich (Dusmatov et al. 1968). Brannockite, the tin analogue of sugilite, occurs in vugs in late hydrothermal portions of a lithium-tin-enriched pegmatite (White et al. 1973). A common feature from these occurrences is the alkaline, hydrothermal, low pressure environment of formation of the minerals.

Natural occurrences and experimental evidence thus seems to indicate that the phases under discussion in this section formed under alkaline hydrothermal conditions at reasonably low pressures.

4 MINERALS ASSOCIATED WITH THE SUGILITE ASSEMBLAGE

In Chapter 2.4 the layered or zoned nature of the mineral assemblages associated with the sugilite assemblage is described. These chemically and mineralogically distinct zones (see Fig. 6) each consist predominantly of one or two minerals, which are described in this Chapter. These minerals appear to have formed under conditions similar to those discussed in Chapter 3.

4.1 AMPHIBOLE GROUP

Amphiboles occur together with the sugilite developed in association with the zoned assemblages. These amphibole grains are small and display a wide colour range. Two groups can be distinguished on the basis of their colours. One group, dark red through red and pink to blue, is strongly pleochroic and where it occurs, sugilite is scarce. The second group consists of pale-green amphiboles, and where these occur sugilite is a major component of the assemblage. The brightly coloured amphiboles are far less common than the pale-green type.

4.1.1 CHEMISTRY AND CLASSIFICATION

The standard amphibole formula contains 8 tetrahedral sites and the general form is:

$$A_{0-1}\ B_2\ C^{[6]}_5\ T^{[4]}_8\ O_{22}\ (OH,F,Cl)_2$$

where A = Na, K

B = Na, Li, Ca, Mn^{2+}, Mg

C = Mg, Fe^{2+}, Mn, Al, Fe^{3+}, Ti, Ca

T = Si, Al

Amphiboles are divided into four principal groups on the basis of their B-group cation occupancy (Leake 1978):

$(Ca + Na)_B$	$B \leq 1,34$	Iron-magnesium-manganese group, orthorhombic and monoclinic
$(Ca + Na)_B$	$B > 1,34$	Calcic amphibole group
Na_B	$B \leq 0,67$	
$(Ca + Na)_B$	$B > 1,34$	Sodic-calcic amphibole group
Na_B	$0,67 \leq B \leq 1,34$	
Na_B	$B > 1,34$	Alkali amphibole group

The distribution of the various cations as to site occupancy is discussed below. The B group contains M(4) sites and the C group contains M(1), M(2) and M(3) sites.

Sodium: Na occupies the A and B (M4) groups of the unit formula. This site allocation has been confirmed by crystal-structure refinement by various authors (Hawthorne 1981).

Calcium: Ca is always assigned to the B group, M(4) site. According to Hawthorne (1976), however, Ca can substitute into the octahedral sites of sodic amphiboles, M(1,2,3). Robinson et al. (1982) suggest that there can be vacancies in M(1,2,3) sites, tending towards a 'dioctahedral' amphibole component.

Lithium: Li can be an important constituent of alkali amphiboles. It is ordered into the C group, preferentially the M(3) site. High Li contents are generally associated with high F contents (Lyons 1976), although this is not a fixed rule.

Manganese: For Mn^{2+} in alkali amphiboles a preference M(3) > M(1) = M(2) is observed (Hawthorne 1976). When Mn is trivalent, however, ordering at the M(2) site is to be expected by analogy with the behaviour of Al^{3+} and Fe^{3+}. Electronic absorption spectra of some Mn-bearing tremolite show the presence of some Mn^{3+}, so amphiboles can contain Mn^{2+} and/or Mn^{3+} (Hawthorne 1981).

Magnesium: Mg in alkali amphiboles occupies the C group.

Iron: Fe^{2+} is generally assigned to the B and C groups of the amphibole formula. Fe^{3+}, however, will only go into the C site. Hawthorne (1981) stated that there is no crystallographic evidence for tetrahedral Fe^{3+} in any amphibole, while Robinson et al. (1982) are of the opinion that since Fe^{3+} occupies tetrahedral positions in pyroxenes and sheet silicates, it should remain an option for amphiboles.

Aluminium: Al^{3+} is both a C and T-group cation.

Potassium: K in the A site is minor in most amphiboles, but can be important in richterites and arfvedsonites. Maximum site occupancy values (Robinson et al. 1982) are given as 0,141 for riebeckite and 0,347 for arfvedsonite, with the highest values for calcic amphiboles from skarns in Japan, where K in A extends to 0,746.

Robinson (1980) showed that all octahedral R^{3+} substitutions in pyroxenes are compensated by tetrahedral Al or Na in M(2). The same octahedral R^{3+} ions in amphiboles are compensated by the same pyroxene-like mechanisms, the main difference being that in amphiboles the sites are differently named and that Na in M(4) (M(2) of pyroxene) may also be compensated by Na in the A site. In the case of the Wessels Mine amphiboles, K , in addition to Na, appears to be present as compensation for the high R^{3+} values. The analyses of the Wessels amphiboles are presented in Table 11.

On the basis of the cation distribution discussed above, therefore, the following list of crystal-chemical limits will be used for the Wessels Mine amphiboles:

K	-	A site only
Na	-	A and M(4) sites only
Ca	-	M(4) and M(1,2,3) sites
$Mn^{3+,2+}$	-	M(1,2,3) sites
$Fe^{3+,2+}$	-	M(1,2,3) sites
Mg	-	M(1,2,3) sites

Al^{3+} - M(2) or T sites

Si - T site only

The method of calculating the formulae is taken from Leake (1978) and Robinson et al. (1982). Since the water plus halogen content is unknown, the formula is calculated on a water- and halogen-free basis to 23(O) and 2(OH, F, Cl). According to Hawthorne (1983), "the normalisation of amphibole formulae on the basis of fixed cation numbers is usually not valid as it often obscures other substitutions, and the use of the 23(O) calculation when H_2O is not analysed for is recommended."

The cations are allocated in the following manner:

T sites: summed to 8,00 using Si, then Al.

C sites: summed to 5,00 using Al, Fe^{3+}, Fe^{2+}, Mn^{3+}, Mn^{2+}, Mg, Ca then Na.

B sites: Ca, then Na to 2,00. If the sum is substantially less than 2,00 there is an analytical problem (e.g. non-determination of Li) or site vacancies in the C or B sites.

A site: left-over Na, then K to 1,00. Any amount of Na + K between 0 and 1 is possible.

If the formulae are calculated on the basis of Fe^{2+} and Mn^{2+} on 23(O), then the Si values are very high indeed, approaching 9 formula units. If Fe^{3+} is used with Mn^{2+}, the value drops

	H86	H84	H811	H104	H103	H1021	H101	H101B	VBX
SiO_2	54,54	55,19	55,81	55,12	55,16	56,18	56,39	55,44	55,33
Al_2O_3	0,31	0,38	0,00	0,06	0,07	0,00	0,12	0,15	0,07
Fe_2O_3*	5,78	6,23	5,46	4,16	4,73	4,50	3,37	3,47	2,03
Mn_2O_3*	19,92	16,22	13,53	12,01	11,34	10,05	10,40	9,83	8,13
MgO	7,77	8,89	11,18	12,33	12,79	13,62	14,57	14,77	16,93
CaO	0,62	0,07	0,40	0,56	0,84	2,18	1,46	1,66	2,52
Na_2O	7,99	7,57	8,28	8,01	7,89	6,30	7,52	7,08	6,77
K_2O	2,11	2,76	3,28	3,68	3,49	3,33	3,00	3,11	3,69
TOTAL	99,04	97,37	97,94	95,93	96,31	96,14	96,83	95,51	95,47
			STRUCTURAL FORMULAE BASED ON 23 OXYGENS						
Si	7,829	7,982	8,001	8,032	8,001	8,088	8,048	8,023	7,993
Al^{3+}	0,053	0,065	0,000	0,010	0,012	0,000	0,020	0,026	0,012
Fe*	0,625	0,678	0,589	0,456	0,517	0,488	0,362	0,378	0,221
Mn*	2,178	1,786	1,477	1,333	1,253	1,102	1,130	1,083	0,894
Mg	1,662	1,916	2,389	2,678	2,765	2,923	3,099	3,186	3,645
Ca	0,095	0,011	0,061	0,087	0,131	0,333	0,223	0,257	0,390
Na	2,224	2,123	2,301	2,263	2,219	1,759	2,081	1,987	1,896
K	0,386	0,509	0,600	0,684	0,646	0,612	0,546	0,574	0,680

*Total Fe and Mn presented as trivalent cations (see text).

Table 11 Amphibole analyses (Group A)

	SS3A	H1024	SS2	H1026	S1384	SS3B	H1022	RDW45	H1025	H1013
SiO_2	56,95	57,30	57,36	57,44	56,41	57,90	56,60	56,19	57,52	56,24
Al_2O_3	0,37	0,19	0,38	0,00	0,29	0,35	0,00	0,25	0,11	0,00
Fe_2O_3*	7,69	5,87	7,29	6,12	7,19	9,38	5,23	9,49	8,38	6,47
Mn_2O_3*	5,64	6,39	4,94	3,20	6,52	3,68	7,86	1,93	2,64	2,26
MgO	16,26	16,97	16,75	12,75	14,97	15,88	15,92	16,12	17,63	8,76
CaO	1,44	1,45	1,48	10,78	2,92	0,99	1,47	1,58	1,57	2,28
Na_2O	7,13	5,55	6,98	5,25	5,97	6,96	6,26	6,80	5,02	7,29
K_2O	4,17	3,16	4,19	2,28	2,80	4,03	3,55	4,09	3,03	3,57
TOTAL	99,65	96,88	99,37	97,82	97,07	99,17	96,89	96,45	95,90	96,87
STRUCTURAL FORMULAE BASED ON 23 OXYGENS										
Si	7,937	8,080	7,983	8,128	8,013	8,058	8,050	8,044	8,143	7,979
Al^{3+}	0,061	0,032	0,063	0,000	0,049	0,058	0,000	0,042	0,018	0,000
Fe*	0,807	0,623	0,764	0,652	0,769	0,983	0,560	0,023	0,893	0,691
Mn*	0,599	0,686	0,524	0,345	0,705	0,390	0,851	0,210	0,285	0,244
Mg	1,378	3,567	3,475	2,689	3,170	3,294	3,375	3,440	3,720	3,967
Ca	0,215	0,219	0,221	1,634	0,444	0,148	0,224	0,242	0,238	0,347
Na	1,927	1,517	1,884	1,440	1,644	1,878	1,726	1,887	1,378	2,005
K	0,741	0,568	0,744	0,412	0,507	0,715	0,641	0,747	0,547	0,646

Table 11 cont. Amphibole analyses (Group B)

	H87	S133	V8L1	V8L12	V8L2	H1027	B8L11	S13S2	H1017	RDW48
SiO_2	54,19	53,93	57,11	55,49	55,77	57,28	56,06	55,89	56,51	56,45
Al_2O_3	0,58	0,11	0,00	0,07	0,18	0,00	0,00	0,09	0,00	0,30
Fe_2O_3*	13,64	9,85	11,82	11,62	9,01	10,48	9,59	7,21	4,27	3,86
Mn_2O_3*	8,42	10,80	8,27	7,62	9,08	7,52	8,59	4,81	4,32	1,75
MgO	8,17	8,91	11,33	11,23	11,40	12,18	12,68	8,50	19,22	20,18
CaO	6,92	0,55	0,26	0,09	0,12	0,21	0,38	10,95	2,17	3,82
Na_2O	8,26	7,95	5,65	7,50	6,65	5,53	6,49	6,03	4,78	5,42
K_2O	0,66	2,47	2,66	3,40	3,64	3,50	3,37	2,17	3,59	4,36
TOTAL	100,84	94,57	97,10	97,02	95,85	96,70	97,16	95,65	94,86	96,14
				STRUCTURAL FORMULAE BASED ON 23 OXYGENS						
Si	7,673	8,020	8,141	8,017	8,104	8,185	8,034	8,177	8,090	8,015
Al^{3+}	0,097	0,019	0,000	0,012	0,031	0,000	0,000	0,016	0,000	0,050
Fe*	1,454	1,103	1,269	1,264	0,986	1,128	1,035	0,794	0,460	0,413
Mn*	0,908	1,223	0,898	0,838	1,005	0,818	0,937	0,536	0,471	0,189
Mg	1,724	1,975	2,407	2,418	2,469	2,594	2,708	1,854	4,101	4,271
Ca	1,050	0,088	0,040	0,014	0,019	0,032	0,058	1,717	0,333	0,581
Na	2,268	2,292	1,562	2,101	1,873	1,532	1,803	1,711	1,327	1,492
K	0,119	0,469	0,484	0,627	0,675	0,675	0,638	0,616	0,656	0,790

Table 11 cont. Amphibole analyses (Group B)

and if both are trivalent then the Si content is usually at or around 8 formula units (see Table 12 for examples). Only two of the analyses treated this way resulted in very low Si values, and some divalent Fe and Mn had to be allocated to adjust these to 8,00 formula units. Robinson et al. (1982) stated that in some low-Al amphiboles, such as these under discussion, calculation of Si + Al = 8,00 can give a reasonable maximum value for Fe^{3+}, which can be compared to the present situation but including the divalent Mn. A problem occurs, however, with the amphiboles, which occur in a wide range of colours from pink red to blue and pale green. This is due to the variation in the oxidation states of the various elements. These minerals have had all their Fe and Mn allocated to the trivalent state due to the difficulty in knowing the proportions of the elements in the various oxidation states. The evidence presented in relation to colour and oxidation state does not enable one to say how much of each cation is in each oxidation state, but the X-ray data (Table 13) confirms the identity of the mineral as one in which both states may be present. For convenience, calculating both Mn and Fe as wholly trivalent may not be correct but allows comparisons to be made. Ishida (1984), in a study on manganoan magnesio-arfvedsonite from manganese-ore deposits in Japan, showed that Mn was generally contained in amounts smaller than 2,0 per formula unit, except for kozulite, and that it went into the M(1,2,3) sites rather than the M4 site, although as the Mn^{2+} rather than the Mn^{3+} ion.

Sample H103

SiO_2	55,16	55,16	55,16
Al_2O_3	0,07	0,07	0,07
Fe_2O_3	4,73	4,73	-
FeO	-	-	4,26
Mn_2O_3	11,34	-	-
MnO	-	10,19	10,19
MgO	12,79	12,79	12,79
CaO	0,84	0,84	0,84
Na_2O	7,89	7,89	7,89
K_2O	3,49	3,49	3,49
	96,31	95,16	94,69
Si	8,001	8,227	8,323
Al^{3+}	0,012	0,009	0,009
Fe^{3+}	0,517	0,531	-
Fe^{2+}	-	-	0,538
Mn^{3+}	1,253	-	-
Mn^{2+}	-	1,287	1,302
Mg	2,765	2,843	2,876
Ca	0,131	0,134	0,136
Na	2,219	2,282	2,308
K	0,646	0,663	0,671

TABLE 12. An example of the effects of allocating iron and manganese to the di- or trivalent state when calculating the structural formulae of the amphiboles in this study, based on 23 oxygens.

Robinson et al. (1982), on the basis of their formula-calculation criteria, showed that it is very difficult to get acceptable analyses of simple amphiboles such as riebeckite ($Na_2Fe^{3+}_2Fe^{2+}_3Si_8O_{22}(OH)_2$) with fixed site occupancies, especially with regard to Al and Na. Elements not analysed for, such as Li^+, OH^-, F^-, Cl^- and O^{-2}, could have a distinct effect on the calculated structural formulae. This has been partly allowed for in the calculation, but the possible presence of appreciable lithium could be a significant source of error. Hawthorne (1983) states that Li can be an important constituent of alkali amphiboles, where it usually occupies the C sites. The structural formulae have been calculated assuming no Li component, for lack of any concrete evidence to the contrary.

There are conflicting opinions on what site allocations are allowed in amphiboles, especially with regard to Ca and Na (Hawthorne 1981, Robinson et al. 1982.). The site allocations in Table 14 are used because if Ca is disallowed in the C sites, then in some analyses it will be allocated to A sites, which is crystal-chemically not allowed. The Na is allocated to fill the C sites before B sites, but in most cases this results in vacancies in the B sites. Na could be allocated to the B site till it is filled, leaving vacancies in the C site, which might be the case (Robinson et al. 1982), but not enough evidence has been found in this study to prefer the one over

W-20		23-495		23-310		23-603		
d	Io	d	Io	d	Io	d	Io	hkl
9,73	20							
8,89	10	8,93	10	8,93	10	9,02	10	020
8,35	80	8,38	80	8,20	75	8,42	100	110
6,80	25							
6,28	20							
		5,03	12	5,04	4			130
								001
4,87	20	4,88	4	4,86	4	4,87	4	$\bar{1}11$
		4,74	6	4,75	6	4,75	6	200
4,41	20	4,45	30	4,47	18	4,50	20	040
4,30	20							
4,04	20	4,01	6	4,01	4	4,16	6	111
								$\bar{2}01$
		3,65	6	3,85	4	3,87	4	131
3,48	40							
3,36	90	3,38	30	3,39	20	3,40	12	131
3,29	15							
3,24	40	3,24	35	3,26	30	3,27	30	$\bar{2}40$
3,20	50							
3,13	100	3,11	100	3,12	100	3,13	90	310
3,02	40	2,947		2,952		2,962		221
				2,920				$\bar{1}51$
2,862	30	2,908		2,798		2,805		330
2,807	30							
2,796	25							
		2,694		2,703		2,712		151
2,677	30							
2,597	30	2,566		2,576		2,590		061
2,520	15	2,525		2,525		2,526		$\bar{2}02$
		2,360				2,378		400
				2,315		2,325		351
		2,306						$\bar{4}21$
2,274	20	2,267				2,288		$\bar{3}31$

Data for the last three from the JCPDS powder diffraction file

TABLE 13. Powder diffraction data for amphibole sample W20 compared with three magnesio-arfvedsonites (JCPDS1986).

TABLE 14. CATION ALLOCATIONS FOR WESSELS MINE AMPHIBOLES, BASED ON 23 OXYGENS AND THE ALLOCATION OF TRIVALENT CATIONS TO ACHIEVE Si = 8,00.

	A = 0 - 1		B(M4) = 2		C(M1+M2+M3) = 5								T = 8	
	K^{+}	Na^{+}	Na^{+}	Ca^{2+}	Na^{+}	Ca^{2+}	Mg^{2+}	Mn^{2+}	Mn^{3+}	Fe^{2+}	Fe^{3+}	Al^{3+}	Al^{3+}	Si^{4+}
H86	0,392		1,874		0,380	0,097	1,685	1,103	1,103		0,633		0,053	7,936
H84	0,509		1,561		0,562	0,011	1,916		1,786		0,678	0,047	0,018	7,892
H811	0,600		1,817		0,484	0,061	2,389		1,477		0,589			8,001
H104	0,684		1,827		0,436	0,087	2,678		1,333		0,456	0,010		8,032
H103	0,646		1,897		0,322	0,131	2,765		1,253		0,517	0,012		8,001
H1021	0,612		1,605		0,154	0,333	2,923		1,102		0,488			8,088
H101	0,546		1,915		0,166	0,223	3,099		1,130		0,362	0,020		8,084
H101B	0,574		1,917		0,070	0,257	3,186		1,083		0,378	0,026		8,023
V8X	0,680	0,051	1,845	0,155		0,235	3,545		0,894		0,221	0,005	0,007	7,993
H87	0,124	0,822	1,544	0,456		0,639	1,798	0,947		1,030	0,485	0,101		8,003
S13-3	0,469		1,700		0,592	0,088	1,975		1,283		1,103	0,019		8,020
V8L1	0,484		1,176		0,386	0,040	2,407		0,879		1,259			8,141
V8L12	0,627		1,647		0,454	0,014	2,418		0,838		1,264	0,012		8,017
V8L2	0,675		1,383		0,490	0,019	2,469		1,005		0,986	0,031		8,104
H1027	0,638		1,104		0,428	0,032	2,594		0,818		1,128			8,185
V8L11	0,616		1,541		0,262	0,058	2,708		0,937		1,035			8,034
S13S2	0,405		1,628		0,083	1,717	1,854		0,536		0,794	0,016		8,177
SS3A	0,741		1,927			0,215	3,378		0,599		0,807		0,061	7,937
H1024	0,568		1,517	0,127		0,092	3,567		0,636		0,623	0,082		8,080
SS2	0,744		1,884	0,030		0,191	3,475		0,524		0,764	0,046	0,017	7,983
H1026	0,412		1,440	0,320		1,314	2,689		0,345		0,652			8,128
S13S4	0,507		1,644	0,137		0,307	3,170		0,705		0,769	0,049		8,013
SS3B	0,715		1,751		0,127	0,148	3,294		0,390		0,983	0,058		8,058
H1022	0,644		1,726	0,010		0,214	3,375		0,851		0,560			8,050
RDW45	0,747		1,844		0,043	0,242	3,440		0,210		1,023	0,042		8,044
H1025	0,547		1,378	0,154		0,084	3,720		0,285		0,893	0,018		8,143
H1013	0,646	0,254	1,751	0,249		0,098	3,967		0,244		0,691			7,979
H1017	0,656		1,327	0,333			4,101		0,471		0,460			8,090
RDW48	0,770		1,492	0,504		0,077	4,271		0,189		0,413	0,050		8,015

the other, so the disparity will be shown for comparative purposes only. Whatever the case, the amphiboles are placed in the alkali amphibole group, as magnesio-arfvedsonites, where magnesio-arfvedsonite is defined with respect to the standard formula as follows (Leake 1978):

$$Na_B > 1,34$$
$$(Na + K)_A > 0,50$$
$$Fe^{2+}/(Fe^{2+},Mg) < 0,50$$
$$Fe^{3+}/(Fe^{3+},Al^{[4]}) > 0,50$$

In Figure 16 it can be seen that two populations of amphibole compositions are present, in which one has a distinct Mg–Mn trend (group A) and the other a more complex Mg–(Fe, Mn) trend (group B). This second group has both low-Ca and high-Ca members. In Figure 17 the two groups are again separated, with group A Mn rich and group B more Fe rich. This distinction between Fe and Mn is mirrored in the garnets and melilites discussed below.

The group-A amphiboles are classified according to the IMA recommendations as:

Potassium-manganese-magnesio-arfvedsonite

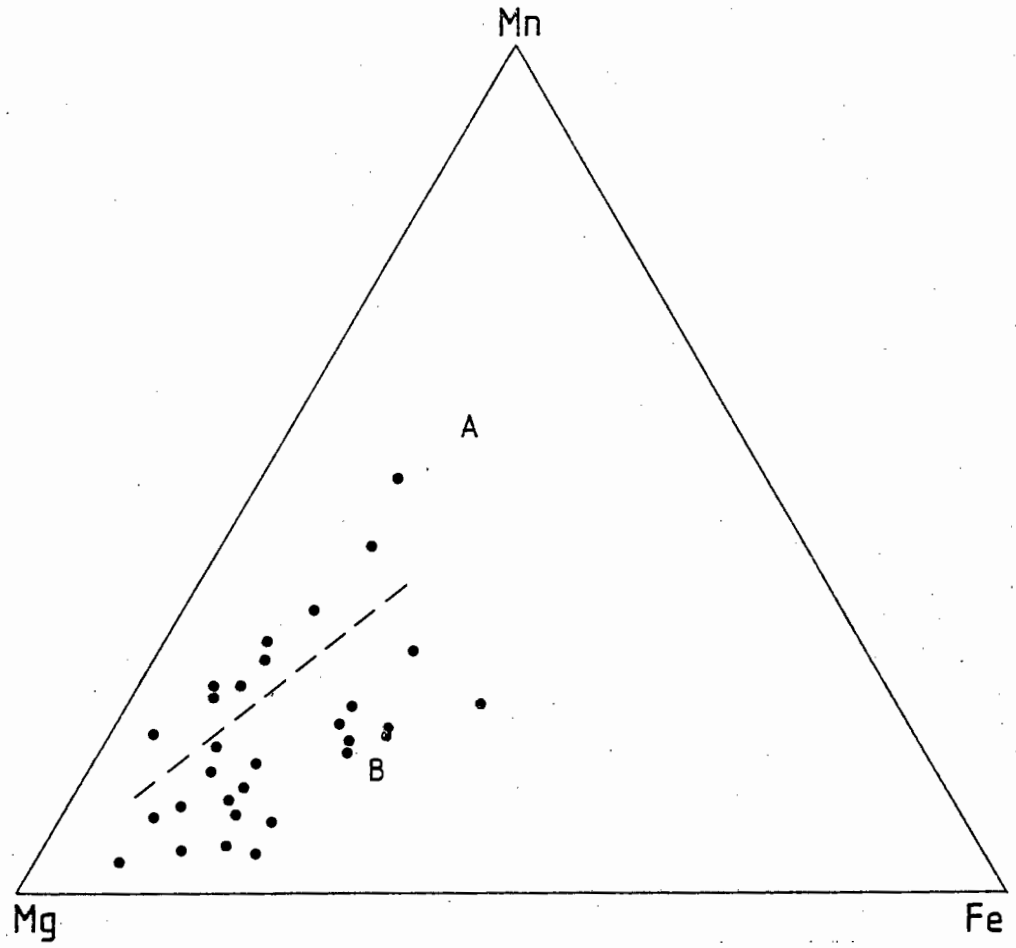

Fig. 16 - Variation in cation proportions between Mg, Mn and Fe in the amphiboles showing the possible separation of group A from group B.

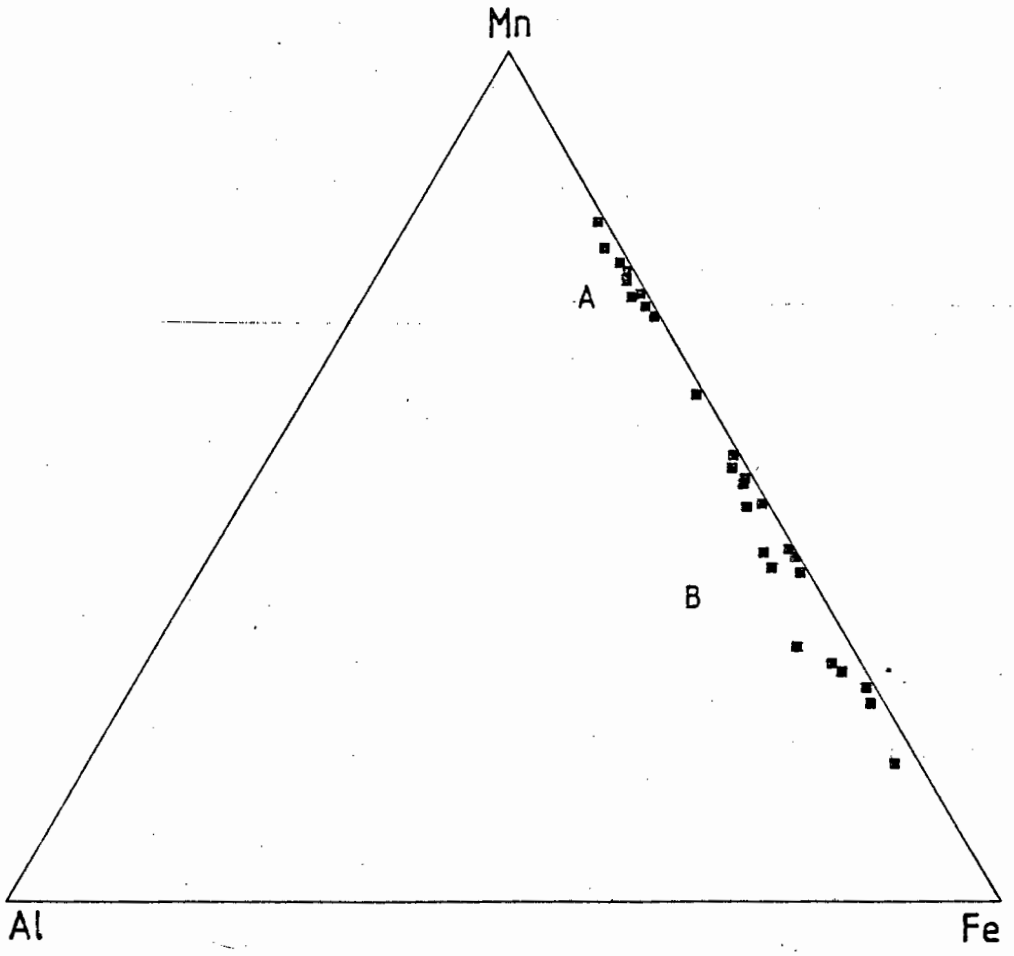

Fig. 17 - Variation diagram for the amphiboles showing wt. per cent proportions of Al_2O_3, total iron as Fe_2O_3 and total manganese as Mn_2O_3. Group A amphiboles are separated from the group B amphiboles.

The group-B amphiboles classify into two further groupings, based on the amount of calcium present:

Manganoan potassium-magnesio-arfvedsonite

and

Calcian potassian manganoan magnesio-arfvedsonite.

4.2 GARNET

The garnet, generally from 0,01 to 1 mm (diameter of grains) in size, is commonly xenoblastic, less commonly subidioblastic. Megascopically the colour of the garnet-rich parts of the rock ranges from pinkish orange to deep reddish orange. Under the microscope the colour varies from pale yellow through brown to bright orange red. The garnet typically occurs in several distinct parageneses, including the following.

i) Garnet occurs together with clinochlore in the lowermost layer in the zoned assemblages (Dixon 1985). The dark red-brown to light pink-brown andradite, massive and fine grained, is in direct contact with manganese--oxide minerals, chiefly braunite II and hausmannite. The contact between the Mn-oxides and the andradite layer is sharp although quite uneven. The andradite layer varies

in thickness from a few millimetres to around twenty centimetres, although the extreme thickness is rare. This andradite also contains acicular hematite crystals in the cores of the larger grains (Figs 18,19).

ii) Discrete grains and aggregates in sugilite- and amphibole-rich areas. These grains are often subidioblastic and are commonly brownish to pinkish brown in colour.

iii) Yellowish grains in wollastonite- and diopside-rich areas in the layered assemblage.

iv) Deep-orange to orange-red veinlets cutting the rock, zoned from darker in the centre of the veinlet to lighter coloured on the rim.

v) In vuggy areas small (up to 1 mm) tetragonal orange red crystals of henritermiérite (Fig. 20) and brownish orange crystals of andradite are found associated with braunite II and hematite.

The brown garnets mentioned in paragraphs (i) and (ii) are often associated with chlorite, and are quite distinct from the garnets described in paragraphs (iii) and (iv).

Fig. 18 - An andradite grain (light grey) showing included hematite (white) in the core and surrounded by clinochlore (dark grey) and diopside (medium grey). Sample RDW2, SEM, 500X.

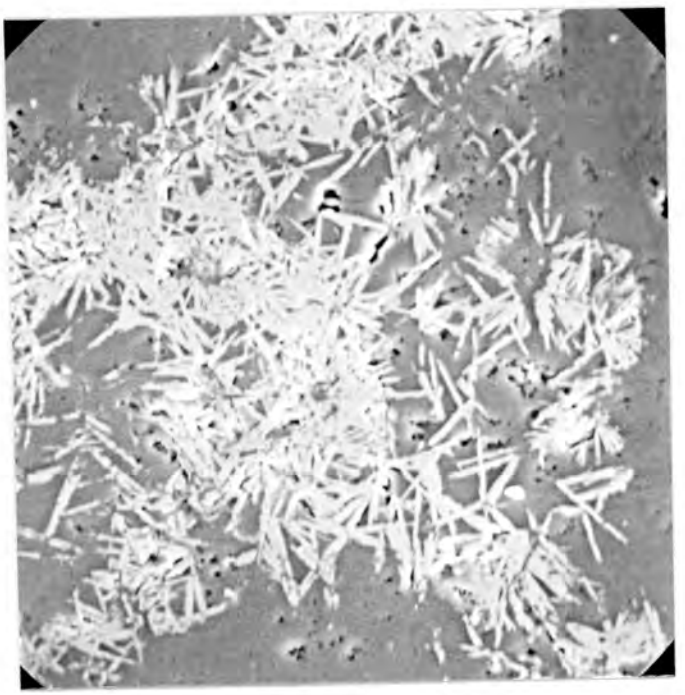

Fig. 19 - Magnified view of the hematite crystals in andradite. Sample RDW2, SEM, 800X.

Fig. 20 - Photomicrograph of henritermiérite crystals in a vug. The large crystal is 0,5 mm long. SEM.

Representative microprobe analyses are given in Tables 15, 16 and 17. Each of the analyses represents the composition at a particular point on a grain, and not of the grain as a whole. The garnets described in this chapter were analysed for all the elements which were detected by means of a wavelength scan by the CAMECA microprobe and shown to be present in a detectable amount. These elements are Si, Al, Fe, Mn, Mg and Ca. Examination of bulk samples by means of XRF analysis reveals only trace amounts (at the ppm level) of other elements. Representative garnets of each group were analysed for H_2O by means of a LECO Rapid Moisture Analyser.

The analytical results show a low summation in many cases, and the analyses can be separated into two main groups on the basis of their chemistry and crystal structure. The first group consists of high analytical total, presumably anhydrous andradite-rich garnet; while the second group consists of low-summing, manganese-rich garnet. The first group correlates with the parageneses described in (i) and (ii) and will be called group F (Table 17). The garnets of parageneses (iii) and (iv) are group H (Tables 15 and 16).

Group F showed no appreciable water content in the samples analysed, although samples analysed by microprobe give totals that vary and may indicate a possible water content of up to 2,5 per cent in some cases.

TABLE 15. MICROPROBE ANALYSES OF HYDROGARNETS FROM WESSELS MINE.

	GROUP HNA			GROUP HNB1		GROUP HNB2			GROUP HNC					
	S4V5	S4V4	H46	GA10A	GA10B	GA9	GA11	GA14	S4V3	S4V2	S4V1B	S4V1A	S4V9	S4V11
SiO_2	33.11	33.43	36.54	33.54	32.21	28.00	27.22	28.15	27.15	28.89	30.71	30.79	30.50	28.62
Al_2O_3	14.42	14.05	13.08	3.40	3.65	4.48	5.69	5.63	10.92	6.02	6.29	5.85	2.72	1.78
Fe_2O_3	0.00	0.00	0.66	1.75	2.13	0.79	1.32	2.23	0.41	10.29	12.44	12.33	17.16	23.78
Mn_2O_3	2.60	3.76	5.75	16.28	17.37	25.17	22.86	20.85	16.47	12.07	10.68	10.24	8.08	3.49
MgO	4.41	5.25	5.53	0.05	0.04	0.16	0.10	0.05	0.47	0.31	0.31	0.28	0.83	1.12
CaO	36.94	36.59	33.45	36.98	36.46	36.46	37.20	37.56	37.43	35.58	35.67	35.90	36.42	36.52
H_2O^*	8.52	6.92	4.99	8.00	8.14	4.94	5.61	5.53	7.15	6.84	3.90	4.61	4.29	4.69

STRUCTURAL FORMULAE ON THE BASIS OF 12 OXYGENS

Si	2.347	2.414	2.669	2.515	2.425	2.250	2.166	2.232	2.068	2.233	2.449	2.434	2.457	2.326
Al^{3+}	1.208	1.200	1.129	0.301	0.325	0.426	0.535	0.528	0.983	0.550	0.593	0.547	0.259	0.171
Fe^{3+}	0.000	0.000	0.036	0.099	0.121	0.048	0.079	0.133	0.024	0.599	0.747	0.734	1.041	1.455
Mn^{3+}	0.140	0.207	0.320	0.930	0.996	1.540	1.385	1.259	0.955	0.711	0.649	0.616	0.496	0.216
Mg	0.466	0.565	0.602	0.006	0.004	0.019	0.012	0.006	0.053	0.036	0.037	0.033	0.100	0.136
Ca	2.805	2.831	2.618	2.971	2.941	3.139	3.171	3.190	3.054	2.947	3.047	3.040	3.143	3.180
OH/4	1.007	0.833	0.608	1.000	1.022	0.622	0.744	0.731	0.908	0.882	0.519	0.608	0.576	0.636

*Difference to 100% assumed to be H_2O.

TABLE 16. MICROPROBE ANALYSES OF GROUP HM HYDROGARNETS FROM WESSELS MINE.

	H41A	H41B	H41B2	H4B	H413	S4V8	V530L1	V530L2A	V530L2B	V519	V5110	V5111	H49
SiO_2	30.28	29.86	29.89	29.88	29.69	29.70	29.54	29.92	30.60	30.35	30.29	30.28	31.43
Al_2O_3	0.30	0.34	0.38	0.12	0.02	1.11	0.51	0.85	0.82	0.08	0.17	0.09	0.37
Fe_2O_3	1.79	1.82	1.78	1.58	0.57	0.07	0.97	1.67	1.74	0.08	0.24	0.11	10.57
Mn_2O_3	34.56	35.40	35.50	35.94	36.53	33.42	34.95	33.28	33.29	36.55	36.81	37.18	24.89
MgO	0.93	0.22	0.24	0.14	0.52	1.39	1.75	2.18	2.07	0.32	0.31	0.20	0.15
CaO	27.53	27.32	27.87	28.12	27.62	28.94	26.92	26.33	26.61	28.89	28.71	28.43	29.82
H_2O^*	4.61	5.04	4.39	4.22	5.15	5.37	5.36	5.77	4.87	3.73	3.47	3.71	2.77

STRUCTURAL FORMULAE BASED ON 12 OXYGENS

Si	2.441	2.402	2.427	2.436	2.388	2.367	2.358	2.363	2.440	2.485	2.490	2.482	2.596
Al^{3+}	0.029	0.032	0.032	0.012	0.002	0.105	0.048	0.105	0.048	0.079	0.077	0.008	0.036
Fe^{3+}	0.109	0.110	0.109	0.097	0.028	0.004	0.058	0.099	0.104	0.005	0.015	0.007	0.657
Mn^{3+}	2.122	2.168	2.196	2.231	2.238	2.028	2.125	2.002	2.022	2.279	2.304	2.320	1.566
Mg	0.112	0.026	0.029	0.017	0.062	0.165	0.208	0.257	0.246	0.039	0.038	0.024	0.018
Ca	2.378	2.354	2.425	2.456	2.380	2.471	2.303	2.228	2.274	2.535	2.529	2.496	2.639
OH/4	0.620	0.676	0.595	0.574	0.691	0.714	0.714	0.760	0.648	0.509	0.476	0.507	0.382

*Difference to 100% assumed to be H_2O

TABLE 17. MICROPROBE ANALYSES OF ANDRADITE FROM WESSELS MINE.

	V53W1A	V512B	V517B	V514A	V513	V518A	V516	V514B	V517A	V53GT2	V53GT1	V53W1B
SiO_2	35.95	35.46	35.45	35.31	34.90	34.94	34.96	34.64	34.95	34.75	35.08	35.04
Al_2O_3	0.32	0.32	0.50	0.15	0.16	0.35	0.59	0.16	0.55	0.23	0.89	0.31
Fe_2O_3	24.53	25.79	27.16	26.20	26.23	23.40	24.01	26.05	27.41	25.11	24.52	24.19
Mn_2O_3	5.99	5.11	3.36	4.61	4.64	6.80	6.12	4.73	3.15	5.43	4.98	6.12
MgO	0.28	0.06	0.11	0.17	0.08	0.28	0.12	0.14	0.11	0.30	1.02	0.26
CaO	33.81	33.97	33.96	34.26	34.29	34.58	34.80	34.27	34.64	34.01	33.14	33.66
H_2O*	0.00	0.00	0.00	0.00	0.00	0.00	0.00	0.00	0.00	0.17	0.37	0.56

STRUCTURAL FORMULAE BASED ON 12 OXYGENS

Si	3.003	2.978	2.978	2.970	2.952	2.950	2.944	2.942	2.939	2.939	2.936	2.935
Al^{3+}	0.032	0.032	0.050	0.015	0.016	0.035	0.059	0.016	0.055	0.023	0.088	0.031
Fe^{3+}	1.543	1.630	1.718	1.659	1.671	1.487	1.522	1.666	1.736	1.599	1.545	1.526
Mn^{3+}	0.381	0.327	0.215	0.295	0.299	0.437	0.392	0.306	0.202	0.350	0.317	0.390
Mg	0.035	0.008	0.014	0.021	0.010	0.035	0.015	0.018	0.014	0.038	0.127	0.032
Ca	3.026	3.056	3.057	3.087	3.108	3.128	3.139	3.118	3.121	3.081	2.972	3.021
OH/4	0.000	0.000	0.000	0.000	0.000	0.000	0.000	0.000	0.000	0.024	0.052	0.078

* Difference to 100% assumed to be H_2O (see text).

TABLE 17(cont.). MICROPROBE ANALYSES OF ANDRADITE FROM WESSELS MINE.

	V515	V5116	GA13	H4-2B	V512A	V518B	V511	GA2	H43	H42A	V53GT5	H47	V53GT5
SiO_2	34.66	35.06	35.87	34.86	34.64	34.46	34.23	34.29	34.52	34.44	34.26	34.43	34.72
Al_2O_3	0.46	1.38	2.34	1.54	0.38	0.38	0.04	1.06	0.92	1.47	0.63	0.90	1.23
Fe_2O_3	25.34	24.84	21.84	24.05	24.74	23.79	27.26	28.42	23.16	24.56	22.11	24.98	23.54
Mn_2O_3	4.55	3.29	3.57	4.66	5.32	6.56	3.42	1.18	5.89	4.45	7.87	4.78	4.31
MgO	0.16	0.30	1.37	0.17	0.05	0.26	0.16	0.12	0.15	0.26	0.15	0.06	3.18
CaO	34.57	34.46	33.40	34.10	34.23	34.15	34.29	34.03	34.06	33.72	33.92	33.37	31.57
H_2O^*	0.26	0.67	1.61	0.62	0.64	0.40	0.60	0.80	1.30	1.10	1.06	1.48	1.45

STRUCTURAL FORMULAE BASED ON 12 OXYGENS

Si	2.927	2.922	2.912	2.910	2.910	2.907	2.889	2.878	2.865	2.861	2.861	2.852	2.844
Al^{3+}	0.046	0.136	0.225	0.152	0.038	0.038	0.004	0.105	0.090	0.144	0.062	0.088	0.119
Fe^{3+}	1.611	1.559	1.335	1.511	1.565	1.511	1.732	1.791	1.447	1.536	1.390	1.558	1.452
Mn^{3+}	0.293	0.209	0.221	0.296	0.340	0.421	0.220	0.075	0.372	0.281	0.501	0.301	0.269
Mg	0.020	0.037	0.166	0.021	0.006	0.033	0.020	0.015	0.019	0.032	0.019	0.007	0.388
Ca	3.128	3.078	2.905	3.049	3.081	3.087	3.101	3.051	3.029	3.001	3.035	2.961	2.770
OH/4	0.037	0.093	0.218	0.086	0.090	0.056	0.084	0.112	0.180	0.152	0.148	0.204	0.198

*Difference to 100% assumed to be H_2O

TABLE 17(cont.). MICROPROBE ANALYSES OF ANDRADITE FROM WESSELS MINE.

	V53GT4	GA12	H1011	GA4	GA5	GA7	V53GT3	GA1A	GA3	GA1B	V53GT7	GA8	GA6
SiO_2	33.95	33.83	33.90	33.87	33.82	34.20	32.89	33.70	33.31	33.24	33.01	33.22	32.74
Al_2O_3	0.48	0.79	0.68	0.92	0.58	1.38	0.23	0.94	0.92	1.06	0.81	0.72	0.81
Fe_2O_3	25.66	28.74	27.17	28.35	29.21	26.13	23.05	27.86	27.94	28.25	25.90	26.98	28.24
Mn_2O_3	4.49	1.17	3.25	1.35	0.92	2.21	11.68	1,70	2.02	1.45	3.36	3.37	1.40
MgO	0.10	0.19	0.19	0.11	0.20	0.16	0.17	0.20	0.19	0.14	2.74	0.22	0.26
CaO	34.20	34.37	33.65	34.27	34.09	34.24	31.80	34.02	34.45	34.30	32.72	33.95	34.48
H_2O^*	1.12	0.91	1.16	1.13	1.18	1.68	0.18	1.56	1.17	1.56	1.46	2.54	2.07
					STRUCTURAL FORMULAE ON THE BASIS OF 12 OXYGENS								
Si	2.842	2.839	2.833	2.831	2.829	2.823	2.810	2.800	2.792	2.769	2.741	2.729	2.717
Al^{3+}	0.047	0.078	0.067	0.091	0.057	0.135	0.023	0.092	0.091	0.104	0.080	0.070	0.079
Fe^{3+}	1.617	1.816	1.710	1.784	1.840	1.624	1.483	1.744	1.763	1.772	1.619	1.669	1.764
Mn^{3+}	0.286	0.075	0.207	0.086	0.059	0.139	0.760	0.108	0.129	0.092	0.212	0.148	0.088
Mg	0.012	0.024	0.024	0.014	0.025	0.020	0.022	0.025	0.024	0.017	0.339	0.027	0.032
Ca	3.067	3.091	3.013	3.069	3.055	3.028	2.911	3.028	3.093	3.061	2.911	2.989	3.065
OH/4	0.156	0.127	0.162	0.158	0.165	0.231	0.026	0.216	0.164	0,217	0.202	0.348	0.286

*Difference to 100% assumed to be H_2O

Group H, however, has a definite water component, clearly demonstrated by analyses performed on the LECO instrument. In Figure 21, the trace produced by the instrument for sample V2 shows loss of water at 475 °C and at 535 °C, for a total of 5,2 per cent H_2O. This trace corresponds well with the DTA traces of hydroandradite of Onuki et al. (1981), with water loss beginning with an exothermic reaction at 460–470 °C and an endothermic reaction at 535 °C. Similar behaviour was described for henritermiérite (tetragonal CaMn hydrogarnet) by Gaudefroy et al. (1969).

In Figure 22 all the garnet analyses have been plotted on the basis of the number of H^+ ions, calculated from the totals assumed to be 100 per cent with the deficiency due to water, versus the sum of all the other cations. The compositions represented by line N in Figure 22 are those that fit normal stochiometry and the normal garnet–hydrogarnet variation, where $H_4O_4^{4-}$ substitutes for SiO_4^{4-} tetrahedra. Line N, of apparent slope 0,25, is the predicted distribution of hydrogrossular compositions based on the formula $X_3Y_2Z_{3-n}H_{4n}O_{12}$ (Meagher 1982).

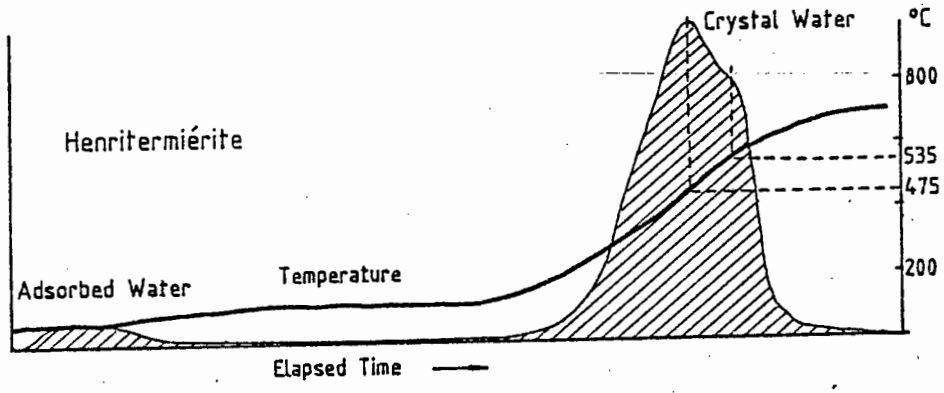

Fig. 21 - Temperature profile of henritermiérite (sample V2) in a LECO RMC-100 Rapid Moisture Analyser. The peak at 110 °C shows the adsorbed water which was driven off, prior to the release of 5,2 % crystal water at 475 °C and 535 °C.

The analyses which plot along line M are of the Mn-rich hydrogarnets and XRD has shown them to be henritermiérite (Table 18). Henritermiérite is unusual in that it is a tetragonal garnet. This is due to the Jahn-Teller distortion effect along the c-axis caused by the Mn^{3+} ion, which disrupts the cubic symmetry of the garnet structure and results in a tetragonal symmetry (Aubry et al. 1969). These garnets occur associated with glaucochroite-kirschteinite and (Fe, Mn)-akermanites and also as the dark orange-red garnet in paragenesis (iv). These analyses do not fit the normal hydrogarnet stochiometry. Birkett and Trzcienski (1984) have shown that the hydroxyl group can occupy other positions in the structure, and that $H_4O_4^{4-}$ substitution for SiO_4^{4-} tetrahedra is not the only way in which water can fit into the hydrogarnet structure. On the basis of this diagram, therefore, Group H is split into two groups, namely group HN (Table 15) for normal stochiometry hydrogarnets and group HM (Table 16) for abnormal stochiometry, manganese-enriched hydrogarnets. The further subdivision of the group HN garnets is by composition, as evidenced in Figures 22, 23 & 24.

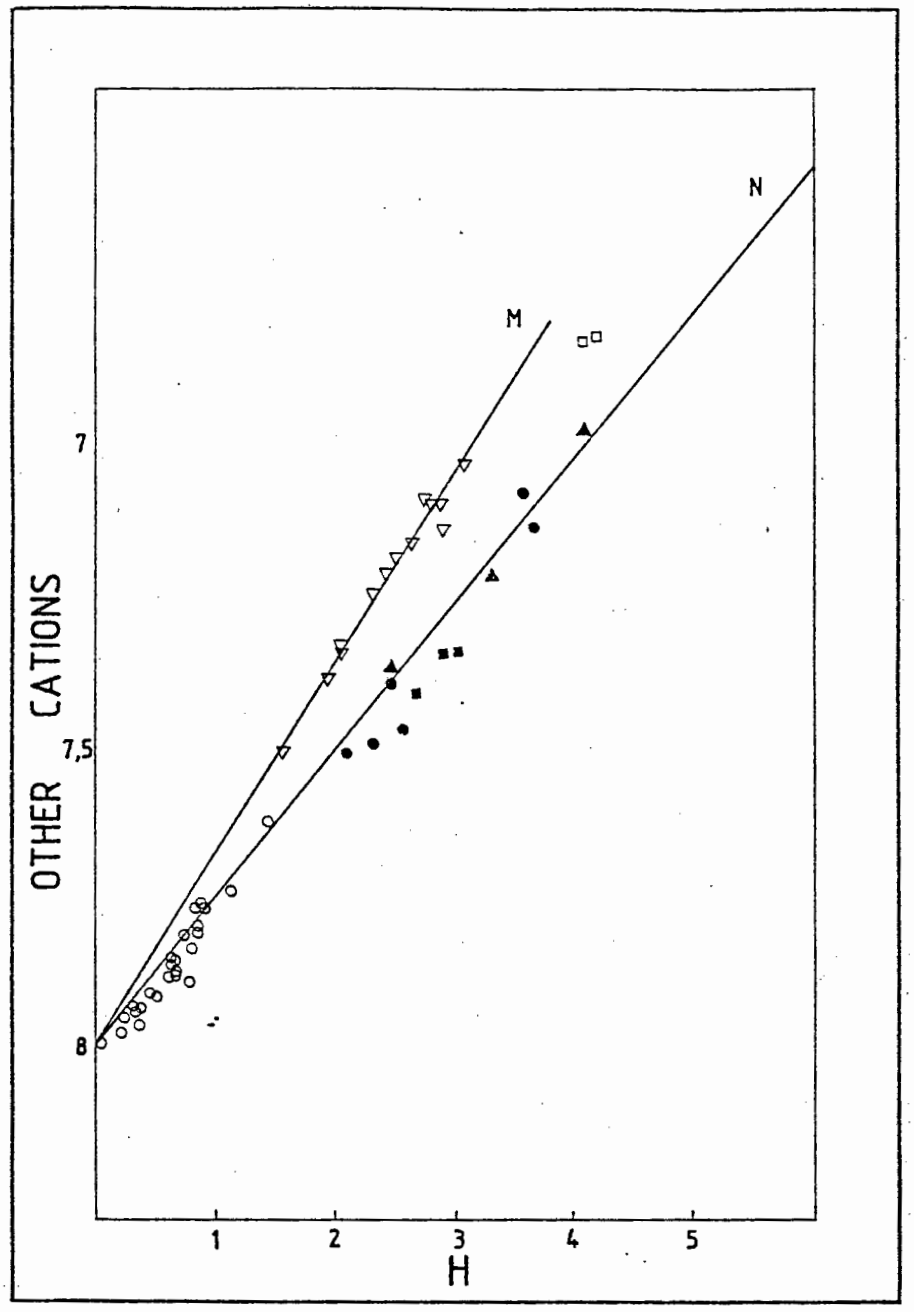

Fig. 22 - Scatter diagram of cation content (except hydrogen) versus hydrogen content (number of cations) of garnet samples, calculated for 12 oxygen atoms. Water is calculated by difference. Line N is the normal substitution trend for hydrogarnets (Meagher 1982). Line M shows the abnormal trend displayed by the group HM hydrogarnets. Symbols explained in Fig. 23.

Henritermiérite					Andradite		
Sample V2		Gaudefroy et al. (1969)					
d(obs)	Io	d(obs)	Io	hkl	d(obs)	Io	hkl
8,63	15						
6,16	15	6,21	30	020			
4,98	25	4,92	30	112			
4,76	25						
4,32	25	4,37	60	220	4,27	15	220
3,853	15						
3,257	20	3,28	20	132			
3,050	50	3,09	60	040			
2,980	20	2,98	60	004	3,019	60	400
2,855	15						
2,732	100	2,75	100	042			
2,684	20	2,684	30	024	2,699	100	420
2,600		2,607	5	233	2,579	10	332
2,503	35	2,516	80	242			
		2,459	5	224	2,466	45	422
		2,428	5	341			
2,397	20						
		2,370	5	134	2,366	15	431

TABLE 18. Powder diffraction data for henritermiérite from Wessels Mine and from Morocco, and andradite from Wessels Mine.

4.2.1 Mn^{3+} IN THE GARNET STRUCTURE

It is unusual to find Mn^{3+} in garnet but it is by no means unique. Gaudefroy et al. (1969) described the mineral henritermiérite from a hydrothermal manganese deposit at Tachgagalt, Morocco. This is a hydrogarnet containing Mn^{3+} as a Y cation and has a tetragonally distorted garnet structure. The hydrogarnet reported in this study contains a large amount of this molecule. When heated to 1 020 °C, the Moroccan henritermiérite gave a cubic garnet X-ray diffraction pattern (Gaudefroy et al. 1969).

Nishizawa and Koizumi (1975) were able to synthesise hydrothermally a reddish-brown cubic garnet, $Ca_3Mn^{3+}_2(SiO_4)_3$, at 60 kbar and 1 100 °C. This garnet showed no evidence for a distorted crystal structure and the lattice parameters were very close to those of andradite, $Ca_3Fe^{3+}_2(SiO_4)_3$. They suggested that the natural occurrence of this garnet end member would be as a relatively high-pressure mineral.
Similarly, Frentrup and Langer (1981) synthesised deep orange-red, idiomorphic Mn^{3+}-bearing cubic garnets, at 23 kbar and 830 °C. According to the latter authors the crystal-field stabilisation energy of Mn^{3+} in the cubic garnet structure is appreciably lower than in other Mn^{3+} silicates, and Mn^{3+} would therefore be strongly concentrated in silicate minerals other than garnet in parageneses of Mn^{3+}-bearing rocks.

Chemically the garnets in Group F consist predominantly of the andradite end member with minor manganese and aluminium present. Attempts to recast analyses of the andradite into end-members according to the scheme of Rickwood (1968) failed, necessitating use of the $Ca_3Mn^{3+}_2Si_3O_{12}$ end member (Table 19), the stability of which Frentrup and Langer (1981) have demonstrated. The andradite analyses treated this way give between 5 and 25 per cent of this end-member (Fig. 25).

The maximum amount of manganese in group-F garnets is 11,68 per cent, that in group HN is 25,17 per cent and group HM 37,18 per cent. In Figure 23 the range of Mn_2O_3 versus calculated H_2O is shown. It can be seen that the variation in manganese contents in groups F and HM is far less than for group HN, which has a wide variation in the amount of substitution of other trivalent ions for manganese in the B site. In paragenesis (iv) the group-HM hydrogarnet is the inner portion of a vein which is rimmed with an outer zone of group-HN garnet. This zonation, which has a more intense colour in the centre, is similar to that obtained by Frentrup and Langer (1981) in their synthesis of Mn^{3+} garnet where in the inner portion more Mn^{3+} was found than in the rim. Birkett and Trzcienski (1984) have postulated that this zonation could be due to the growth of the garnet in a migrating or ephemeral fluid phase during a prograde metamorphic reaction with decreasing P_{H2O} as the reaction proceeds.

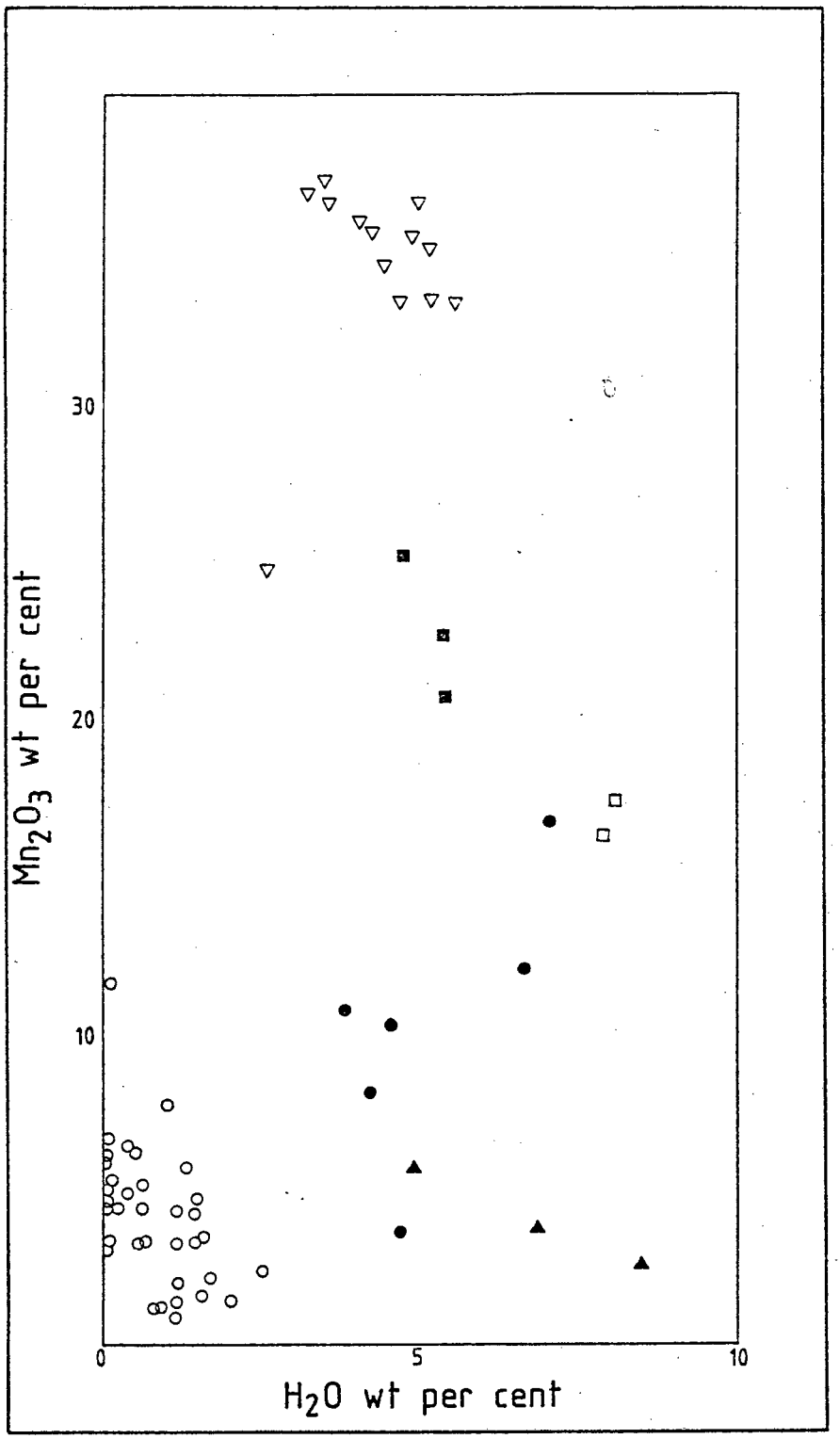

Fig. 23 - Mn_2O_3 versus calculated H_2O (wt. per cent) for all the garnets. Symbols for groups discussed in text are: ○ = F; ▲ = HNA; □ = HNB-1; ■ = HNB-2; ● = HNC; ▽ = HM.

	Weight %	Cation proportion	Andradite	Pyrope	Spessartine
SiO_2	35,95	0,5983	0,1375	0,1306	0,1282
Al_2O_3	0,32	0,0062		0,0016	Nil
Fe_2O_3	24,53	0,3072	Nil		
MnO	5,83	0,0822			0,0798
MgO	0,28	0,0069		Nil	
CaO	33,81	0,6029	0,1421		
	100,72	1,6037	0,1536	0,0023	0,0008

78,17 % cations allocated: Andradite 98,0%; Pyrope 1,5%; Spessartine 0,5%.

	Weight %	cation proportion	Andradite	Mn^{3+} Andradite	Pyrope	Grossular
SiO_2	35,95	0,5983	0,1375	0,0238	0,0169	0,0145
Al_2O_3	0,32	0,0062			0,0016	Nil
Fe_2O_3	24,53	0,3072	Nil			
Mn_2O_3	5,99	0,0758		Nil		
MgO	0,28	0,0069			Nil	
CaO	33,81	0,6029	0,1421	0,0284		0,0260
	100,88	1,5973	0,1536	0,0379	0,0023	0,0008

97,46 % cations allocated: Andradite 78,9%; Mn^{3+}-Andradite 19,5%; Pyrope 1,2%; Grossular 0,4%.

TABLE 19. Calculation of the percentage end-member molecules of garnet V53W1A with and without the Mn^{3+}-andradite molecule, after Rickwood (1968).

4.2.2 THE GARNET-HYDROGARNET SERIES

Although the hydrogen content of garnet is reported as wt. per cent H_2O, X-ray and neutron diffraction studies, as well as infrared absorption spectroscopy, indicate that H_2O does not occur as a molecular group in hydrogarnets to any appreciable extent (Deer et al. 1982). The general formula for hydrogarnet is:

$$X_3Y_2(SiO_4)_{3-n}(H_4O_4)_n.$$

The substitution $4H^+ = Si^{4+}$ appears to be the operative mechanism whereby each of the four oxygens about the tetrahedral site is strongly bonded to one hydrogen. Although numerous end-member hydrogarnets ($n = 3$) have been synthesised, natural garnet beyond intermediate ($0<n<2$) composition is not known to occur (Meagher 1982). Natural hydrogrossular is most often compositionally intermediate between grossular ($Ca_3Al_2(SiO_4)_3$) and hibschite ($Ca_3Al_2(SiO_4)_2(OH)_4$) (Deer et al. 1982). Zabinski (1966) has shown that the majority of hydrogrossular compositions are closer to hibschite than grossular, possibly due to a more stable crystal structure.

Varieties more hydrous than hibschite have been reported and a continuous solid solution exists between grossular and hydrogarnet at low temperature. Above 200 °C Shoji (1974) showed experimentally that the series is not continuous, but is composed of a limited hydrogrossular series

$Ca_3Al_2(SiO_4)_{3-n}(H_4O_4)_n$ where $0 < n < 1$ or 2,

and a hydrogarnet series

$Ca_3Al_2(SiO_4)_n(H_4O_4)_{3-n}$ where $0 < n < 0,4$.

The silica-free end member decomposes above 250 °C and the hydrogen content in the grossular–hydrogrossular series decreases with increasing temperature. When n = 1 the mineral persisted up to 300 °C (1 kbar), and at n = 0,5 the temperature was increased to 425 °C although its stability was unknown.

The low-temperature stability of andradite as a function of temperature, XCO_2 and fO_2 at a constant P_{fluid} of 2 kbar was investigated by Taylor and Liou (1978) who demonstrated that the reaction

$$3\ SiO_2 + 3\ CaCO_3 + 0,25\ Fe_2O_3 + 0,5\ Fe_3O_4 + 0,125\ O_2 = Ca_3Fe_2Si_3O_{12} + CO_2$$

occured at 550±10 °C at XCO_2 = 0,22, and rising with increasing X_{CO2}. Gustafson (1974) showed that below 550 °C a member of this andradite–hydroandradite series occurred, the amount of water in the structure increasing with decreasing temperature.

The structure refinement of Aubry et al. (1969) of henritermiérite reveals a similar substitution of the type $4H^{+} = Si^{4+}$. The iron-rich end member of the hydrogarnet group, hydroandradite, is rare (Peters 1965, Onuki et al. 1981), and shows similar behaviour to the hydrogrossular series. Even rarer is hydrospessartine, which was reported by Wilkens and Sabine (1973).

4.2.3 COMPOSITIONAL VARIATION IN THE GARNETS

The garnet analyses in Tables 15, 16 and 17 display wide variations in the type and degree of cation substitions. H_2O in these tables is by deduction, after considering the results of those few samples of which enough material was available for more complete analysis. Five distinct hydrogarnet divisions can be distinguished in the group-H analyses. In addition, it would appear that the andradite-hydroandradite series of Gustafson (1974) is also present. In Figure 24 the analyses are plotted on the basis of trivalent cation proportions. There is a clear differentiation of these analyses into four groups, one a cluster in the hydrogrossular field (group HNA), two clusters in the henritermierite field (groups HNB and HM), and the fourth group a substitution trend, at a constant Al^{3+}/Mn^{3+} ratio of 1, from hydroandradite to manganoan hydrogrossular (group HNC).

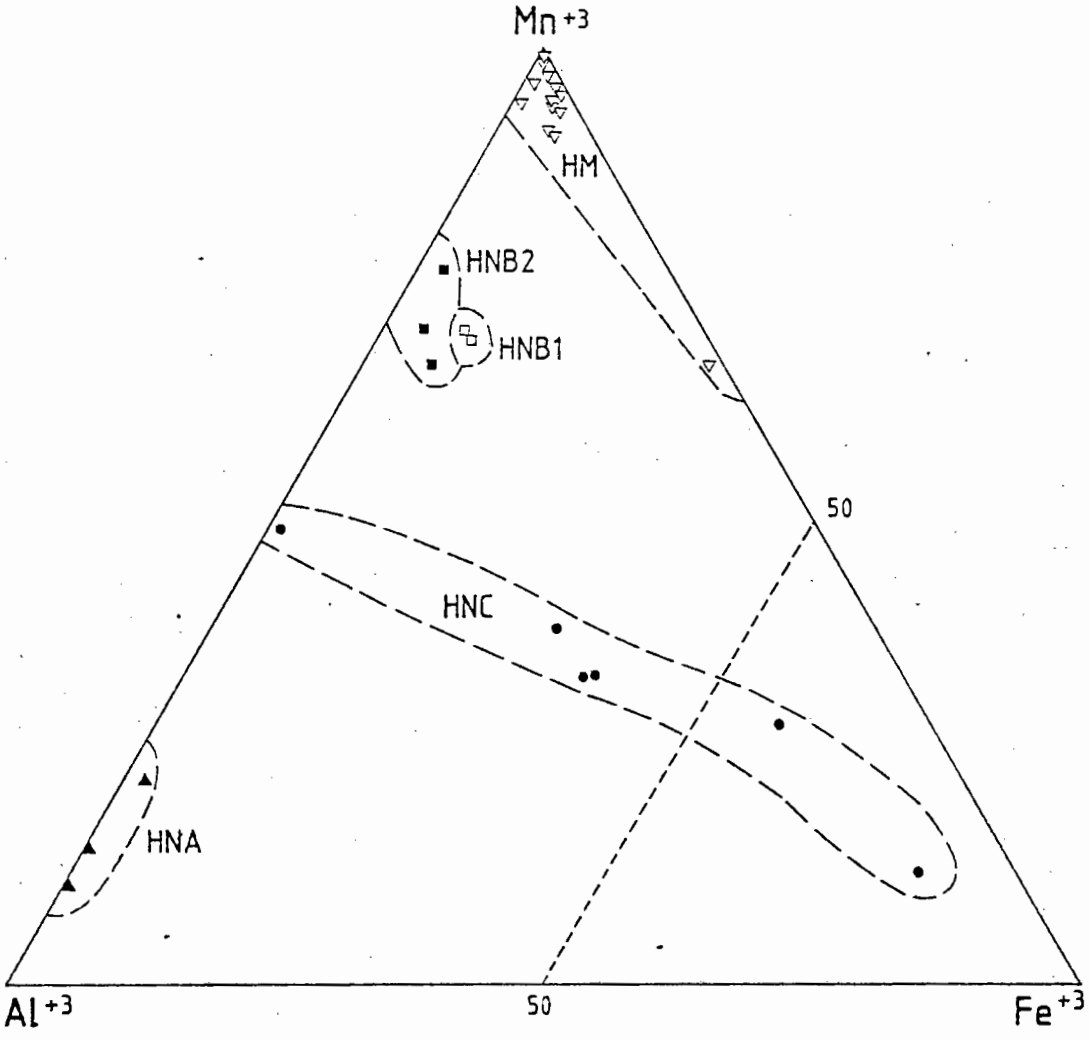

Fig. 24 - Plot of Y^{3+} cations (mole proportions) of the garnets, excluding group F. All Al, Fe and Mn assumed to be trivalent for the purposes of this plot. Symbols as in Fig. 23. See Fig. 25 for triangle at Fe^{3+} apex (group F).

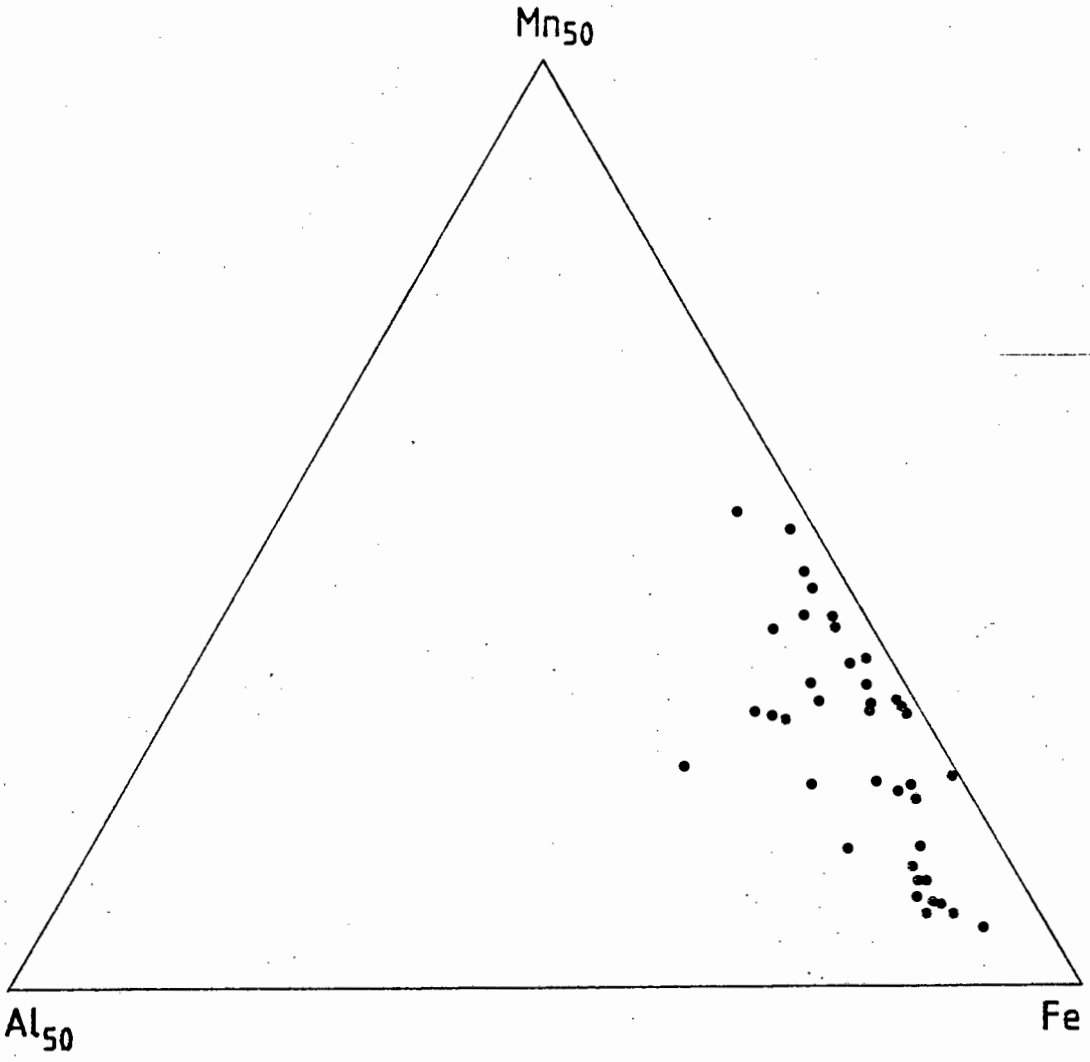

Fig. 25 - Plot of Y^{3+} cations (mole proportions) for group F andradites.

In the henritermiérite cluster HNB, however, two sub-groups are apparent. The one sub-group (group HNB-1) shows normal hydrogarnet stochiometry and plots on line N in Fig. 22, while the other (group HNB-2) plots between lines N and M, possibly indicating that it also has abnormal $H_4O_4^{4-}$ substitution mechanism, although different to that in group HM. Another anomaly is the large amount of Mg present in group HNA (Fig. 26), which cannot all be allocated to the X site. Here another substitution mechanism, perhaps involving a Mg-OH complex, could occur, because Aines and Rossman (1984) showed that the hydrogen speciation in garnets is OH^-, not H_2O. The abnormal cation distributions of groups HM, HNA and HNB-2 are clearly displayed in Figure 27, which is a plot of divalent, trivalent and quadrivalent cations.

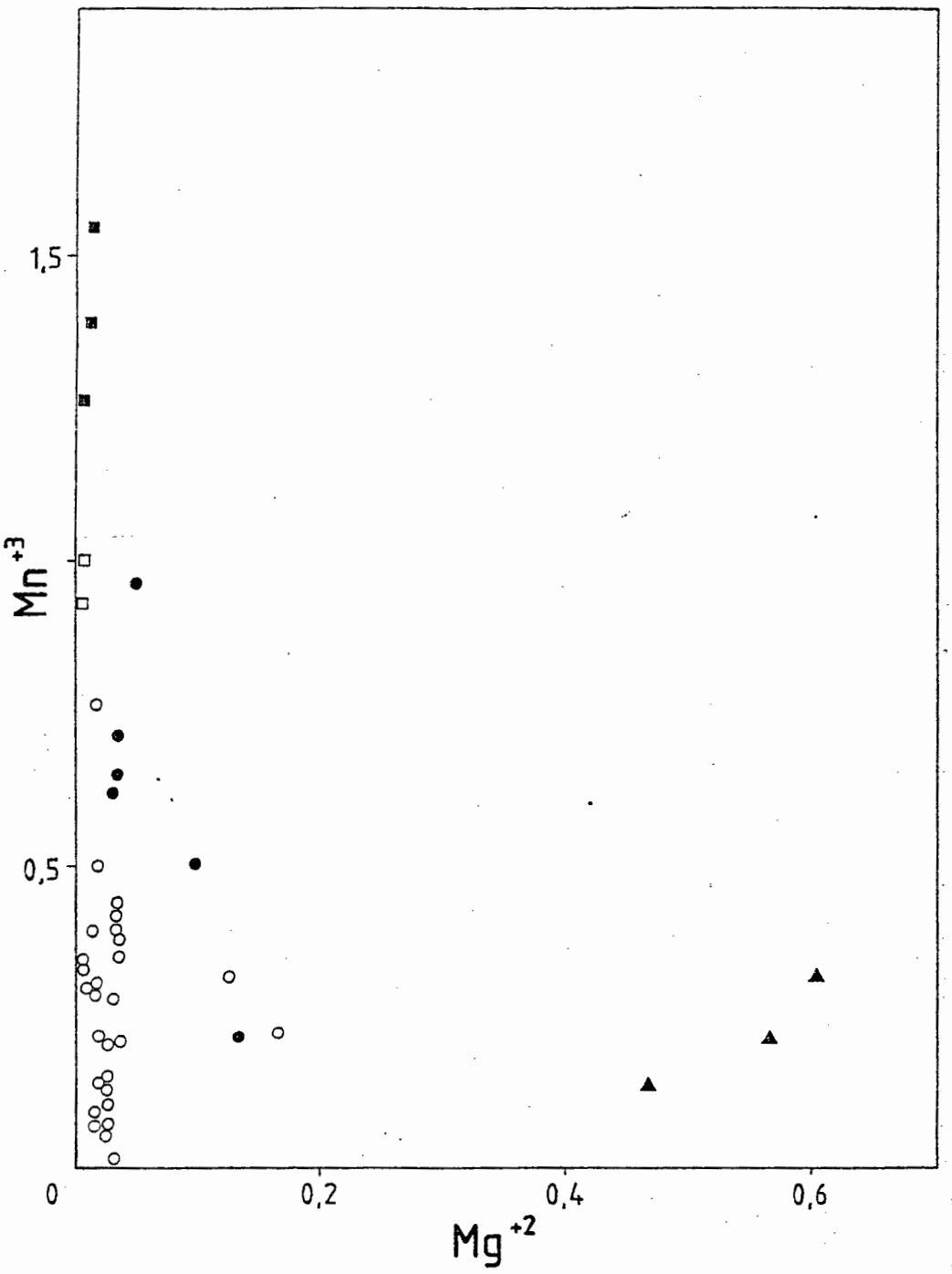

Fig. 26. Mn versus Mg cation distribution in the garnets and hydrogarnets. Symbols as in Fig. 23.

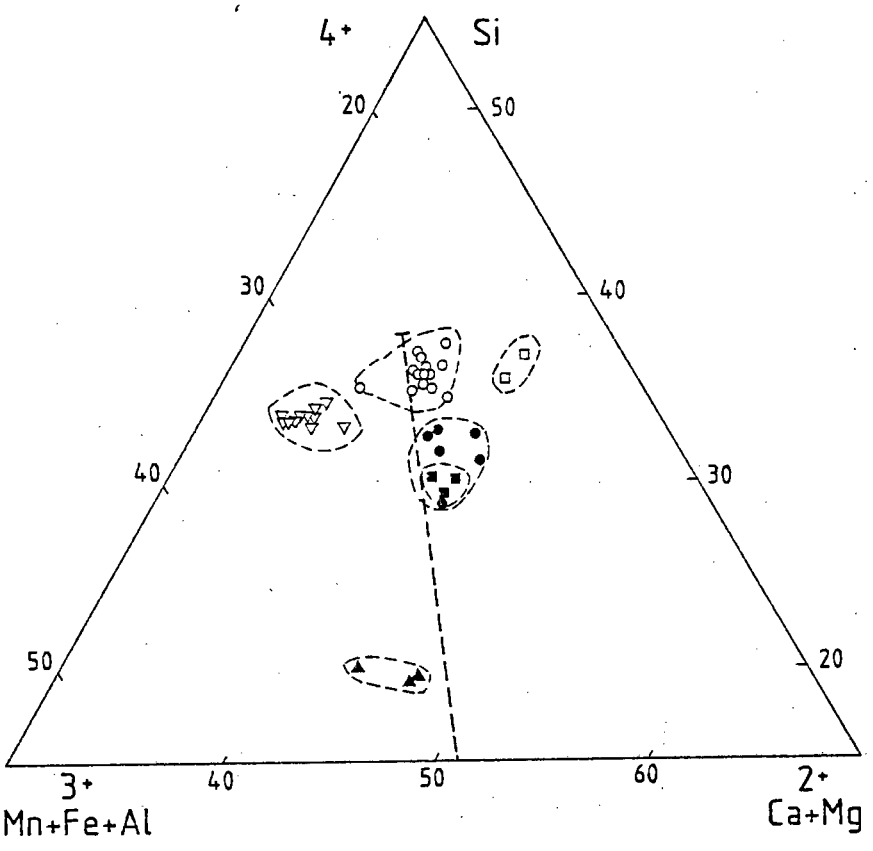

Fig. 27 - Cation variation between X^{2+}, Y^{3+} and Z^{4+}. All Mn assumed trivalent to demonstrate the difference between group HM and the other hydrogarnets. Symbols as in Fig. 23. The dotted line is the theoretical substitution trend for normal hydrogarnets (line N in Fig. 22).

4.3 SHEET SILICATES

Two Mg-Al sheet silicates occur in the zoned assemblage, both associated with garnet.

4.3.1 CHLORITE

Coexisting with the andradite in the zoned assemblage is clinochlore (Bayliss 1975) which occurs as small colourless domains in and around the garnet. It appears to be cogenetic with the andradite. Clinochlore is also found associated in other assemblages with diopside and phlogopite. Chemically, the clinochlore is an almost pure end member with only a small amount of Fe and Mn in its structure (Table 20), as is shown in Figure 28.

4.3.2 PHLOGOPITE

Phlogopite occurs between euhedral Mn-rich andradite, diopside and clinochlore (sample V53) in the heterogeneous leucocratic assemblages, and adjacent to the orange-red henritermiérite (see Chapter 4.1). It has also been found associated with almost pure end-member iron akermanite (sample H4).

The phlogopite approaches the ideal composition

$$K_2Mg_6(Si_6Al_2)O_{20}(OH)_{16}$$

	RDW21	V53Y2	RDW2PX4	RDWCh13	RDW22A	RDWCh12	RDW22
SiO2	34,96	35,40	35,15	34,73	34,78	35,67	35,79
Al2O3	14,94	9,84	12,92	14,03	16,32	14,25	15,36
FeO	0,35	0,61	0,33	0,36	0,25	0,54	0,41
MnO	0,51	1,14	0,57	0,39	0,30	0,50	0,40
MgO	33,99	38,43	36,60	36,76	35,10	36,70	35,71
CaO	0,11	0,10	0,11	0,12	0,12	0,11	0,10
Na2O	-	-	-	-	-	-	-
K2O	-	-	-	0,08	-	-	-
H2O*	15,14	14,42	14,32	13,54	13,13	12,24	12,23
	STRUCTURAL FORMULAE ON THE BASIS OF 36(O,OH)						
Si	6,345	6,535	6,452	6,417	6,417	6,657	6,657
Al^{3+}	3,197	2,141	2,795	3,055	3,550	3,135	3,368
Fe^{2+}	0,053	0,094	0,051	0,056	0,039	0,084	0,064
Mn	0,078	0,178	0,089	0,061	0,047	0,079	0,063
Mg	9,194	10,574	10,012	10,123	9,651	10,209	9,898
Ca	0,021	0,020	0,022	0,024	0,021	0,022	0,020
Na	-	0,021	-	-	-	-	-
K	-	-	-	0,019	-	-	-
OH	18,336	17,685	17,462	16,621	16,164	15,178	15,179

*Difference to 100% assumed to be H2O

TABLE 20. Microprobe analyses of clinochlore from Wessels Mine.

	H45	S5114	S5113	V53X3	V53X1	V53X2	V53Y1
SiO2	40,90	40,97	43,51	43,79	42,61	43,10	43,06
Al2O3	12,36	11,58	12,03	10,80	11,05	11,35	11,17
FeO	0,07	0,83	0,47	0,50	1,07	0,93	1,04
MnO	0,40	0,33	0,17	0,55	0,22	0,09	-
MgO	30,20	33,37	29,56	28,50	28,57	28,93	29,20
CaO	0,81	-	-	-	1,58	-	-
NaO	-	0,04	0,01	-	-	-	-
K2O	4,45	5,15	7,73	8,37	8,38	9,62	9,30
H2O*	10,82	7,73	6,52	7,49	6,53	6,07	6,22
	STRUCTURAL FORMULAE ON THE BASIS OF 22(O,OH)						
Si	5,890	5,761	6,065	6,200	6,030	6,064	6,065
Al^{3+}	2,098	1,920	1,977	1,803	1,844	1,882	1,855
Fe^{2+}	0,008	0,098	0,055	0,059	0,127	0,109	0,123
Mn	0,049	0,039	0,020	0,066	0,026	0,011	-
Mg	6,482	6,993	6,141	6,014	6,028	6,066	6,130
Ca	0,125	-	-	-	0,240	-	-
Na	-	0,011	0,003	-	-	-	-
K	0,818	0,924	1,375	1,512	1,513	1,727	1,671

* Difference to 100% assumed to be H2O. (Not used in structural formula calculation)

TABLE 21. Microprobe analyses of phlogopite from Wessels Mine.

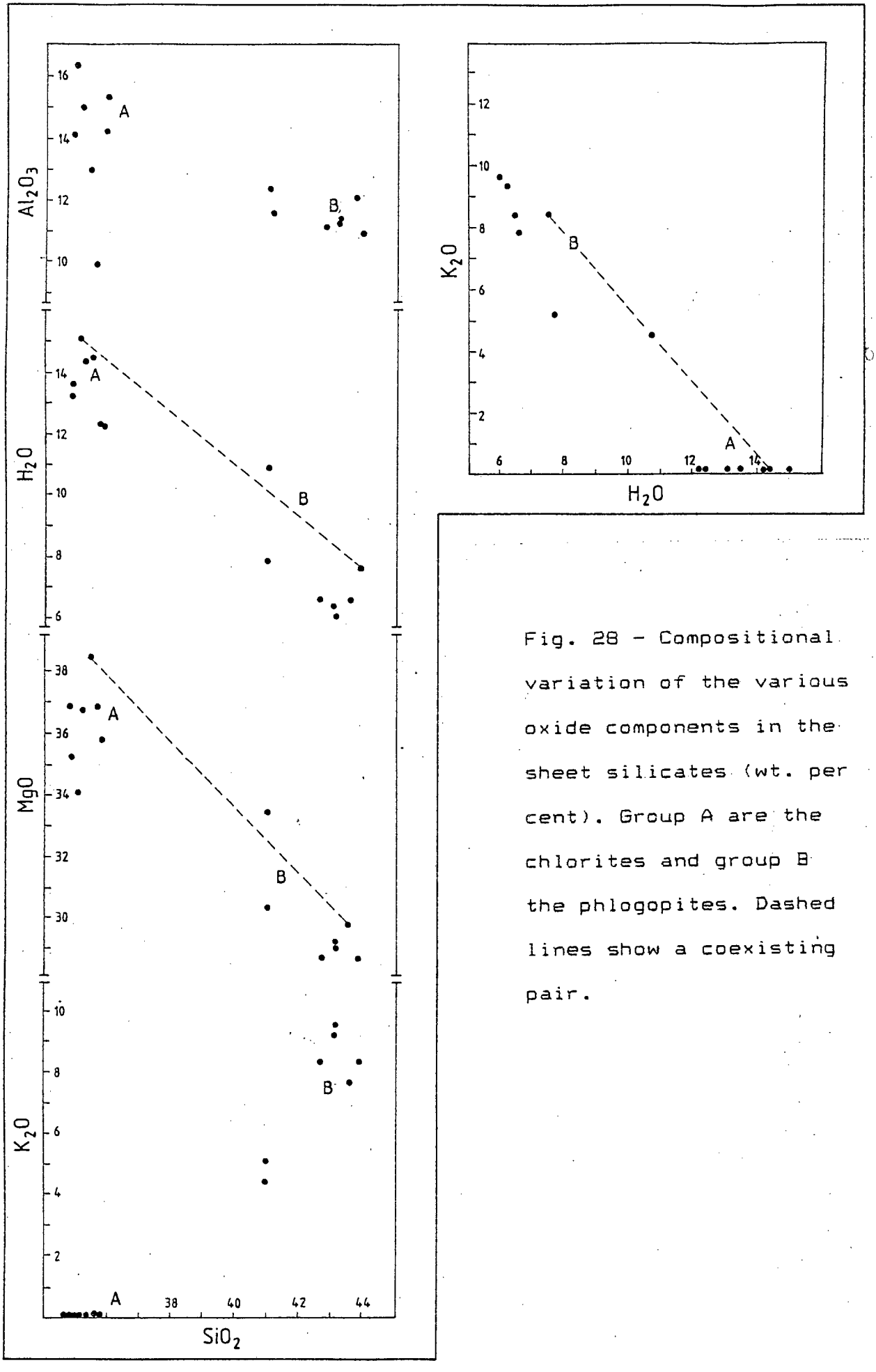

Fig. 28 - Compositional variation of the various oxide components in the sheet silicates (wt. per cent). Group A are the chlorites and group B the phlogopites. Dashed lines show a coexisting pair.

although the compositions in Table 21 show that the amount of K^+ cations is much less than ideal for some analyses and that the water content is too great, if the deficiency in their totals is assumed to be due solely to H_2O.

4.4 OLIVINE AND MELILITE

Patches of bright orange glaucochroite, ferroan akermanite and hydrogarnet occur in a fine-grained orange to dark blackish-brown calc-silicate rock which occurs as thin (5 cm thick) discontinuous layers between manganese ore. In places this rock appears purple with development of sugilite and then the minerals discussed in this section are no longer found. In thin section the rock displays a brownish, very fine-grained matrix with larger colourless blebs up to 1 mm in diameter (Fig. 29). The matrix consists predominantly of andradite garnet, wollastonite and pectolite, and the blebs consist mainly of wollastonite, pectolite and diopside.

4.4.1 GLAUCOCHROITE-KIRSCHSTEINITE

Glaucochroite [$Ca(Mn,Fe)SiO_4$] was originally described from the Franklin Zn-Fe-Mn deposit, in Sussex County, New Jersey by Penfield and Warren (1899), where it occurred as minute blue crystals embedded in nasonite. It also occurs in association with willemite, garnet, manganaxinite, clinohedrite, hardystonite, tephroite and franklinite (Palache 1935). Frondel and Baum (1974) considered the Franklin-

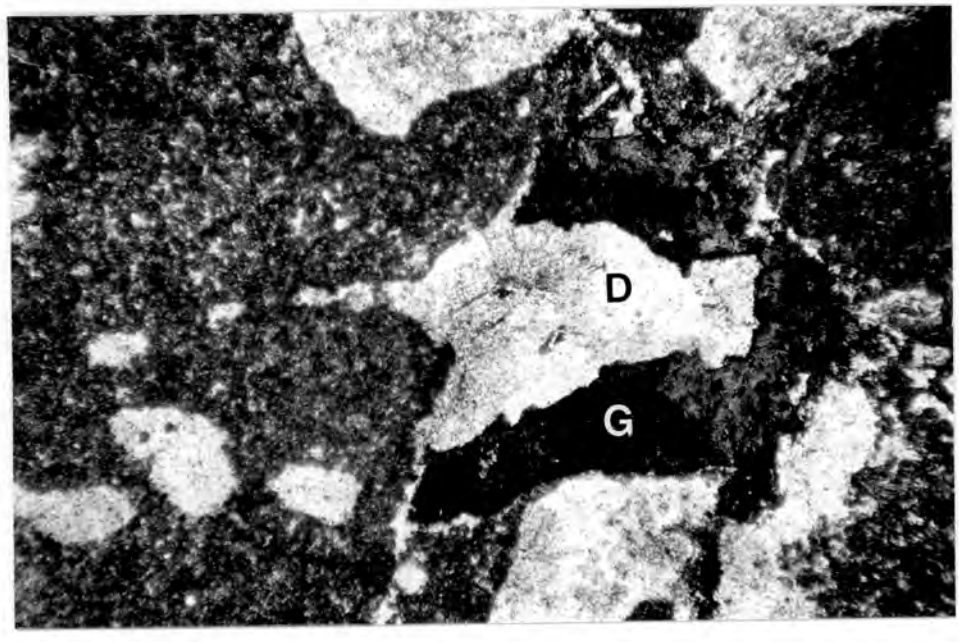

Fig. 29 - Glaucochroite (G) and diopside (D) in blebs in the orange calc-silicate rock. Note the very fine-grained groundmass which consists mainly of andradite, wollastonite and pectolite. The diffraction pattern in Table 22 is of the marked glaucochroite grain. Field of view 2 mm, plane polarised light.

WESSELS MINE			FRANKLIN		
d(obs)	Io	d(calc)	d(obs)	Io	hkl
5,532	40	5,567	5,54	30	020
4,259	20	4,255	4,23	40	021
3,947	10	3,950	3,91	10	101
			3,69	60	120
			3,25	20	002
3,016	50	2,965	2,96	60	130
2,834	20	2,838	2,81	20	022
2,698	100	2,705	2,69	80	131
			2,63	80	112
2,582	40	2,565	2,56	20	041
2,459	40	2,460	2,44	30	122
2,262	20	2,261	2,25	20	220
2,204	20	2,205	2,19	20	132
2,018	20	2,030	2,03	20	150
1,961	20	1,961	1,95	20	113
1,845	50	1,846	1,85	100	222
			1,79	20	061
			1,77	20	241
1,767	20	1,766	1,75	20	133
1,744	20	1,739			160
			1,72	20	152
1,719	20	1,726	1,71	20	043
1,609	100	1,595	1,62	40	310
			1,61	40	213
1,571	20	1,576	1,58	20	311
1,530	20	1,533			321
			1,52	30	170
1,446	20	1,441	1,43	20	134
1,420	20	1,418	1,42	30	322
1,314	20	1,317			303
1,263	20	1,266			115
			1,23	20	400
1,184	20	1,181	1,19	20	191,135

TABLE 22. X-ray diffraction data for glaucochroite. The relative intensities of the peaks of the Wessels material were estimated visually. D-spacing calculated using the Appleman least squares computer program. Data for Franklin glaucochroite from the JCPDS powder diffraction manual (14-376).

	GL 7	H4GL12	H4GL11	H4GL10	H4GL9	H4GL8	H4GL5	H4GL4	H4GL3	OL2	GL1
SiO_2	33,71	32,81	32,61	33,25	31,26	32,01	31,40	33,68	29,64	31,37	31,89
Al_2O_3	1,41	0,80	0,54	0,46	0,31	0,52	0,73	1,85	0,50	0,51	0,93
FeO	18,08	11,88	10,31	0,97	0,67	0,54	3,14	11,90	0,52	1,84	0,66
MnO	14,64	21,89	26,50	35,91	38,75	37,08	36,66	19,53	40,60	37,12	37,34
MgO	0,15	0,31	0,33	1,97	0,33	0,48	0,81	0,16	0,19	0,71	1,07
CaO	31,44	31,55	30,31	27,77	27,79	28,97	26,66	32,06	27,73	27,38	27,61
Na_2O	-	-	-	-	-	-	0,17	0,19	0,18	-	-
K_2O	-	-	-	-	-	-	0,13	0,08	0,11	-	-
TOTAL	99,43	99,24	100,60	100,33	99,11	99,60	99,70	99,45	99,47	98,93	99,50
					STRUCTURAL FORMULAE ON THE BASIS OF 4 OXYGENS						
Si	1,027	1,011	1,002	1,013	0,987	0,996	0,982	1,020	0,946	0,988	0,990
Al^{3+}	0,051	0,029	0,020	0,017	0,012	0,019	0,027	0,066	0,019	0,019	0,034
Fe^{2+}	0,460	0,306	0,265	0,025	0,018	0,014	0,082	0,301	0,014	0,048	0,017
Mn	0,378	0,571	0,690	0,927	1,036	0,977	0,971	0,501	1,097	0,990	0,982
Mg	0,007	0,014	0,015	0,089	0,016	0,022	0,038	0,007	0,009	0,033	0,050
Ca	1,026	1,042	0,998	0,907	0,940	0,966	0,893	1,040	0,948	0,924	0,919
Na	-	-	-	-	-	-	0,010	0,001	0,011	-	-
K	-	-	-	-	-	-	0,005	0,003	0,004	-	-
TOTAL	2,949	2,973	2,990	2,978	3,009	2,994	3,010	2,951	3,050	3,002	2,992

TABLE 23. Microprobe analyses of glaucochroite from Wessels Mine.

Sterling Hill orebodies to be the product of amphibolite facies regional metamorphism of a limestone which is present between Zn-rich (with accessory Mn) ore lenses and beds. This highly deformed deposit was metamorphosed at temperatures of at least 650-750 °C (Frondel and Klein 1965) and pressures of several kilobars (Hague et al. 1956).

A second occurrence of glaucochroite was described by Pertsev and Laputina (1975) from the Anakit skarns, Lower Tunguska, U.S.S.R., where it occurs with andradite, diopside-hedenbergite and calcite in a skarn formed by the contact metamorphism of marly carbonate beds by an instrusive dolerite. They proposed that the glaucochroite formed by reaction of rhodonite and calcite.

Kirschsteinite [$CaFeSiO_4$], the iron analogue of glaucochroite, was first described in the form of magnesian kirschsteinite from Mt. Nyiragongo, Zaire, by Sahama and Hytonen (1957) and Sahama (1961). Magnesian kirschsteinite has been described from calcareous skarn xenoliths in Tazheran, U.S.S.R., from an alkali syenite, associated with wollastonite, diopside, melilite, grossular-andradite and other minerals as a late mineral in thin veins around garnet, diopside and calcite (Konev et al. 1970). Prinz et al. (1977) also recorded magnesian kirschsteinite from the Angra dos Reis achondrite from Brazil.

At Wessels Mine the glaucochroite is orange red in thin section and strongly pleochroic. It has a high birefringence partially masked by its strong colour, and the pleochroism is X = Y = light yellow-orange, Z = red-orange. It has a high relief and all the grains are polycrystalline. It is biaxial negative with 2V approximately 60 degrees. It differs from the Franklin and Anakit glaucochroite in its strong color and pleochroism. The Franklin material is bluish green in colour with some very small crystals white or pinkish (Penfield and Warren 1899), and the Anakit material is brownish rose coloured on fresh fractured surfaces (Pertsev and Laputina 1975). No pleochroism is noted from these two localities

X-ray powder diffraction confirms the identity of the mineral, the results agreeing reasonably with those of O'Daniel and Tscheischwili (1943), O'Mara (1951), and Lager and Meagher (1978) (Table 22). The unit-cell dimensions obtained are $\underline{a}$ = 4.93 $\pm$ 0,02 Å, $\underline{b}$ = 11.14 $\pm$ 0,04 Å and $\underline{c}$ = 6,60 $\pm$ 0,01 Å.

The analyses show a range of compositions from almost pure glaucochroite to manganoan kirschsteinite (Table 23, Figs 30,31). The presence of small amounts of aluminium in olivines is unusual. Dodd (1973) stated that terrestrial olivines (olivine sensu stricto) of all parageneses contain essentially no aluminium (0,01 wt. per cent), while many workers have reported amounts up to 0,15 wt. per cent in olivines in lunar basalts. Up to 2,55 wt. per cent Al_2O_3, however, has been recorded in the monticellite -

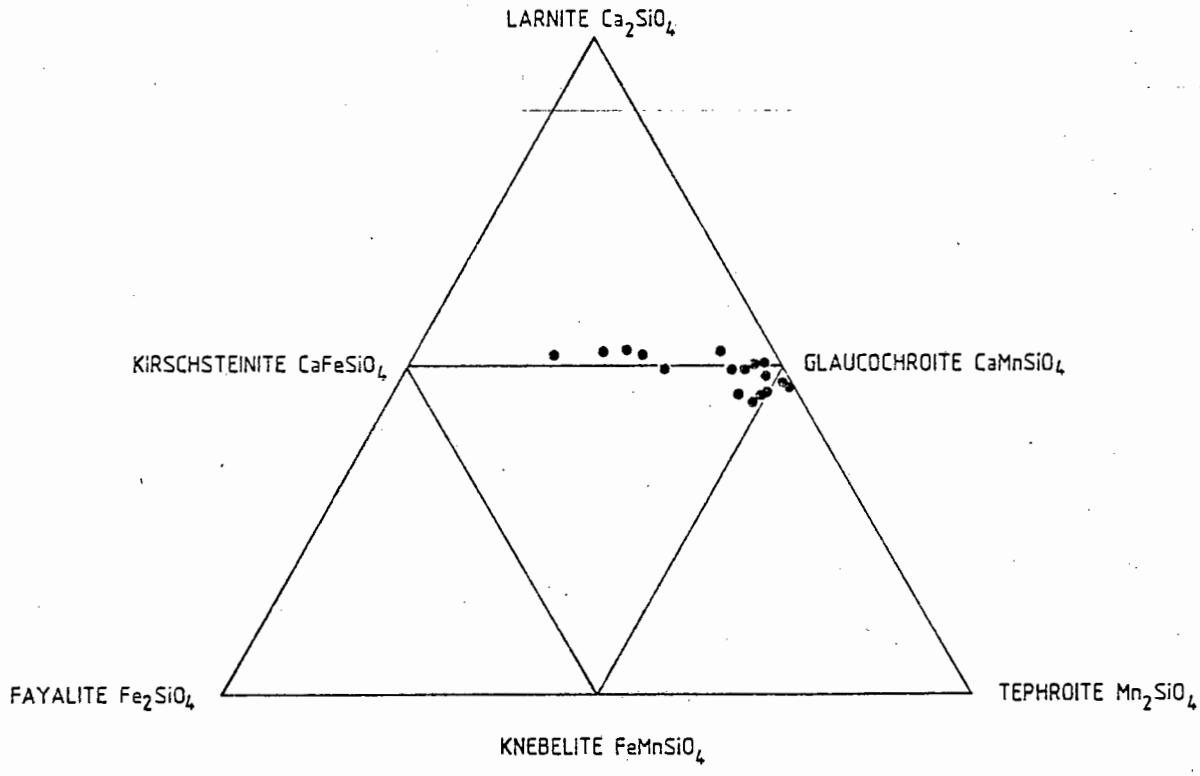

Fig. 30 - The solid solution developed between glaucochroite and kirschsteinite at Wessels Mine.

kirschsteinite solid-solution series (Gold 1966, quoted in Deer et al. 1982). Since the analysed grains showed no signs of alteration or impurity, the aluminium is presumed to be primary. The striking orange-red colour is probably due to the presence of trivalent cations in the M(1) site. Inesite [$Ca_2(Mn,Fe)_7Si_{10}O_{28}(OH)_2.5H_2O$] from the Kokuriki mine, Hokkaido, Japan displays a bright-orange colour in contrast to the more normal pinkish colour for the mineral. This has been shown to be due to the presence of small amounts of Mn^{3+} (Togari et al. 1986). The substitution of trivalent ions for divalent ions, in view of the absence of replacement of Si and the lack of appreciable amounts of monovalent cations, would require corresponding vacancies in the structure (Deer et al. 1982):

$$3(Mn^{2+},Fe^{2+}) = 2(Mn^{3+},Fe^{3+},Al^{3+}) + [\ ]^{6}$$

In olivine there are two non-equivalent octahedral sites for (Mg,Fe) at a centre of symmetry and one on a mirror plane (001), while in monticellite Ca ions occupy the sites on the mirror planes and Mg ions are at the centre of symmetry (Deer at al. 1982). Lager and Meagher (1978) have shown that site preferences in monticellite and glaucochroite for Ca in the M(2) and Mn, Fe and Mg in the M(1) sites exist, as opposed to (Fe,Mg) olivines which have no preferences. It has also been shown by Mössbauer spectroscopy that in synthetic kirschsteinite the Fe^{2+} is in a single site, corresponding to the monticellite structure (Eibschutz and Ganiel 1967).

4.4.2 AKERMANITE

An iron- and manganese-rich member of the melilite group occurs in close association with the glaucochroite, sometimes in the same composite grain. It varies in colour from yellow brown (high Fe content) to an orange brown (high Mn content) and is moderately pleochroic. Some grains display a distinct yellow-brown to pink pleochroism. Identification was difficult due to the very small size and scarcity of the mineral and its similarity to glaucochroite (similar colour and texture). An X-ray diffraction identification was finally made from a mixture of the two minerals which yielded six identifiable lines which were indexed by comparison with file 10-391 (akermanite) (JCPDS 1986) and a calculated pattern based on the unit-cell data of Seifert (1974) for synthetic ferroakermanite (his terminology).

The analyses (Tables 24 and 25) show a variation in Fe, Mn and Mg proportions (Fig. 31), and reveal the presence of two distinct groups on the basis of Fe and Al content. The analyses designated H4 in these two tables are from one thin section and are highlighted to show the compositional heterogeneity present in this association. In Figure 32 a plot of Si-Al-Total cations distinctly separates the analyses into a high-Al group, group A, and a low-Al group, group B. The two groups can be defined as follows:

	H4			H4	H4			H4
SiO_2	43,65	43,63	41,14	41,10	38,37	38,49	37,78	37,26
Al_2O_3	5,71	11,41	7,33	10,00	10,47	11,51	14,16	13,91
FeO	6,60	0,92	8,95	0,69	6,08	0,55	1,70	0,78
MnO	2,76	4,36	4,51	4,44	6,50	3,92	4,38	5,11
MgO	9,06	4,22	6,83	11,13	1,75	9,67	2,94	5,54
CaO	31,94	35,13	30,57	29,54	35,66	35,65	39,03	37,34
Na_2O	0,06	0,10	0,20	-	-	0,11	-	-
K_2O	0,12	0,11	0,11	1,88	-	0,08	-	-
TOTAL	100,00	100,03	99,74	98,78	98,83	100,07	99,99	99,94
	STRUCTURAL FORMULAE ON THE BASIS OF 7 OXYGENS							
Si	1,994	1,956	1,921	1,872	1,831	1,749	1,741	1,712
Al^{3+}	0,307	0,603	0,404	0,537	0,589	0,617	0,769	0,753
Fe^{2+}	0,252	0,034	0,350	0,026	0,243	0,021	0,066	0,030
Mn	0,107	0,166	0,178	0,171	0,263	0,151	0,171	0,199
Mg	0,617	0,282	0,475	0,756	0,124	0,655	0,202	0,379
Ca	1,563	1,687	1,530	1,442	1,824	1,736	1,927	1,838
Na	0,005	0,009	0,018	-	-	0,010	-	-
K	0,007	0,010	0,007	0,109	-	0,005	-	-
TOTAL	4,855	4,750	4,887	4,804	4,874	4,947	4,876	4,911

TABLE 24. Microprobe analyses of group-A melilites from Wessels Mine.

			H4	H4	H4	H4		H4	H4	
SiO_2	41,58	41,30	40,49	39,82	38,58	36,96	37,90	36,40	35,26	36,79
Al_2O_3	0,30	0,58	0,14	0,81	1,38	0,80	2,07	1,27	2,20	1,47
FeO	17,12	17,29	12,44	9,57	19,90	17,84	18,12	20,62	22,52	19,32
MnO	3,51	2,54	10,77	11,86	5,99	8,36	4,50	6,03	3,60	4,67
MgO	0,49	0,16	4,34	5,37	1,77	1,56	2,82	0,13	0,14	6,29
CaO	35,43	36,05	32,25	32,47	31,81	33,02	33,78	35,01	35,56	31,35
Na_2O	0,11	0,90	-	-	-	0,13	0,19	-	0,18	-
K_2O	0,08	0,12	-	-	-	0,25	0,12	-	0,09	-
TOTAL	98,83	99,15	100,43	99,90	99,43	99,03	99,63	99,46	99,68	99,92
	STRUCTURAL FORMULAE ON THE BASIS OF 7 OXYGENS									
Si	2,085	2,068	1,888	1,964	1,956	1,913	1,910	1,886	1,833	1,850
Al^{3+}	0,018	0,034	0,008	0,047	0,083	0,049	0,123	0,078	0,134	0,088
Fe^{2+}	0,715	0,721	0,514	0,395	0,844	0,771	0,762	0,893	0,976	0,812
Mn	0,149	0,107	0,450	0,496	0,257	0,366	0,192	0,265	0,158	0,200
Mg	0,036	0,012	0,319	0,395	0,134	0,120	0,211	0,010	0,011	0,471
Ca	1,896	1,926	1,706	1,716	1,728	1,829	1,944	1,975	1,689	
Na	0,011	0,087	-	-	-	0,013	0,019	-	0,018	-
K	0,005	0,008	-	-	-	0,016	0,008	-	0,006	-
TOTAL	4,915	4,963	4,996	5,013	5,002	5,076	5,044	5,076	5,111	5,108

TABLE 25. Microprobe analyses of group-B melilites from Wessels Mine.

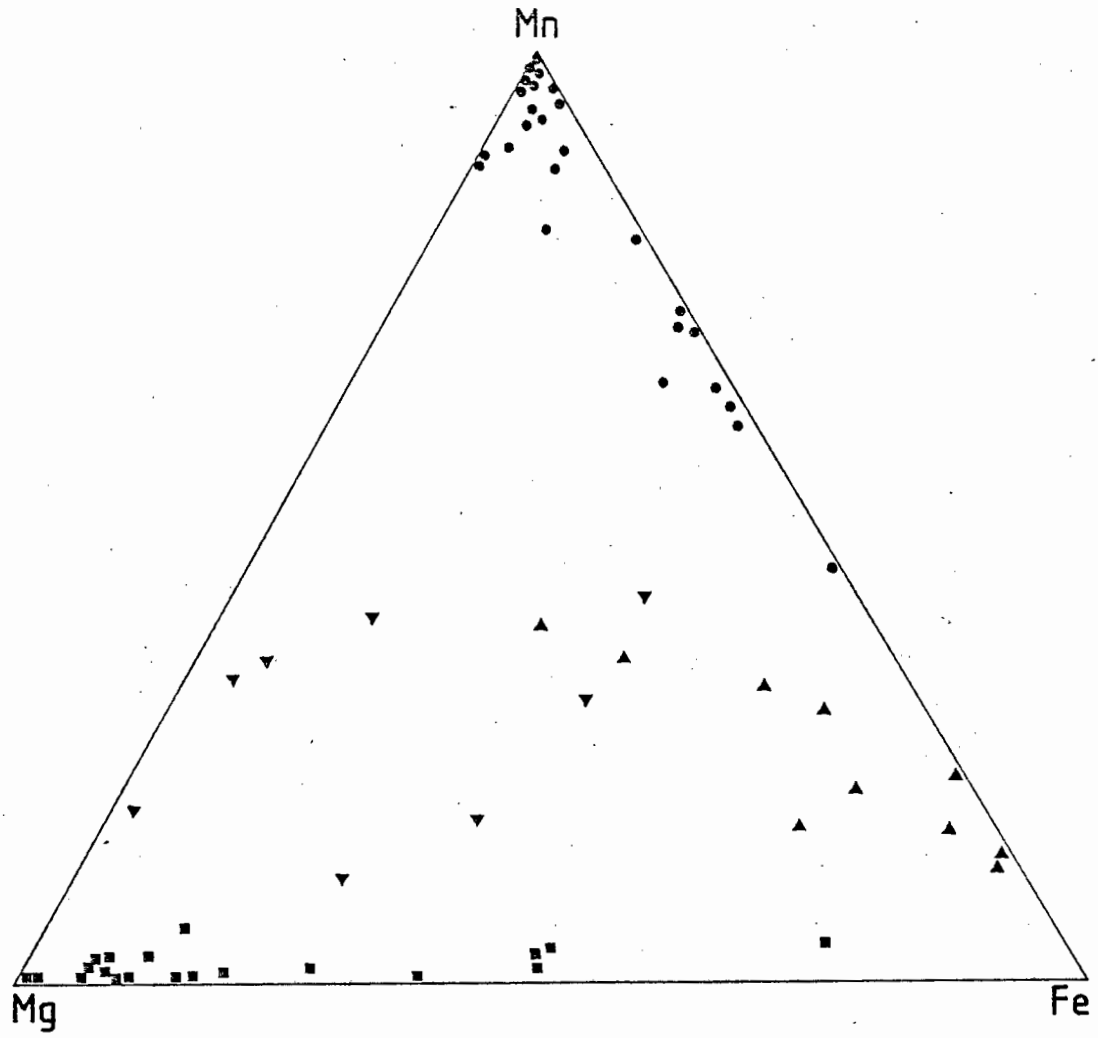

Fig. 31 – Cation variation in the olivine and melilite between total Mn (Mn^{2+} + Mn^{3+}), total Fe (Fe^{2+} + Fe^{3+}) and Mg. The glaucochroite solid-solution data (circles) are from this study and sources quoted in the text. Group A (inverted triangles) and B (triangles) melilite from this study and monticellite (squares) from quoted sources.

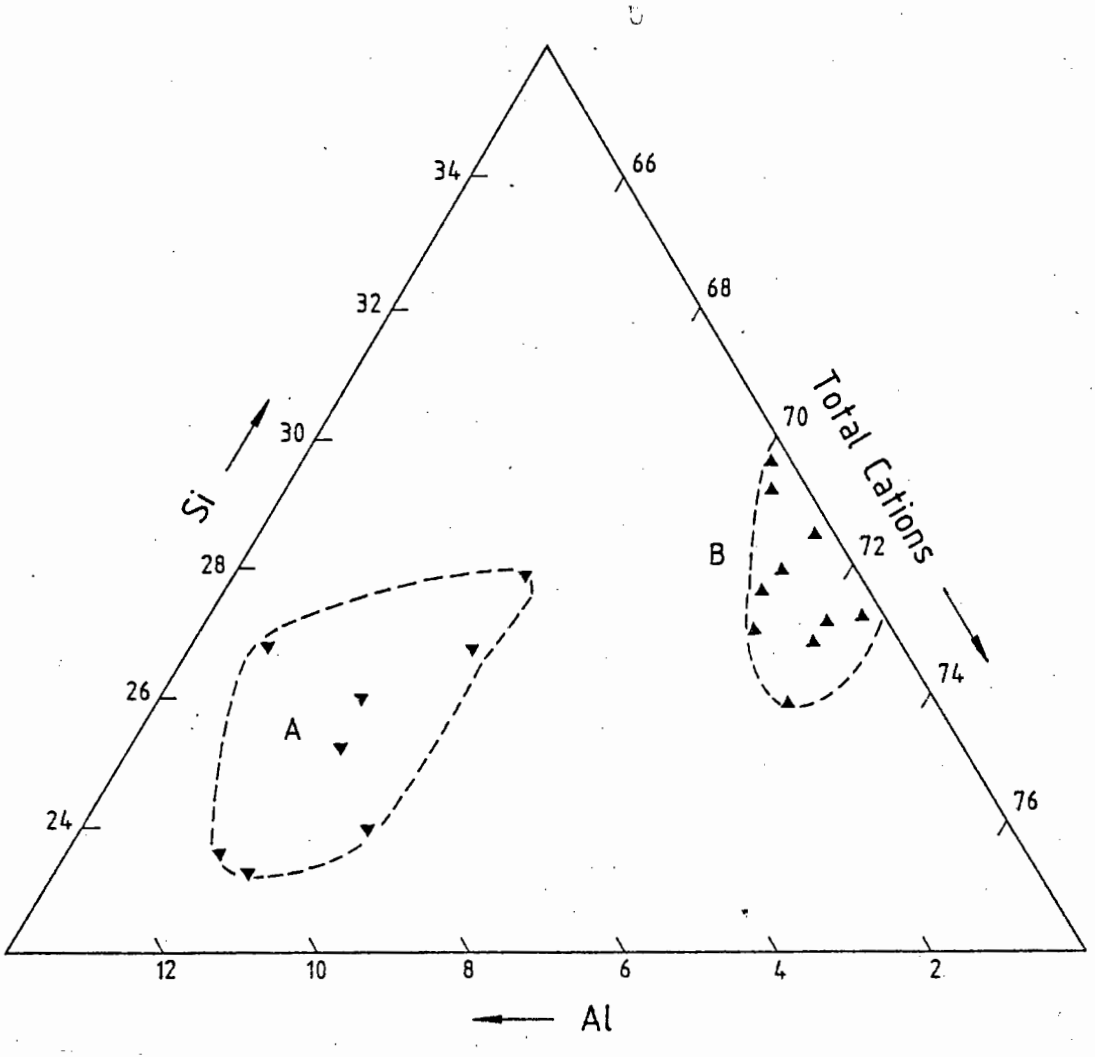

Fig. 32 - Variation between Si^{4+}, Al^{3+} and total cations showing the separation between the two melilite groups: A = akermanite and B = iron-rich akermanite.

Group A - high-Al, high-Mg, low-Fe melilite = akermanite

Group B - high-Fe, low-Al, low-Mg melilite = iron-rich akermanite

The deficiency in Ca (Theoretically 2 atoms per 7 Oxygen atoms) suggests a partial replacement by Mn^{2+}. The previous highest ferrous-iron content reported for melilite was 22 per cent $Ca_2FeSi_2O_7$ (Tilley 1929). In some of the grains analysed in this study the value is more than 90 per cent. A few of the analysed grains have a higher Mn than Fe content, indicating a possible Fe^{2+} = Mn^{2+} substitution (see Fig. 31). Seifert (1986), however, states that when the Z cations in the melilite structure are larger than Zn, the melilite structure collapses - $Ca_2Fe^{2+}Si_2O_7$ melilite can only form metastably and a $Ca_2MnSi_2O_7$ compound cannot be synthesised. The analyses do not show that the latter compound was formed in a pure end-member composition, but rather that the presence of the Fe in the mineral acted to stabilise the melilite structure.

4.4.3 FORMATION OF GLAUCOCHROITE AND AKERMANITE

Based on the mineralogy of the Treburland Mine in Cornwall, where bustamite-tephroite is the typical assemblage and glaucochroite is absent, Tilley (1946) suggested that glaucochroite would form by the reaction:

$$\text{bustamite} + \text{tephroite} + \text{calcite} = \text{glaucochroite} + CO_2$$

$$CaMnSi_2O_6 + Mn_2SiO_4 + 2CaCO_3 = 3CaMnSiO_4 + 2CO_2$$

at a higher temperature than the reaction

$$\text{rhodonite} + \text{calcite} = \text{bustamite} + \text{tephroite} + CO_2$$

$$2MnSiO_3 + CaCO_3 = CaMnSi_2O_6 + Mn_2SiO_4 + CO_2$$

Glasser (1961) studied the crystallisation of melts in the system Ca_2SiO_4-Mn_2SiO_4. This system has a minimum in the liquidus curve approximately midway between the tephroite and glaucochroite compositions, but shows complete solid solution between tephroite and an olivine even richer in Ca than the glaucochroite composition. Glasser suggested that a complete range of compositions from tephroite to olivine, more calcic than glaucochroite, might occur naturally. Burt (1972) suggested that glaucochroite could form by the gradual extension of tephroite to more calcic composition at high grades of metamorphism but at low to moderate pressures; whereas at high oxygen fugacities the solid solution was probably broken by tie lines between oxide phases and phases along the pyroxene join which would account for the separate occurrence of glaucochroite and tephroite at Franklin.

The system $CaFeSiO_4$-Fe_2SiO_4, investigated by Mukhopadhyay and Lindsley (1983), also has a minimum in the liquidus curve approximately midway between the two compositions. They inferred that this minimum indicated that there should be a

miscibility gap in the subsolidus region of the system. A similar gap probably exists between tephroite and glaucochroite.

In contrast to the other two occurrences, glaucochroite at Wessels Mine has a compositional variation along the kirschsteinite = glaucochroite solid-solution trend (Fig. 31) and in fact displays a range of compositions from $Glc_{100}Kir_0$ to $Glc_{45}Kir_{55}$. Its substitution of Mg for Mn is limited to 9 per cent of the monticellite molecule, well within the range given by Leavens and Dunn (1987) for Franklin glaucochroite. At Wessels Mine the glaucochroite is commonly associated with iron-rich akermanite, and in Figure 31 the compositional variation of the two minerals is plotted. A distinct feature is that the fields for glaucochroite (analyses from this study, Leavens and Dunn 1987, Pertsev and Laputina 1975, and Palache 1935), monticellite-kirschsteinite (analyses from Deer et al. 1982, Sahama 1961, Tilley 1929) and akermanite (this study) do not overlap. From textural relationships and the compositional differences it is inferred that the two phases are cogenetic. The presence of Al^{3+} ions in the crystal structure appears to have been the controlling influence as to which crystal structure was formed, with higher Al^{3+} resulting in the formation of melilite rather than olivine.

The limited solid solution of glaucochroite towards monticellite and tephroite found in this study, and the limited solid solution of tephroite with glaucochroite

reported by Palache (1935) and Leavens and Dunn (1987) show that glaucochroite did not form by extension of tephroite solid solution to calcic compositions, as suggested by Burt (1972) (Fig. 30).

4.5 WOLLASTONITE GROUP

Wollastonite and pectolite occur intimately associated in most assemblages in which they are present at Wessels Mine, and because of this, and the fact that they are isomorphous (Buerger 1956), they are discussed together.

Pectolite is commonly associated with sugilite in sugilite-rich parageneses, and is also found associated with wollastonite in the glaucochroite and the layered assemblages. It is usually white (rarely tinged with blue) in appearance and acicular in habit, and becomes green with increasing manganese content.

In appearance, the pectolite zone in the zoned paragenesis is similar to the wollastonite zone below it. This zone is distinguished by the presence of pectolite with minor wollastonite and acmite. Optically they can be distinguished by the greater birefrigence of the pectolite compared to the wollastonite. The pectolite and wollastonite zones are commonly developed wherever the andradite zone occurs, and reach thicknesses of up to 10 cm. The pectolite zone is thicker than the wollastonite zone, and the contact between the two is

abrupt but ragged, as is their contact with the andradite zone below. The wollastonite zone is whitish in colour and translucent in places. It consists predominantly of wollastonite with minor pectolite and diopside. The wollastonite and pectolite display a fibrous, very fine-grained vertical habit. The diopside, which forms only a few percent of the zone, occurs as small angular to subrounded grains, with a slight greenish tinge in thin section. The diopside can be distinguished from wollastonite by its much higher relief. Thin wollastonite veinlets cut across the zone and can be traced to the zones above and below.

4.5.1 PECTOLITE-SERANDITE

The pectolite compositions vary from pure pectolite to calcian serandite (Table 26). Pectolite associated with sugilite shows a wide variation in composition and is more manganese rich than pectolite from other assemblages. In Figure 33 the variation between CaO and MnO is shown. Although pectolite is commonly found in a very pure state, Mn^{2+} can replace Ca^{2+} forming an isostructural series to serandite, in which all the calcium has been replaced by manganese (Schaller 1955):

$$Ca_2NaH(SiO_3)_3 \longrightarrow Mn_2NaH(SiO_3)_3$$

Magnesium and iron may be present in small amounts, and aluminium can replace silicon. The reported content of directly determined structural water is often high, giving more than

	H1012	RDW2PX2	RDW11	RDW54	RDW53	RDW8	RDW3A25	RDW23	RDW3A2	RDW3B14	RDW3B13	RDW3A1A	RDW3A1B	RDW3B15
SiO2	52,43	51,65	55,61	52,29	53,50	52,75	52,93	53,35	53,03	54,04	53,87	52,16	52,70	52,92
Al2O3	-	-	0,99	0,14	0,24	0,15	0,12	0,16	0,13	0,21	0,12	0,15	0,13	0,16
FeO	-	-	0,77	0,09	1,71	0,13	0,14	0,15	0,13	0,19	0,22	0,14	0,17	0,20
MnO	-	0,14	0,17	0,20	0,26	0,25	0,31	0,37	0,37	0,45	0,77	1,57	1,99	2,29
MgO	-	-	2,68	0,64	0,08	0,08	0,06	0,09	0,08	0,10	0,17	0,07	0,09	0,25
CaO	34,17	39,49	27,65	32,88	33,91	32,96	33,65	32,33	33,22	32,49	32,86	33,43	32,06	31,93
Na2O	9,17	3,31	7,72	7,92	7,95	8,12	8,36	7,20	8,47	8,28	8,36	8,18	7,96	8,03
K2O	-	-	0,98	0,07	0,07	0,05	0,07	0,08	0,08	0,06	0,10	0,06	0,07	0,18
H2O*	4,23	5,43	3,43	5,77	2,28	5,51	4,36	6,27	4,49	4,18	3,53	4,24	4,83	4,04
STRUCTURAL FORMULAE ON THE BASIS OF 18 OXYGENS														
Si	5,738	5,567	5,996	5,595	5,986	5,658	5,764	5,644	5,762	5,861	5,905	5,722	5,720	5,801
Al^{3+}	-	-	0,126	0,018	0,032	0,019	0,015	0,020	0,017	0,027	0,016	0,019	0,017	0,021
Fe^{2+}	-	-	0,069	0,008	0,160	0,012	0,013	0,013	0,012	0,017	0,020	0,013	0,015	0,018
Mn	-	0,013	0,016	0,018	0,025	0,023	0,029	0,033	0,034	0,041	0,072	0,146	0,183	0,213
Mg	-	-	0,430	0,102	0,013	0,013	0,010	0,014	0,013	0,016	0,028	0,011	0,015	0,041
Ca	4,007	4,561	3,195	3,770	4,065	3,788	3,926	3,665	3,867	3,776	3,860	3,390	3,729	3,751
Na	1,946	0,692	1,614	1,643	1,725	1,688	1,765	1,477	1,784	1,741	1,777	1,740	1,765	1,707
K	-	-	0,135	0,010	0,010	0,007	0,010	0,011	0,011	0,008	0,014	0,008	0,010	0,025
OH	3,089	3,891	2,468	4,210	1,702	3,944	3,168	4,426	3,255	3,025	2,582	3,104	3,499	2,955

	S13S55	BIGSUG2	H10B	H1010	SMLSUG4	SMLSUG5	BIGSUG1	SMLSUG	V8L5	V8L6	H82	H812	H81	V8L7
SiO2	53,43	52,21	52,39	52,70	52,04	53,63	51,58	53,33	52,38	52,66	51,87	51,93	50,46	52,38
Al2O3	0,06	1,77	-	-	0,17	0,24	0,14	0,19	-	-	-	-	-	-
FeO	0,08	0,19	-	-	0,20	0,16	0,18	0,23	-	-	-	-	-	0,28
MnO	4,12	7,28	7,36	8,01	8,94	10,51	12,88	13,28	18,99	19,50	20,26	20,91	26,13	26,23
MgO	0,01	0,15	-	0,07	0,09	0,18	0,19	1,24	0,11	0,16	0,11	0,09	0,07	0,17
Cao	28,78	27,01	26,59	26,87	25,31	23,91	22,70	21,44	16,84	17,29	16,14	15,92	10,70	9,41
Na2O	7,30	7,77	6,87	9,21	7,73	7,95	8,06	8,33	6,53	6,04	7,75	7,77	7,28	8,64
K2O	-	0,11	-	-	0,08	0,23	0,07	0,24	-	-	-	-	-	-
H2O	6,22	3,51	6,79	3,14	5,44	3,19	4,20	1,72	5,14	4,35	3,86	3,34	5,37	2,89
STRUCTURAL FORMULAE ON THE BASIS OF 18 OXYGENS														
Si	5,684	5,788	5,586	5,911	5,675	5,992	5,769	6,105	5,800	5,888	5,880	5,932	5,692	6,061
Al^{3+}	0,008	0,231	-	-	0,022	0,032	0,018	0,026	-	-	-	-	-	-
Fe^{2+}	0,007	0,018	-	-	0,018	0,015	0,017	0,022	-	-	-	-	-	0,027
Mn	0,371	0,684	0,665	0,761	0,826	0,995	1,220	1,288	1,781	1,847	1,945	2,023	2,497	2,571
Mg	0,002	0,025	-	0,012	0,015	0,030	0,032	0,212	0,018	0,027	0,019	0,015	0,012	0,029
Ca	3,281	3,209	3,038	3,229	2,957	2,862	2,720	2,630	1,998	2,072	1,960	1,949	1,293	1,167
Na	1,506	1,670	1,420	2,003	1,634	1,722	1,748	1,849	1,402	1,310	1,703	1,721	1,592	1,938
K	-	0,016	-	-	0,011	0,033	0,010	0,035	-	-	-	-	-	-
OH	4,415	2,597	4,831	2,350	3,958	2,378	3,134	1,314	3,805	3,246	2,927	2,576	4,035	2,231

*Difference to 100% assumed to be H2O

TABLE 26. Microprobe analyses of pectolite-serandite from Wessels Mine.

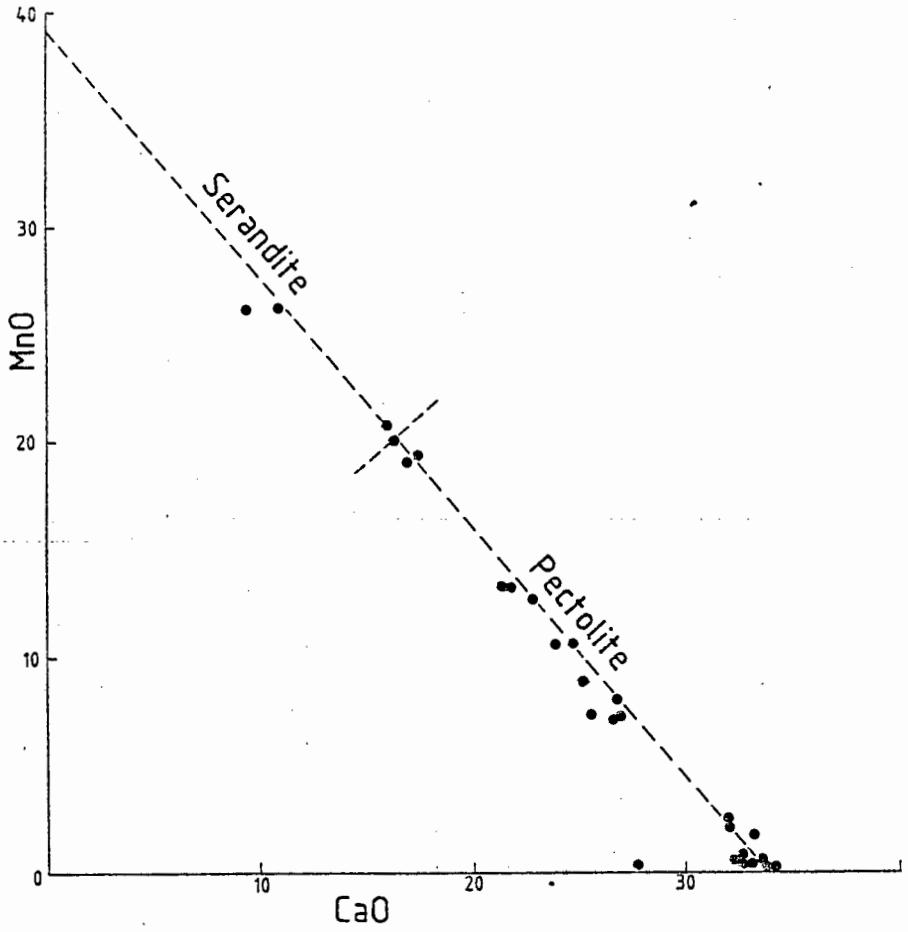

Fig. 33 - The theoretical MnO-CaO substitution trend (wt. per cent) between serandite and pectolite (long dotted line) with the range of compositions found in this study.

two OH ions on recalculating on the basis of 18(O,OH). Deer et al. (1978) show that in these cases the Z group is low, and the excess would appear to fit the formula

$$Na_2Ca_4Si_{6-m}O_{18}H_{2+4m}$$

similar to hydrogrossular. This might be the case with the Wessels Mine pectolites if the low totals are not due to analytical error.

4.5.2 WOLLASTONITE

Wollastonite is commonly fairly close in composition to $CaSiO_3$ although the wollastonite structure can accept considerable amounts of Fe and Mn, and lesser amounts of Mg, all replacing Ca. A maximum of 38 mol per cent $MnSiO_3$ can be accommodated in its structure (Albrecht and Peters 1975), and up to 10 per cent $FeSiO_3$ (Deer et al. 1978). The analyses in Table 27 show limited amounts of substitution for CaO, with maxima of 0,68 per cent MnO and 2,48 per cent MgO.

The analyses do, however, show a wide range in analytical totals, which may be partly due to the presence of water.

4.5.3 FORMATION

	RDW2A	RDW2P6	S4V7	RDW217	RDW2B	S4V6	RDW3A24	S4V10	RDW3A1	RDW21
SiO_2	49,78	50,23	50,11	49,86	50,87	49,32	49,21	50,23	48,14	48,58
Al_2O_3	-	-	-	-	-	-	-	-	0,35	-
FeO	-	-	-	-	-	-	-	-	0,25	-
MnO	0,23	0,68	-	0,23	0,22	-	0,14	-	0,36	0,19
MgO	1,51	-	-	2,48	0,70	-	-	-	0,53	-
CaO	47,84	47,83	48,00	44,52	44,81	47,02	46,54	45,39	43,29	44,83
Na_2O	-	-	-	-	1,41	-	-	-	0,96	-
K_2O	-	-	-	-	-	-	-	-	0,52	-
H_2O^*	0,64	1,26	1,89	2,91	3,40	3,65	4,11	4,38	5,60	6,41
STRUCTURAL FORMULAE ON THE BASIS OF 18 OXYGENS										
Si	5,766	5,778	5,710	5,574	5,594	5,506	5,464	5,524	5,266	5,244
Al^{3+}	-	-	-	-	-	-	-	-	0,045	-
Fe^{2+}	-	-	-	-	-	-	-	-	0,023	-
Mn	0,022	0,066	-	0,022	0,020	-	0,014	-	0,033	0,038
Mg	0,262	-	-	0,414	0,115	-	-	-	0,086	-
Ca	5,938	5,896	5,862	5,332	5,290	5,626	5,538	5,348	0,075	5,186
Na	-	-	-	-	0,301	-	-	-	0,204	-
K	-	-	-	-	-	-	-	-	0,073	-
OH	0,496	0,964	1,434	2,170	2,495	2,722	3,044	3,212	4,088	4,616

*Difference to 100% assumed to be H_2O, on the basis that since the bulk assemblage contains water, and since pectolite has a structural water component, the possibility exists that some water is being taken up by the wollastonite, which has a similar structure. It could also be due to poor sample surface, although care was taken to ensure optimum analysing conditions.

TABLE 27. Microprobe analyses of wollastonite from Wessels Mine.

Wollastonite is a common constituent of thermally metamorphosed impure limestone and in most cases is the result of the reaction

$$CaCO_3 + SiO_2 = CaSiO_3 + CO_2$$

(Harker and Tuttle 1956, Thompson 1971). Under water-free conditions, wollastonite is stable above 670 °C under CO_2 pressure corresponding to 1 000 atm. (Greenwood 1967). In CO_2-free conditions it is stable above 410 °C at a water pressure of 1 000 atm. (Buckner et al. 1960). According to Greenwood wollastonite is stable above 500 °C in fluid containing 10 mole per cent CO_2 and a fluid pressure of 1 000 atm. The formation temperature rises rapidly with increased mole fraction of CO_2.

4.6 PYROXENE

In Figure 34 the two distinct pyroxene species which occur in the assemblages under discussion at Wessels Mine, diopside and acmite, are shown.

4.6.1 ACMITE

Although the term acmite has generally been adopted to describe the $NaFe^{3+}Si_2O_6$ molecule, both aegirine and acmite have been used for pyroxene of approximately this composition. Aegirine is generally restricted to the green and black

crystals and acmite to the brown varieties (Deer et al. 1978). The preferred name for pyroxene of this composition is acmite (Fleischer 1987).

The acmite occurs mainly as pale to medium-green anhedral grains in the pectolite-rich layers, and as a dark orangy brown layer at the base of the layered assemblage in contact with manganese oxide minerals. Representative analyses of both types are given in Table 28 and plotted in Figure 34. The additional data points in Figure 34 are of analyses not presented here but occurring in the same assemblages.

Acmite shows a wide range in chemical composition but in most the main replacement is $NaFe^{3+}$ --> $Ca(Mg,Fe^{2+})$ (Deer et al. 1978). Sabine (1950) showed that Na varies directly with Fe^{3+}, Ca with Mg and Fe^{2+}, and that Ná and K vary inversely with Ca. The replacement of Si by Al in acmite is negligible. Acmite can take a small amount of Mn into its structure, with up to 6 per cent recorded (Klein 1966). The possible replacement trend observed in Figure 34, although based on a limited data set, shows that Fe^{3+} is replaced by Mn^{3+}, the oxidation state of which is assumed because of the trivalent state of iron in acmite and the high proportion of Mn^{3+} in the manganese ore.

4.6.2 DIOPSIDE

Colourless to pale-green diopside is found as small grains associated with the wollastonite-pectolite assemblages, and

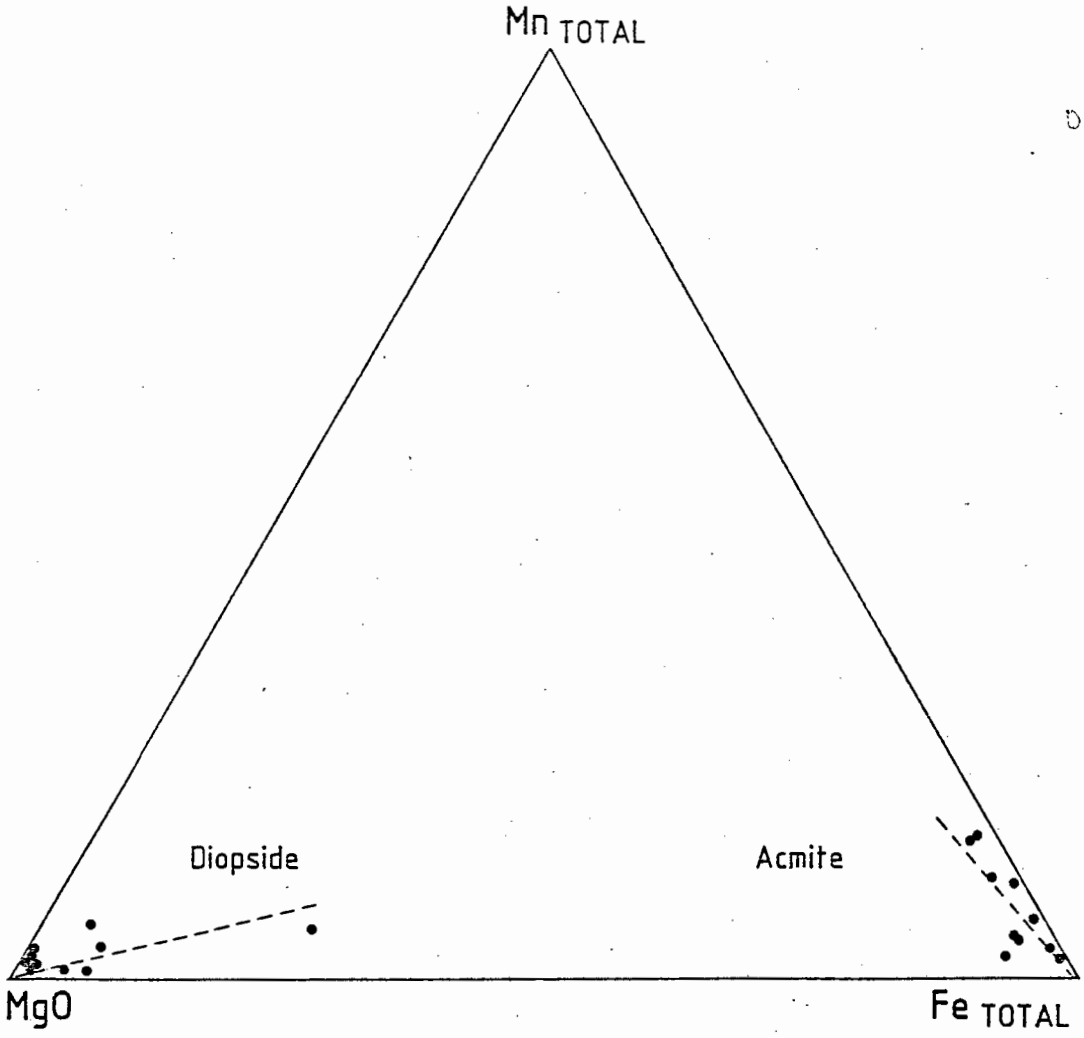

Fig. 34 - Oxide variation (wt. per cent) in the pyroxene showing limited Fe <==> Mn substitution in acmite (Fe apex) and Fe <==> Mg substitution in diopside (Mg apex).

	S13S6	S1357	RDW23a	RDW23b
SiO_2	52,27	52,36	51,50	51,20
Al_2O_3	0,07	0,04	0,84	2,45
Fe_2O_3	26,21	29,92	30,23	21,70
Mn_2O_3	4,73	2,21	1,22	0,61
MgO	0,74	0,24	0,24	1,29
CaO	0,91	0,46	3,68	11,26
Na_2O	13,42	14,00	11,84	10,71
K_2O	-	-	0,07	0,08
TOTAL	98,35	99,23	99,62	99,20
STRUCTURAL FORMULAE ON THE BASIS OF 6 OXYGENS				
Si	2,027	2,020	1,988	1,969
Al^{3+}	0,003	0,002	0,038	0,111
Fe^{3+}	0,765	0,869	0,878	0,625
Mn	0,140	0,065	0,040	0,020
Mg	0,043	0,014	0,014	0,074
Ca	0,038	0,019	0,152	0,464
Na	1,009	1,048	0,886	0,798
K	-	-	0,003	0,004
TOTAL	4,025	4,037	3,999	4,065

TABLE 28. Microprobe analyses of acmite from Wessels Mine.

colourless to light-brownish diopside is found in association with glaucochroite and melilite in the orange calc-silicate rock and associated with andradite, clinochlore and phlogopite in more leucocratic parageneses. The analyses in Table 29 show that substitutions in the diopside are limited to a small amount of Fe^{2+} and Mn^{2+} replacing Mg. The manganese content of the diopside increases proportionately to the amount of iron present, but the amounts of both are small (Fig. 34). Generally, a very low-average MnO content of 0,09 per cent is observed, although up to 1,9 per cent has been observed in manganoan diopside from manganese ores elsewhere (Roy 1971).

4.7 VESUVIANITE

Vesuvianite occurs as a thin greenish-brown layer above the pectolite zone in the layered assemblage. It has a smooth, irregularly undulating surface above and below, and where it occurs it forms a distinctive boundary between the pectolite and sugilite zones. It is sometimes associated with quartz. The vesuvianite layer is seldom more than 5 mm thick, is impersistent and found only where the layered assemblage is well developed.The analyses presented in Table 30 show that the vesuvianite composition is reasonably stochiometric, with a substantial amount of manganese present.

The formation of vesuvianite in the layered assemblage took

	RDW2PX1A	RDW2PX1B	RDW2PX3	RDW2PX5	H412	H44	V5321	H4	WM1A	RDW22	RDW2C	H4
SiO_2	54,85	55,17	54,99	55,35	54,28	53,69	53,42	53,76	48,63	52,09	51,20	54,
Al_2O_3	0,17	0,13	0,50	0,17	0,07	0,32	1,79	0,30	0,34	0,45	3,30	0,
FeO	0,46	0,97	0,35	1,32	0,32	1,23	0,38	0,88	5,59	0,26	0,33	0,
MnO	0,21	0,12	0,22	0,13	0,31	0,71	0,14	1,14	1,01	0,18	0,45	0,
MgO	18,63	18,25	19,07	18,26	18,55	17,25	20,77	17,64	15,25	19,96	22,96	19,
CaO	26,09	25,65	24,98	25,75	25,27	26,01	21,31	26,01	27,03	25,92	19,29	24,
Na_2O	0,23	0,34	0,17	0,34	0,08	0,08	0,11	-	0,11	0,08	0,08	0,
K_2O	-	-	0,35	-	-	0,05	1,40	-	0,08	0,06	0,11	0,
											SrO 0,70	
TOTAL	100,64	100,63	100,62	101,32	98,87	99,34	99,31	99,73	98,04	99,01	98,43	100,
					STRUCTURAL FORMULAE ON THE BASIS OF 6 OXYGENS							
Si	1,976	1,988	1,977	1,984	1,986	1,973	1,940	1,968	1,850	1,918	1,869	1,
Al^{3+}	0,007	0,006	0,021	0,007	0,003	0,014	0,077	0,013	0,015	0,020	0,142	0,
Fe^{2+}	0,014	0,029	0,010	0,039	0,010	0,038	0,012	0,027	0,181	0,008	0,010	0,
Mn	0,006	0,004	0,007	0,004	0,010	0,022	0,004	0,035	0,033	0,006	0,014	0,
Mg	1,000	0,980	1,022	0,976	1,011	0,945	1,124	0,962	0,879	1,095	1,249	1,
Ca	1,007	0,990	0,962	0,989	0,990	1,024	0,829	1,020	1,119	1,022	0,755	0,
Na	0,016	0,024	0,012	0,024	0,006	0,006	0,008	-	0,008	0,006	0,006	0,
K	-	-	0,016	-	-	0,002	0,065	-	0,004	0,003	0,005	0,
											Sr 0,015	
TOTAL	4,026	4,021	4,027	4,023	4,016	4,024	4,024	4,059	4,025	4,099	4,065	4,

TABLE 29. Microprobe analyses of diopside from Wessels Mine.

	RDW3A21	RDW3A22	STRUCTURAL FORMULAE BASED ON 78 OXYGENS		
SiO_2	38,71	36,91	Si	18,767	18,026
Al_2O_3	13,63	15,00	Al^{3+}	7,787	8,632
Fe_2O_3	1,22	1,33	Fe^{3+}	0,445	0,489
Mn_2O_3	3,92	4,27	Mn^{3+}	1,447	1,586
MgO	2,43	3,05	Mg	1,756	2,221
CaO	37,02	36,70	Ca	19,228	19,201
H_2O^*	3,07	2,74	OH	9,927	8,926
	$Ca_{19,23}(Al_{7,79}Mg_{1,76}Mn_{1,45}Fe_{0,45})_{11,44}Si_{18,77}O_{68,07}(OH)_{9,93}$				
	$Ca_{19,20}(Al_{8,63}Mg_{2,22}Mn_{1,59}Fe_{0,49})_{12,93}Si_{18,03}O_{69,07}(OH)_{8,93}$				

*Difference to 100% assumed to be H_2O

TABLE 30. Microprobe analyses of vesuvianite from Wessels Mine.

place at very low XCO_2 and high H_2O activities. The association of vesuvianite occurring between layers of mosaic-fabric quartz and wollastonite and pectolite is consistent with equilibrium in a system including CO_2 and H_2O. Reactions leading to the formation of wollastonite and vesuvianite were controlled by gradients in the chemical potentials of volatiles during metamorphism. Trommsdorff (1968) found from layered calc-silicate rocks at Claro in the Lepontine Alps that the above was true, and showed that the reaction

2 grossular + 2 diopside + 2 calcite + 2 H_2O

$Ca_3Al_2(SiO_4)_3$ $CaMgSi_2O_6$ $CaCO_3$

= 1 vesuvianite + 1 quartz + 2 CO_2

$Ca_{10}Mg_2Al_4[(OH)_4(SiO_4)_5(Si_2O_7)$ SiO_2

was operative. In Figure 35 it is shown that the lower the temperature, the smaller the XCO_2 has to be to form vesuvianite. Grossular and vesuvianite are almost identical in composition, the distinction being the presence of Mg and (OH) in vesuvianite. High CO_2 activity favours the formation of grossular, probably due to lowering of H_2O in the system. Vesuvianite is much more sensitive to compositional changes than to P_{H2O}–T variation, and forms at lower temperatures in a Ca- and Mg-rich, strongly alkaline environment (Ito and Arem 1970).

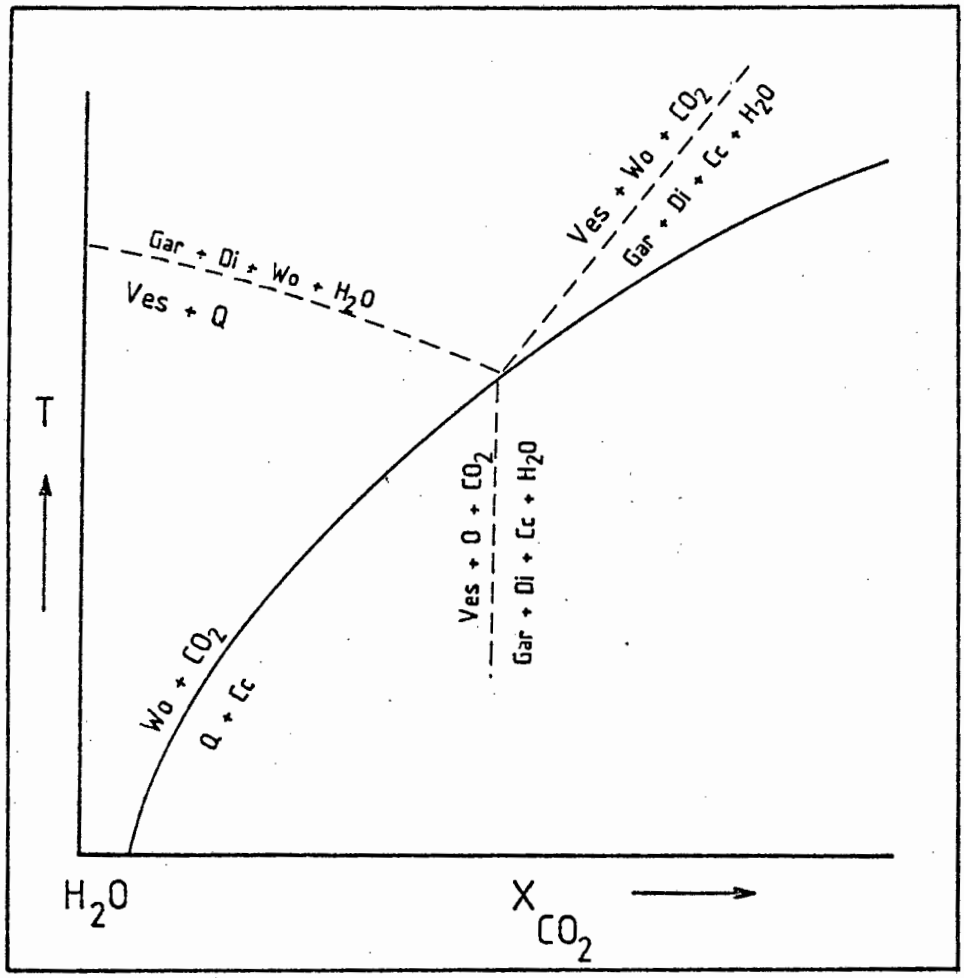

Fig. 35 - Hypothetical $T-XCO_2$ diagram for the system SiO_2-$(Al,Fe^{3+})_2O_3$-$(Mg,Fe^{2+})O$-CaO-CO_2-H_2O. The reaction at the top left marks the transition in the layered assemblage from the **Wo**llastonite + **Di**opside + **Gar**net to **Ves**uvianite + **Q**uartz. (after Trommsdorff 1968).

4.8 QUARTZ

Pure quartz is found as patches at the top of the layered assemblage, commonly associated with iron-rich sugilite and hematite. It also occurs as a zone in the layered assemblage, above the pectolite zone. In Figure 6 it can be seen that the quartz displays a pronounced polygonal texture with the individual grains up to 0,5 mm in size, which gives the rock a sugary appearance in hand specimen.

5 AGE OF METAMORPHISM

Rb-Sr and Pb isotopic studies were undertaken on the sugilite in an attempt to determine its age and provide information on its genesis. In addition Pb-isotopic analyses were made of galena which is found in fissures at N'chwaning and post-dates the sugilite formation. This galena is thought to represent the last stage of the hydrothermal event which caused the development of the metamorphic minerals at Wessels and N'chwaning Mines. Wessels and N'chwaning are adjacent mines and share the same orebody, and it is assumed that the information obtained from the galena is applicable two both mines, as would be the case with the sugilite which has only been found at Wessels. Rb-Sr and Pb isotopic analyses were also performed on the fine-grained bostonite dykes which could have played a part in the formation of the sugilite and associated minerals.

5.1 SAMPLING AND ANALYSIS

This chapter is a summary of work by Dr F. Walraven and R. Dixon. The isotopic determinations were performed by the first author at the geochronology laboratory of the Bernard Price Institute of the University of the Witwatersrand, Johannesburg. The analytical procedures are described in another publication (in preparation). All the mineral samples, as well as the geological descriptions, were provided by the second author. The bostonite dykes were sampled underground at

Wessels Mine and an attempt was made to collect samples that were as fresh as possible, although the rock proved to be highly altered.

5.1.1 SUGILITE Rb-Sr ISOTOPES

Six samples of sugilite from various parageneses and localities in Wessels Mine were examined. An attempt was made to obtain pure material, but due to the extremely fine-grained nature of some of the samples some intergrowth with other mineral phases was present in the samples. Regression of the data yielded an errorchron with an apparent age of 1 351±291 Ma and an initial $^{87}Sr/^{86}Sr$ ratio of 0,7098±0,0005.

5.1.2 SUGILITE Pb ISOTOPES

The above-mentioned six samples were also analysed for their Pb isotopic compositions. The sugilite examined contained no detectable U or Th, so its Pb isotopic composition should reflect its age of formation, 1 270±30 Ma. Very little spread in the Pb isotopic composition was found.

5.1.3 GALENA Pb ISOTOPES

Clean euhedral galena crystals from a fissure in section 28 South in N'chwaning 2 Mine were used. The Pb isotopic compositions showed a very small spread, similar to that found in the sugilite, and, in fact, they are indistinguishable within

analytical uncertainty. This similarity points strongly to a genetic relationship between the two, at least in terms of the source of the lead and time of formation of the minerals. An age of 1 270±20 Ma was obtained for the galena.

5.1.4 BOSTONITE Rb-Sr ISOTOPES

Rb-Sr isotopic analyses were performed on nine samples, six from the main dyke trending east-west through the mine, and three from a smaller dyke with a north-south strike. A considerable amount of scatter in the data was found and the errorchron obtained suggests that the scatter is, to a large degree the result of geological processes such as hydrothermal alteration, which is evident from the rather altered nature of the dykes. Although the data points do not define an isochron, they do conform moderately well to a 1 350-Ma reference line. The most deviation from this line is in the most altered samples. The data do not rule out the possibility of isotopic resetting of bostonite of an older age by a circa 1 350-Ma event.

5.1.5 BOSTONITE Pb ISOTOPES

The trend shown by the bostonite Pb does not coincide with the galena and sugilite data. It is unlikely to have resulted from radiogenic evolution of the bostonite Pb. It is considered to represent mixing between partly evolved lead from the bostonite dykes and the lead involved in the galena and

sugilite formation, combined with subsequent evolution of the Pb isotopic composition (Walraven and Dixon in prep).

5.2 DISCUSSION

The ages indicated by the analyses are all in the region of 1 300 Ma and are considered to point to an event at about that time.

TABLE 31. ISOTOPE AGES FROM WESSELS AND N'CHWANING MINES

Sugilite	1 350 ± 269 Ma	Errorchron from Rb-Sr data
Sugilite	1 270 ± 30 Ma	Pb-Pb
Galena	1 270 ± 20 Ma	Pb-Pb
Bostonite	1 350 Ma	Rb-Sr whole rock data

In the case of the sugilite it is considered that the age obtained reflects the age of formation of the mineral. It is considered highly unlikely that isotopic homogenisation of the sugilite from widely separated areas in the mine took place. The close correspondence between the isotopic compositions of the sugilite lead and that of the galena from N'chwaning strongly suggests that the formation of the two minerals took place at the same time and that the lead for both was derived from the same source.

The isotopic data obtained for the bostonite-dyke samples show clear evidence of post-crystallisation disturbance. The coincidence of the Rb-Sr data points to the 1 300 Ma reference line reflects this event, and the spread of the Pb data supports this as they cannot represent the effects of isotopic evolution of the bostonite lead through the decay of uranium, but most probably indicate mixing between isotopically evolved lead in the bostonite with lead being introduced during the sugilite and galena mineralisation.

This implies that the bostonite was already emplaced when the galena and sugilite were formed and must therefore be older than 1 300 Ma. The bostonite therefore most probably played no part in the formation of the sugilite, galena and associated minerals, nor is it likely to have been responsible for the upgrading of the manganese ore.

6 METAMORPHIC CONDITIONS

The presence of many unusual and rare minerals in the Wessels, N'chwaning and Black Rock Mines is indicative of unusual conditions of formation. Many of the minerals encountered are either unique to the Kalahari Manganese Field or described from only one or two other localities in the world (Von Bezing et al. in press).

Among these assemblages are those that have counterparts from a wide range of radically different origins. These vary from the regionally metamorphosed Franklin, New Jersey orebody (glaucochroite + wollastonite + andradite) (Palache 1935), to ipnitically metamorphosed volcanic rocks from Zaire (kirschsteinite + Fe-akermanite) (Sahama 1961) and the hydrothermal manganese deposits at Tachgagalt, Morocco (henritermiérite + gaudefroyite + jouravskite) (Gaudefroy et al. 1969).

The metasomatic zoning sequences such as those observed at Wessels Mine are similar to those of exoskarns which can be explained by simple diffusion models that assume simultaneous development of all major zones, as a result of chemical-potential gradients set up between iron- and silica-rich solutions and carbonate host rocks (Burt 1974). There is a general tendency for the minerals to be segregated into more or less monominerallic bands around the presumed passageways for the skarn-forming solutions, which in the case of Wessels

Mine consist of sedimentary contacts, cross-cutting fractures and faults. The rock which was replaced by these sugilite and zoned parageneses is thought to have been originally a carbonate-rich rock type. The variation in the width of these assemblages at Wessels mine would reflect the local variation in the porosity and permeability of the rock.

6.1 DEPTH AND PRESSURE OF FORMATION

As shown in Chapter 2, the maximum thickness of rock above the Hotazel Member could have been 4 500 m, which would give a load pressure of approximately 1 kbar. With erosion and other processes, the figure could be much less. At present the depth of the manganese ore at Wessels Mine is approximately 400 m.

6.2 ORIGINAL COMPOSITION OF THE ROCK

This has been covered in Chapter 2, but, to summarise, the major components of the iron formation in the Hotazel Member are calcium, iron, magnesium and manganese carbonates, hematite, braunite and chert, with some minor magnetite in places. Trace amounts of alkalis and other elements are also found. These are the results of a period of chemical sedimentation in a shallow marine environment, with the majority of the deposited material originating from a volcanogenic source area.

6.3 SEQUENCE OF METAMORPHIC MINERAL FORMATION

The minerals examined in this study are found in a restricted paragenesis in the Wessels Mine. The localisation of the zoned assemblages, which are often terminated abruptly upwards, is thought to be due to the presence of siliceous layers directly above the carbonate-rich layers in which the sugilite formed. These acted as temporary barriers to the hydrothermal fluids, where increasing fluidisation and concentration of the mobile elements, in the space previously occupied by the carbonate-rich host rock, enhanced the formation of the zoned assemblages. The following sequence of events is suggested starting with the original fine-grained pisolith-bearing rock:

i) The groundmass recrystallises to a mixture of andradite, diopside, wollastonite and pectolite, with glaucochroite, akermanite, diopside and wollastonite forming mainly in the lighter coloured blebs (originally pisoliths).

ii) The groundmass in the orange layer becomes more coarsely grained and the glaucochroite and akermanite alter to hydrogarnet; along fractures hydrogarnet and sheet silicates form.

iii) Above the orange layer, either in contact with it or some centimetres away in more hematite- and chert-rich

layers, acmite forms and this in turn is succeeded by sugilite.

iv) With increasing amounts of fluid, which contains large quantities of alkalis, the orange-coloured calc-silicate rock becomes stratified into mineralogically distinct layers and the sugilite development now produces patches of purple rock which is alkali rich and very hydrous.

v) At this stage of development the whole assemblage starts to exhibit a swirled texture at the top, contacts between individual mineral zones are sharp but display a raggedness oriented in the direction of the swirled texture, indicating a very fluid-rich environment.

vi) In a few places the sugilite part of the zoned assemblage becomes vuggy with the development of large sugilite crystals on pectolite, some of which are associated with large euhedral hydroxylapophyllite and quartz crystals.

Paragraph (i) above is classified as Stage 1 of the metamorphic event, which is followed by Stage 2 [(iii) to (v)]. The sugilite-cemented breccia illustrated in Figure 5 is contemporaneous with the formation of the sugilite and may be an indication of rupture of the rock through the agency of a fluid under pressure, and is further evidence of the very

hydrous conditions prevailing at this stage. The third and last stage which is beginning in (vi) is widespread throughout Wessels and N'chwaning Mines. It is distinguished by the formation of many varied silicate, sulphate, hydrate, sulphide, borate, fluoride, phosphate and carbonate minerals (Wilson and Dunn 1978; Dixon 1986; Von Bezing et al. in press).

6.4 DISCUSSION

The zones of the assemblage under discussion are terminated by sharp boundaries both mineralogically and chemically, while the composition of the mineral species within each zone remains relatively constant within that zone. These characterisrics are distinctive of infiltration metasomatic zoning (Korzhinskii 1970) in which irreversible reactions are effected at sharp replacement fronts, while the solution between them is in equilibrium with the minerals of the rock. This zoned assemblage is distinctive of Stage 2 of the metamorphism. In Stage 1, however, mineral compositions are heterogeneous, and a proportion of the minerals contain divalent iron and manganese, in contrast to their predominantly trivalent nature in Stage 2.

6.4.1 STAGE 1

In terms of solid solution with Ca^{2+} in skarn minerals, Mn^{2+} exhibits the highest degree, Fe^{2+} somewhat less, and Mg^{2+} the

least. Although most decarbonation reactions in the Mg system and to a lesser extent in the Fe system involve minerals that are close to being pure substances, most in the Mn system involve minerals that are solid solutions. Because of the similar ionic radii of Mn^{2+} and Ca^{2+}, formation of minerals in the Ca-Mn-Si skarn system occurs at lower temperatures than related minerals in the analogous system with Fe or Mg (Burt 1972). In comparison with the minerals of the later stages, the initial olivine and melilite display large amounts of solid solution between divalent cations, although the intense orange and red colours of these minerals and the presence of andradite indicate that a trivalent component was present, which according to Seifert (1974) would be the case at the high fO_2 neccessary for the formation of iron-rich akermanite.

In Stage 1 with prograde metamorphism the fluid coexisting with the original carbonate-silicate iron formation will be buffered to moderate or high XCO_2 as the reaction

carbonate + quartz --> silicates + CO_2

proceeds. The presence of olivine is an indication of the presence of such a CO_2-rich fluid. In iron formation the metamorphism of a wide range of primary mineral assemblages will lead to olivine-bearing assemblages, indicating that such metamorphism is accompanied by reduction, which is an artefact of the buffering reaction (Frost 1979). fO_2 can be buffered over many orders of magnitude without changing the abundance

of any of the solid phases or the composition of the fluid phase. However, if the fluid phase were externally controlled, the final assemblage would be dependant upon the fO_2 of the incoming fluid. The formation of hydrogarnet from olivine and melilite, and as a primary mineral lining small cracks, in the orange layer, is evidence of a cessation of CO_2-producing reactions coupled with a greater amount of infiltrating H_2O-rich fluids. Hsu (1980) states that at $P_{H2O} \leq$ 1kbar, any occurrence of hydrogarnet may be used as a temperature indicator setting the maximum temperature of formation around or even below 400 °C. Christie (1961) showed that the decomposition products of akermanite-gehlenite in a hydrothermal environment produced the assemblage

vesuvianite + wollastonite + diopside + hydrogarnet

above 450 °C, and that below this the products were

diopside + xonotlite + hydrogarnet.

Additionally, the presence of pectolite, clinochlore and phlogopite shows that this fluid was rich in alkalis. Frost (1979) has shown that hydrous Fe-silicate assemblages are stable only with extremely H_2O-rich fluids, and that with prograde metamorphism the silicates formed in the above reaction would break down as the fluid became H_2O-enriched.

6.4.2 STAGE 2

Amphibole-rich assemblages are commonly considered to have originated under high P_{H2O} conditions, and the assemblage hematite + quartz is only stable at high fO_2 (see Fig. 36). Sugilite occurs in association with both amphiboles and with polygonal quartz and hematite where the zoned assemblages are well developed. It has been shown that osumilite-type structures nucleate with ease in the presence of liquid over a wide range of chemical composition, under experimental conditions of low pressure and short time not dissimilar to those which must have obtained in a volcanic environment (Chinner and Dixon 1973, Abraham et al. 1983).

James (1955) suggested that the gradual increase of grain size of microcrystalline chert to quartz could be used as an indicator of metamorphic grade in iron formations. He noted that in low metamorphic grade (chlorite and biotite facies) SiO_2-rich assemblages, the grain size of quartz tended to be less than 0,10 mm, and with increasing time and metamorphic grade this gradually enlarged to a maximum of more than 0,20 mm. Klein (1973) showed that correlation of SiO_2 grain size with metamorphic grade is possible in silica-rich rocks that have undergone at least chlorite-facies metamorphism. Severe heterogeneity in quartz grain sizes does occur, and it is

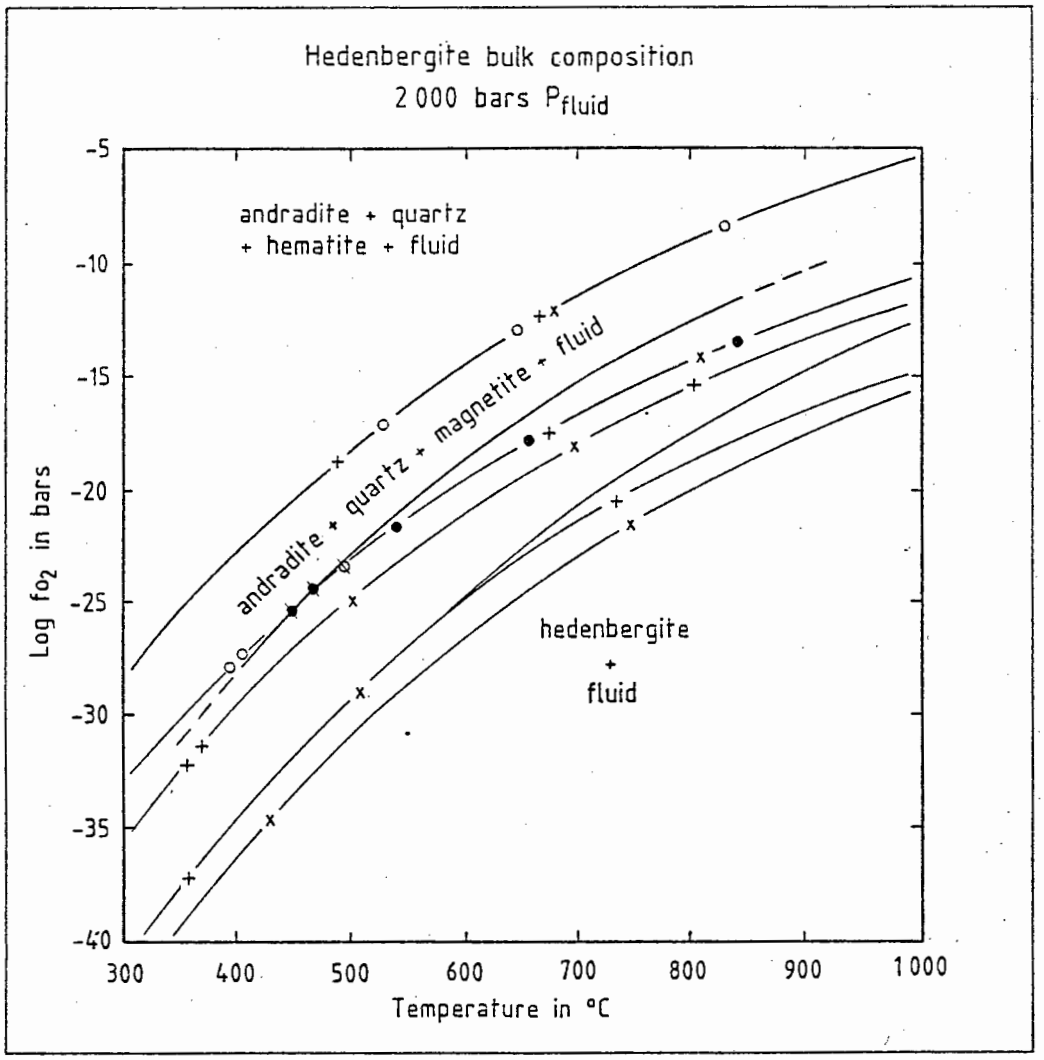

Fig. 36 - Log f_{O2}-T diagram for the hedenbergite bulk composition + excess H_2O at 2kbar P_{fluid}. Symbols indicate starting materials as follows: (●) indicates reversals of the reaction hedenbergite = andradite + quartz + magnetite + O_2, (+) reduced iron oxide starting mix, (×) oxidised iron oxide starting mix, and (⊗) indicates that no reaction took place. From Gustafson (1974).

possible that SiO_2-rich units saturated with H_2O would recrystallise more easily and to larger grain sizes than those which behaved as impermeable and less hydrous systems.

A very high fO_2 is generally manifested by the presence of hematite, and the results of this are the production of Fe^{3+} from Fe^{2+} and the depletion of the amount of Fe^{2+} available to form silicates. In the case of the second stage of metamorphism at Wessels Mine the effect for manganese is similar. This resulted in the production of diopside instead of hedenbergite or johannsenite, phlogopite instead of biotite, and so forth.

The assemblage hematite + andradite found in this study has also been reported from prehnite-pumpellyite facies metavolcanic rocks from New Zealand (Coombs et al. 1977) and this is interpreted to indicate that the metamorphic fluid prevailing during the crystallisation of the andradite was H_2O-rich with X_{CO2} lower than 0,02 (Taylor and Liou 1978), and similarly the hydroandradite described by Peters (1965) indicates a very H_2O-rich metamorphic fluid.

The introduction of the andradite component into the grossular garnet decreased the temperature of formation for grandite garnet and expands the stability field towards both higher and lower temperatures as well as more CO_2-rich environments at higher temperature. With decreasing fO_2 the stability limit of andradite in quartz-bearing calcareous rocks is significantly

decreased and hedenbergite may become an important phase (Gustafson 1974; Liou 1974). Taylor and Liou (1978) have shown experimentally in the hydrothermal synthesis of andradite in the system Ca-Fe-Si-C-O-H that the amount of Fe^{2+} in andradite is directly proportional to the fO_2. With decreasing fO_2 the amount of Fe^{2+} in the andradite increases.

As seen from the assemblages involving andradite, coexisting minerals containing divalent cations do not contain appreciable amounts of Fe^{2+}, so it can be assumed that the fO_2 was high enough for all the Fe^{2+} originally in the system to be oxidised to Fe^{3+}. In addition, the presence of large amounts of Mn^{3+} is additional proof that when the andradite formed fO_2 was very high indeed.

The transition from Stage 1 to Stage 2 may be represented by the following

$$3CaMn^{2+}SiO_4 + H_2O \longrightarrow (Ca,Mn)_3Mn^{3+}{}_2(SiO_4)_n(H_4O_4)_{3-n}$$

glaucochroite group HM henritermiérite

With increasing temperature and fluid influx, henritermierite in turn breaks down, with the Mn^{3+} taken up in sugilite and andradite and other silicate phases.

7 CONCLUSIONS

According to Zharikov (1970) the development of calcareous skarns requires the participation of post-magmatic hydrothermal solutions. The magmatism needed can possibly be found in the presence of the bostonite dykes which are intrusive into the Voëlwater Jasper Formation. The only observed contact-metamorphic effect, however, is the development of a narrow aureole of jacobsite around the intrusion (De Villiers 1983), and the results of the isotopic study discussed in Chapter 5 would seem to preclude this possibility.

The delimitation of Kleyenstüber (1984) of a widespread hydrothermal event in the northwestern portion of the Kalahari Manganese Field, the isotopic study by Walraven and Dixon (in prep), and the results of this study indicate that at around 1 300 Ma a widespread hydrothermal event affected the Kalahari Manganese Field, reaching a maximum of around 450 °C in the Wessels, N'chwaning and Black Rock area. This had the effect of decarbonating portions of the Hotazel Member to the northwest, thus upgrading the Mn content of the ore and producing a wide range of rare minerals and unusual mineral assemblages. The presence of the zoned assemblage and the extent of the hydrothermal event presuppose a magmatic source for the heat generated. At present there is little evidence to establish the nature of this presumed magmatic source.

8 REFERENCES

ABRAHAM, K., GERBERT, W., MEDENBACH, O., SCHREYER, W. and HENTSCHEL, G., 1983. Eifelite, $KNa_3Mg_4Si_{12}O_{30}$, a new mineral of the osumilite group with octahedral sodium: Contr. Mineral. Petrol., 82, p 252-258.

AINES, R.D. and ROSSMAN, G.R., 1984. The hydrous component in garnets: pyralspites: Am. Mineral., 69, p 1 116-1 126.

ALBRECHT, J. and PETERS, T.J., 1975. Hydrothermal synthesis of pyroxenoids in the system $MnSiO_3$-$CaSiO_3$ at Pf = 2 kbari Contr. Mineral. Petrol., 50, p 241-246.

AUBRY, A., DUSAUSOY, Y., LAFFAILLE, A. and PROTAS, J., 1969. Détermination et étude de la structure cristalline de l'henritermiérite, hydrogrenat de symétrie quadratique: Bull. Soc. Fr. Minéral. Cristallogr., 92, p 126-133.

BANK, H., BANERJEE, A., PENSE, J., SCHNEIDER, W. and SCHRADER, W., 1978. Sogdianite - ein neues Edelstein mineral?: Zeit. Deut. Gemmol. Ges., 27, p 104-105.

BAYLISS, P., 1975. Nomenclature of the trioctahedral chlorites: Can. Mineral., 13, p 178-180.

BENCE, A. E. and ALBEE, A. L., 1968. Empirical correction factors for the electron microanalysis of silicates and oxides: J. of Geol., 76, p 382-403.

BEUKES, N.J., 1980. Suggestion towards a classification of and nomenclature for iron-formation: Trans. geol. Soc. S. Afr., 83, p 285-290.

_____, N.J., 1983. Palaeoenvironmental setting of iron-formation in the depositional basin of the Transvaal Supergroup, South Africa in Developments in Precambrian Geology 6 - Iron-formation: Facts and problems (A.F. Trendall and R.C. Morris, eds): Elsevier, Amsterdam, p 131 - 209.

BUERGER, M. J., 1956. The rearrangement of atoms in crystals of the wollastonite group of metasilicates: Proc. Nat. Acad. Sci. USA, 42, p 113 - 116.

BIRKETT, T.C. and TRZCIENSKI, W.E., 1984. Hydrogarnet: multi-site hydrogen occupancy in the garnet structure: Can. Mineral., 22, p 675-680.

BONATTI, E., KRAEMER, T. and RYDELL, H.S., 1972. Classification and genesis of submarine iron - manganese deposits in Ferromanganese deposits of the ocean floor (D.R. Horn, ed): National Science Foundation, Washington, D.C., p 159-166.

BUCKNER, D.A., ROY, D.M. AND ROY, R., 1960. Studies in the system CaO - Al_2O_3 - SiO_2 - H_2O. II. The system $CaSiO_3$ - H_2O: Am. J. Sci., 258, p 132-147.

BUNCH, T. E. and FUCHS, L., 1969. Yagiite, a new sodium-magnesium analogue of osumilite: Am. Mineral., 54, p 14-18.

BURT, D.M., 1972. Decarbonation sequence in the system CaO - MnO - SiO_2 - CO_2: Yb. Carnegie Institn, 71, p 427-433.

____, D.M., 1974. Metasomatic zoning in Ca - Fe - Si exoskarns in Geochemical transport and kinetics (A.W. Hoffman, B.J. Giletti, H.S. Yoder and R.A. Yund, eds): Pub. Carnegie Instn., 634, p 287-293.

ČERNY, P., HAWTHORNE, F. C. and JAROSEWICH, E., 1980. Crystal chemistry of milarite: Can. Mineral., 18, p 41-57.

CHINNER, G.A. and DIXON, P.D., 1973. Irish osumilite: Min. Mag., 39, p 189-192.

CHRISTIE, O.H.J., 1961. On sub-solidus relations of silicates. I. The lower breakdown temperature of akermanite gehlenite mixed crystal series at moderate water pressure: Norsk Geologisk Tids-skrift, 41, p 255-269.

CLARK, A.M., FEJER, E.E., BEARNE, G.S., DIN, V.K. AND COUPER, A.G., 1980. Additional data on sugilite: Min. Mag., 43, p 947-949.

COOMBS, D.S., KAWACHI, Y., HOUGHTON, B.F., HYDEN, G., PRINGLE, I.J. and WILLIAMS, J.G., 1977. Andradite and andradite - grossular solid solutions in very low grade regionally metamorphosed rocks in southern New Zealand: Contrib. Mineral. Petrol., 63, p 229-246.

DEER, W.A., HOWIE, R.A. and ZUSSMAN, J., 1978. Rock-forming minerals - 2nd ed. Vol. 2A: Single-chain silicates: Longmans, London, 668p.

_____, 1982. Rock-forming minerals - 2nd ed. Vol. 1A: Orthosilicates: Longmans, London, 919p.

DE VILLIERS, J.E., 1983. The manganese deposits of Griqualand West, South Africa: some mineralogic aspects: Econ. Geol., 78, p 1 108-1 118.

DE VILLIERS, P.R., 1970. The geology and mineralogy of the Kalahari manganese field north of Sishen, Cape Province: Mem. geol. Surv. S. Afr., 59, 84p.

DIXON, R.D., 1985. Sugilite and associated minerals from Wessels mine, Kalahari manganese field: Trans. geol. Soc. S. Afr., 88, p 11-17.

_____, 1986. Metamorphism in the Kalahari manganese field: Ext. Abstr. Geocongress '86 geol. Soc. S. Afr., p 505-508.

DODD, R. T., 1973. Minor element abundances in olivines of the Sharps (H-3) achondrite: Contr. Mineral. Petrol., 42, p 159-167.

DODD, R. T., VAN SCHMUS, W. R. and MARVIN, U. B., 1965. Merrihueite, a new alkali-ferromagnesian silicate from the Mezo-Madaras Chondrite: Sci., 149, p 972-974.

DUNN, P.J., BRUMMER, J.J. and BELSKY, H., 1980. sugilite a second occurrence: Wessels mine, Kalahari manganese field, Republic of South Africa: Can. Mineral., 18, p 37-39.

_____, ROUSE, R. C., CANNON, B. and NELEN, J. A., 1977. Zektzerite: A new lithium sodium zirconium silicate related to tuhualite and the osumilite group: Am. Mineral., 62, p 416-420.

DUSMATOV, V. D., YEFIMOV, A. F., KATAYEVA, Z. T., KHOROSHILOVA, L. A. and YANULOV, K. P., 1968. Sogdianite, a new mineral: Dokl. Acad. Sci. USSR, Earth Sci. Sec., 182, p 137-139.

EIBSCHUTZ, M. and GANIEL, U., 1967. Mössbauer studies of Fe^{2+} in paramagnetic fayalite (Fe_2SiO_4): Solid State Commun., 5, p 267-270.

FLEISCHER, M., 1987. Glossary of mineral species - 5 ed: Mineralogical Record Inc., Tucson, 227p.

FORBES, W.C., BAUR, W.H. and KHAN, A.A., 1972. Crystal chemistry of milarite-type minerals: Am. Mineral., 57, p 463-472.

FRENTRUP, K.R. and LANGER, K., 1981. Mn^{+3} in garnets: optical absorption spectrum of a synthetic Mn^{3+}-bearing silicate garnet: Mh. N. Jb. Miner., 6, p 245-256.

FRICK, C., 1986. The mineralogy and geochemistry of the banded ironstones in the Griqualand West and Olifantshoek Sequences: Ext. Abstr. Geocongress '86 geol. Soc. S. Afr., p 513-517.

FRONDEL, C. and BAUM, J.L., 1974. Structure and mineralogy of the Franklin zinc - iron - manganese deposits, New Jersey: Econ. Geol., 69, p 157-180.

_____. and KLEIN, C., 1965. Exsolution in franklinite: Am. Mineral., 50, p 1 670-1 680.

FROST, B.R., 1979. Metamorphism of iron-formation: parageneses in the system Fe - Si - C - O - H: Econ. Geol., 74, p 775-785.

FUCHS, L.H., FRONDEL, C. and KLEIN, C., 1966. Roedderite, a new mineral from the Indarch meteorite: Am. Mineral., 51, p 949-955.

GAUDEFROY, C., ORLIAC, M., PERMINGEAT, F. and PARFENOFF, A., 1969. L'henritemiérite, une nouvelle espèce minerale: Bull. Soc. Fr. Minéral. Cristallogr., 92, p 185-190.

GLASSER, F.P., 1961. The system Ca_2SiO_4 - Mn_2SiO_4: Am. J. Sci., 259, p 46-59.

GOLD, D.P., 1966. The minerals of the Oka carbonatite and alkaline complex, Oka, Quebec: Papers and Proc. I.M.A. 4th Gen. Meeting, New Delhi, Min. Soc. India, p 109-125.

GREENWOOD, H.J., 1967. Wollastonite: Stability in H_2O - CO_2 mixtures and occurrences in a contact-metamorphic aureole near Salmo, British Colombia, Canada: Am. Mineral., 52, p 1 669-1 680.

GROBLER, N.J. and BOTHA, B.J.V., 1976. Pillow-lavas and hyaloclastite in the Ongeluk Andesite Formation in a road-cutting west of Griquatown, South Africa: Trans. geol. Soc. S. Afr., 79, p 53-57.

GUSTAFSON, W.I., 1974. The stability of andradite, hedenbergite and related minerals in the system Ca - Fe - Si - O - H: J. Petrol., 15, p 455-496.

HAGUE, J.M., BAUM, J.L., HERRMANN, L.A. and PICKERING, R.J., 1956. Geology and structure of the Franklin - Sterling Hill area, N.J.: Bull. geol. Soc. Am., 67, p 435-473.

HARKER, R.I. and TUTTLE, O.F., 1956. Experimental data on the P_{CO2} - T curve for the reaction: calcite + quartz = wollastonite + carbon dioxide: Am. J. Sci., 254, p 238-256.

HAWTHORNE, F.C., 1976. The crystal chemistry of amphiboles: V. The structure and chemistry of arfvedsonite: Can. Min., 14, p 346-356.

_____, 1981. Crystal chemistry of the amphiboles in Amphiboles and other hydrous pyriboles - Mineralogy (D.R. Veblen, ed): Rev. Mineral., Mineral. Soc. Am., 9A, p 1-102.

_____, 1983. The crystal chemistry of the amphiboles: Can. Mineral., 21, p 173-480.

HSU, L.C., 1980. Hydration and phase relations of grossular - spessartine garnets at P_{H2O} = 2Kb.: Contr. Mineral. Petrol., 71, p 407-415.

HUTTON, C. O., 1956. Re-examination of the mineral tuhualite: Min. Mag., 31, p 96-106.

ISHIDA, K., 1984. A mineralogical study of manganoan alkali-calcic amphiboles from manganese ore deposits: J. Mineral. Soc. Japan, 16, p 353-364. (in Japanese).

ITO, J. and AREM, J.E., 1970. Idocrase: synthesis, phase relations and crystal symmetry: Am. Mineral., 55, p 880-912.

ITO, T., MORIMOTO, N. and SADANAGA, R., 1952. The crystal structure of milarite: Acta Crystallogr., 5, p 209-213.

JAMES, H.L., 1955. Zones of regional metamorphism in the Precambrian of northern Michigan: Bull. geol. Soc. Amer., 66, p 1 455-1 487.

JCPDS INTERNATIONAL CENTRE FOR DIFFRACTION DATA, 1986. Mineral Powder Diffraction File: Data Book. 1396p.

KLEIN, C., 1966. Mineralogy and petrology of the metamorphosed Wabush Iron Formation, southwestern Labrador: J. Petrol., 7, p 246-305.

_____, 1973. Changes in mineral assemblages with metamorphism of some banded Precambrian iron-formations: Econ. Geol., 6, p 1 075-1 088.

KLEYENSTÜBER, A.S.E., 1984. The mineralogy of the manganese-bearing Hotazel Formation of the Proterozoic Transvaal Sequence in Griqualand West, South Africa: Trans. geol. Soc. S. Afr., 87, p 257-272.

KONEV, A.A., USHCHAPOVSKAYA, Z.F. and LEBEDEVA, V.S., 1970. First find of magnesian kirschsteinite in the U.S.S.R.: Dokl. Acad. Sci. U.S.S.R., Earth Sci. Sect., 190, p 136-138.

KORZHINSKII, D.S., 1970. Theory of Metasomatic Zoning: Clarendon Press, Oxford, 162p.

LAGER, G.A. and MEAGHER, E.P., 1978. High-temperature structural study of six olivines: Amer. Mineral., 63, p 365-377.

LEAKE, B.E., 1978. Nomenclature of amphiboles: Am. Min., 63, p 1 023-1 052.

LEAVENS, P.B. and DUNN, P.J., 1987. Glaucochroite (olivine, $CaMnSiO_4$) from Franklin, New Jersey: its composition, occurrence and formation: Am. Mineral., 72, p 423-428.

LIOU, J.G., 1974. Stability relations of andradite - quartz in the system Ca - Fe - Si - O - H: Am. Mineral., 59, p 1 016-1 025.

LYONS, P. C., 1976. The chemistry of riebeckite of Massachusetts and Rhode Island: Min. Mag., 40, p 474-499.

MEAGHER, E.P., 1982. Silicate garnets in Orthosilicates - 2nd Ed. (D.H. Ribbe, ed.): Rev. Mineral., Mineral. Soc. Amer., 5, p 25-66.

MIYANO, T. and BEUKES, N. J., 1987. Physicochemical environment for the formation of quartz-free manganese oxide ores from the early Proterozoic Hotazel Formation, Kalahari Manganese Field, South Africa: Ec. Geol., 82, p 706-718.

MIYASHIRO, A., 1956. Osumilite, a new silicate mineral, and it's crystal structure: Am. Mineral., 41, p 104-166.

MUKHOPADHYAY, D.K. and LINDSLEY, D.H., 1983. Phase relations in the join kirschsteinite ($CaFeSiO_4$) - fayalite (Fe_2SiO_4): Amer. Mineral., 68, p 1 089-1 094.

MURAKAMI, N., KATO, T., MIURA, Y. and HIROWATARI, F., 1976. Sugilite, a new silicate mineral from Iwagi Islet, southwest Japan: Mineral. J. (Japan)., 8, p 110-121.

NEL, C.J., 1984. Die mineralogie en geochemie van die Manatwan-ertsliggam, Kalaharimangaanveld, Transvaal-Supergroep: M Sc Thesis (unpubl.), Rand Afrikaans Univ., 119p.

NISHIZAWA, H. and KOIZUMI, M., 1975. Synthesis and infra-red spectra of $Ca_3Mn_2Si_3O_{12}$ and $Cd_3B_2Si_3O_{12}$ (B:Al,Ga,Cr,V,Fe,Mn) garnets: Am. Mineral., 60, p 84-87.

O'DANIEL, H. and TSCHEISCHWILI, L., 1943. Strukturuntersuchungen an Tephroit Mn_2SiO_4, Glaukochroite $(Mn,Ca)_2SiO_4$ und Willemit Zn_2SiO_4 von Franklin Furnace: Z. Kristallogr., Abteiling A. 105, p 273-278.

OLIVIER, C., GIHWALA, D., PEISACH, M., PINEDA, C.A. and PIENAAR, H.S., 1983. Determination of lithium in the gem mineral sugilite: J. Radioanalytical Chem., 76, p 241-248.

O'MARA, J.H., 1951. Unit cell and space group of glaucochroite: Am. Mineral., 36, 918p.

ONUKI, H., YOSHIDA, T. and NEDACHI, M., 1981. Electron probe study of Ti-rich hydroandradites in the Sanbagawa metamorphic rocks: J. Japan. Assoc. Min. Petr. Econ. Geol., 76, p 239-247.

PALACHE, C., 1935. The minerals of Franklin and Sterling Hill, Sussex County, New Jersey: Prof. Pap. U. S. G. S., 180, p 79-80.

PENFIELD, S.L. and WARREN, C.H., 1899. Some new minerals from the zinc mines at Franklin, N.J. and note concerning the chemical composition of ganomalite: Am. J. Sci., 4th ser., 8, p 339-353.

PERTSEV, N.N. and LAPUTINA, I.P., 1975. Glaucochroite in the Anakit skarns, Lower Tunguska: Dokl. Acad. Nauk U.S.S.R., Earth Sci. Sect., 216, p 173-175.

PETERS, T.J., 1965. A water-bearing andradite from the Total serpentinite (Davos, Switzerland): Am. Mineral., 50, p 1 482-1 486.

PRINZ, M., KEIL, K., HLAVA, P.F., BERKLEY, J.F., GOMES, C.B. and CURVELLO, W.S., 1977. Studies of Brazilian meteorites. III. Origin and history of the Angra dos Reis achondrite: Earth Planet. Sci. Letters, 35, p 317-330.

RICKWOOD, P.C., 1968. On recasting analyses of garnet into end-member molecules: Contr. Mineral. Petrol., 18, p 175-198.

ROBINSON, P., 1980. The composition space of terrestrial pyroxenes - internal and external limits in Pyroxenes. (C.T. Prewitt, ed): Rev. Mineral., Mineral. Soc. Am., 7, p 419-494.

_____, SPEAR, F.S., SCHUMACHER, J.C., LAIRD, J., KLEIN, C., EVANS, B.W. and DOOLAN, B.L., 1982. Phase relations of metamorphic amphiboles: natural occurrence and theory in Amphiboles: Petrology and experimental phase relations (D.R. Veblen and P.H. Ribbe, eds): Rev. Mineral., Mineral. Soc. Am., 9B, p 1-227.

ROY, S., 1971. Studies on manganese-bearing silicate minerals from metamorphosed manganese formations of India. II. Blandfordite, manganoan diopside and brown manganiferous pyroxene: Min. Mag., 38, p 32-42.

_____, 1981. Manganese deposits: Academic Press, London, 458p.

SABINE, P.A., 1950. The optical properties and composition of acmitic pyroxenes: Min. Mag., 29, p 113-125.

SAHAMA, Th. G., 1961. Thermal metamorphism of the volcanic rocks of Mt. Nyiragongo (Eastern Congo): Bull. de la commn geol. de Finlande, 196, p 151-174.

_____. and HYTONEN, K., 1957. Kirschsteinite, a natural analogue to synthetic iron monticellite, from the Belgian Congo: Min. Mag. 31, p 698-699.

SAMANCOR, 1979. Brochure describing the manganese and iron ore interests of the Samancor Group of Companies: SAMANCOR, Johannesburg, 20p.

SCHALLER, W.T., 1955. The pectolite - schizolite - serandite series: Am. Min., 40, p 1 022-1 031.

SCHREYER, W. and SEIFERT, F., 1967. Metastability of an osumitite end member in the system K_2O - M_gO - Al_2O_3 - SiO_2 - H_2O and its possible bearing on the rarity of natural osumilites: Contr. Mineral. Petrol., 14, p 343-358.

SEIFERT, F., 1974. The join akermanite - ferroakermanite: Yb. Carnegie Instn., 73, p 436-440.

_____, 1986. Synthesis of $Ba_2CdSi_2O_7$, an end member of the $X^{2+}{}_2Z^{2+}Si_2O_7$ melilites: Mh. N. Jb. Miner., 1, p 8-12.

SEMENOV, E. I., DUSMATOV, V. D., KHOMYAKOV, A. P., VORONKOV, A. A. and KAZAKOVA, M. E., 1975. Darapiosite, a new mineral of the milarite group: Zapish. Vses. Mineralog. Obshch., 104, p 583-585.

SHIGLEY, J. E., KOIVULA, J. I. and FRYER, C. W., 1987. The occurrence and gemological properties of Wessels Mine sugilite: Gems Gemol., 23, p 78-89.

SHOJI, T., 1974. $Ca_3Al_2(SiO_4)_3$ - $Ca_3Al_2(SiO_4)_3$ - $Ca_3Al_2(O_4H_4)_3$ series garnet: composition and stability: J. Mineral. Soc. Japan, 11, p 359-372. (In Japanese).

SÖHNGE, P.G., 1977. Timing aspects of the manganese deposits of the Northern Cape Province (South Africa) in Time and Stratabound ore deposits (D. D. Klemm and H.J. Schneider, eds): Springer-Verlag, Heidelberg, p 115-122.

SOUTH AFRICAN COMMITTEE FOR STRATIGRAPHY (SACS)., 1980. Stratigraphy of South Africa. Part I (Comp. L.E. Kent). Lithostratigraphy of the Republic of South Africa, South West Africa/Namibia and the Republics of Bophuthatswana, Transkei and Venda: Handbk geol. Surv. S. Afr., 8, 690p.

STANTON, R.L., 1972. Ore Petrology: McGraw Hill, New York, 713p.

TAYLOR, B.E. and LIOU, J.G., 1978. The low-temperature stability of andradite in C - O - H fluids: Am. Mineral., 63, p 378-393.

THOMPSON, A.B., 1971. PCO_2 in low-grade metamorphism: Zeolite, carbonate, clay mineral, prehnite relations in the system CaO - Al_2O_3 - SiO_2 - CO_2 - H_2O: Contrib. Mineral. Petrol., 33, p 145-161.

TILLEY, C.E., 1929. On melilite as a product of interaction of limesto and basaltic liquid: Geol. Mag., 66, p 378-393.

_____, 1946. Bustamite from Treburland manganese mine, Cornwal and paragenesis: Mineral. Mag., p 236-241.

TOGARI, K., AKASAKA, M. And KAWAGUCHI, Y., 1986. Inesite from the Kokuriki mine, Hokkaido, Japan: J. Fac. Sci., Hokkaido Univ., Ser. IV 21, p 669-677.

TROMMSDORFF, V., 1968. Mineralreaktionen mit Wollastonit und Vesuvian einem Kalksilikatfels der alpinen Disthenzone (Claro, Tessin): Schwei: Mineral. Petrog. Mitteil., 48, p 655-666.

UPTON, B. G. J., HILL, P. G., JOHNSEN, O. and PETERSEN, O. V., 1978. Emeleusite; a new Li Na Fe^{3+} silicate from south Greenland: Min. Mag. 42, p 31-34.

VON BEZING, K-L., DIXON, R.D., POHL, D. and CAVALLO, G. Famous minera localities: Kalahari manganese field - an update: Mineral. Rec. (in press.).

WALRAVEN, F. and DIXON, R.D. Isotopic studies on sugilite and associat minerals and rocks in the Kalahari manganese field, Northern Cape Province: (in prep).

WHITE, J. S., AREM, J. E., NELEN, J. A., LEAVENS, P. B. and THOMSSEN, W., 1973. Brannockite, a new tin mineral: Mineral. Rec., 4, p 73-76.

WILKENS, R.W.T. and SABINE, W., 1973. Water content of some nominally anhydrous silicates: Am. Mineral., 58, p 508-526.

WILSON, W.E. and DUNN, P.J., 1978. Famous mineral localities: the Kalahari manganese field: Mineral. Rec., 9, p 137-153.

ZABINSKI, W., 1966. Hydrogarnets: Polska Akademia Nauk, Komisja Nauk Mineralogicsnych, Prace Mineralogiczne, 3, 71p.

ZHARIKOV, V.A., 1970. Skarns (Part II): Int. Geol. Rev., 12, p 619-647